8-1-2014

An Investigation of Geochemical Evidence for Three Paleo-Environments

John Paul Jones

An investigation of geochemical evidence for three paleo-environments

By

John Paul Jones

A Dissertation
Submitted to the Faculty of
Mississippi State University
in Partial Fulfillment of the Requirements
for the Degree of Doctor of Philosophy
in Earth and Atmospheric Sciences
in the Department of Geosciences

Mississippi State, Mississippi

August 2014

An investigation of geochemical evidence for three paleo-environments

By

John Paul Jones

Approved:

Rinat I. Gabitov
(Major Professor)

John E. Mylroie
(Committee Member)

Brenda L. Kirkland
(Committee Member)

Darrel W. Schmitz
(Committee Member)

Michael E. Brown
(Graduate Coordinator)

R. Gregory Dunaway
Dean
College of Arts & Sciences

Name: John Paul Jones

Date of Degree: August 15, 2014

Institution: Mississippi State University

Major Field: Earth and Atmospheric Sciences

Major Professor: Rinat I. Gabitov

Title of Study: An investigation of geochemical evidence for three paleo-environments

Pages in Study: 117

Candidate for Degree of Doctor of Philosophy

Three paleo-environments were studied. The first project concerned the Manson Impact and the effect of the Black Hills on the resulting fall-out from this asteroid strike. Samples of the Crow Creek Member were taken east of the Black Hills in Nebraska and South Dakota and samples from the Red Bird Member were taken from the west, in Wyoming. These samples were examined for chemical weathering, soot, shocked quartz, and fossils. The Crow Creek samples had shocked quartz (indicative of an impact), severe chemical weathering, soot, and evidence of tsunamis. There were few calcareous fossils. The Red Bird showed no signs of chemical weathering, a distinct absence of soot and shocked quartz and an abundance of fossils. These results indicate that the Black Hills were large enough to pose an atmospheric and oceanic barrier to the effects of the Manson Impact.

The second project dealt with dinosaur eggs which were found in Montana. The eggs were examined and subjected to Computed Tomography Scans. The egg-shell, matrix, and volcanic ash were studied. The egg-shell was found to be from an undescribed oolithic species, and revealed that a transgressive event transpired after the

eggs had fossilized. The matrix revealed that the eggs were laid in a flood-plain. The ash revealed a high amount of tungsten and yielded a high percentage of potassium for future dating. The eggs themselves revealed that intact embryos were within. This project has provided information on dinosaur nesting behavior.

In the third project corals were examined to determine the usefulness of sampling different architectural structures for evaluating environmental proxies. Coral was collected at the Verde Reef. The different architectural structures were sampled using SIMS, and LA-ICP-MS to selectively sample the small architectural structures. Oxygen isotope ratios and elemental: calcium ratios were compared among the different structures. It was found that dissepiments intake isotopic oxygen and elements at different rates than other structures. This has an impact in sampling corals for environmental proxies, but, because of the very small amount of mass contained in the dissepiments that bulk analyses would not be significantly affected.

.

DEDICATION

I would like to dedicate this page to my parents, Dr. and Mrs. James Paul and Dudie Jones who supported me and stood behind me, as well as sending much appreciated CARE packages.

ACKNOWLEDGEMENTS

I would like to acknowledge many people in this long and at times painful process. I would like to thank my advisor, Dr. Rinat Gabitov, who made it all possible and generously used part of his budget to pay for analyses. Dr. Brenda Kirkland who took an interest in the eggs and encouraged me to investigate them further, to Dr. John E. Mylroie and his lovely wife, Joan who acted as mentors since before my sojourn here at MSU. Dr. Darrel Schmitz was instrumental in providing me summer employment which kept me going, even before I started the program. I also wish to thank him for his valuable comments and interesting field trips. I want to thank Dr. Giselle T. Munn for donating the CT scans which proved an embryo was in the eggs, and Amanda Lawrence and all the other people who helped me at I2AT. I also want to thank all the interesting and informative professors which all had a role in helping me through this. I would definitely like to thank the rancher in Montana and his two sons who helped me extract the first eggs and donated the land for further digs, though they wish to remain anonymous, and Tyler Anderson, geologist who helped me on the last dig. Finally I would like to thank my friends, both here at MSU and else-where who supported me, especially Jeremy Weremeichik, who provided a lot of technical assistance when needed..

TABLE OF CONTENTS

LIST OF TABLES

LIST OF FIGURES

CHAPTER I

INTRODUCTION

The study of paleo-environments is an important aspect of geology due to the changing environment man-kind finds itself in. By looking at how paleo-environments have evolved and the impacts that have been caused by these changes, the events our ecosystems are going through can be better envisioned. Rising sea-levels, climate change, storms are all making an impact on our lives. In addition these studies can guide us in understanding the evolution of species and climates in the geologic past. In the following dissertation three paleo-environments were explored using geochemical methods. Those methods explored the timing of certain events in the Campanian Stage (Late Cretaceous epoch). The Manson Impact and its effects (~74.1mya) will be examined through sedimentary diagenesis, sedimentary structures, and fossil dissolution first. Next the eggs from a dinosaur which nested during the Campanian, though slightly later (probably a couple of million years but that is yet to be determined) will be examined both morphologically and geochemically in order to understand the habitat at time of nesting as well as any environmental changes (such as transgressions) which took place after fossilization. An attempt to identify the dinosaur which laid them, either by egg-shell classification or from embryonic means will also be attempted.

Scleractian corals have been around since the Mesozoic and then, as now, have played a role in recording seawater chemistry and temperature (Suzuki, 2012; Stanley, et al., 2010). . However, it was shown that temperature and environment are not the only factors that control coral geochemistry (Storz, et al., 2013; Guzman, et al., 1998). Previous studies showed that isotopic and elemental ratios vary with respect to different architectural structures in corals grown at the same environmental conditions (Storz, et al., 2013; Guzman, et al., 1998). Because of this fact bulk analyses of coral samples often contain multiple signatures from kinetic and biological effects, which could distort the use of temperature proxies. Therefore, isotopic and chemical examinations of individual architectural structures of modern corals will allow us to estimate kinetic or vital effects and improve environmental proxies. The difference in elemental ratios may also distort the usage of corals for other environmental factors such as wind, turbidity, sun-light, salinity, etc (Suzuki, 2012; Barnes & Lough, 1993).

Various techniques such as Thin Section Microscopy (TSM), Scanning Electron Microscopy (SEM), Elemental Dispersive Spectroscopy (EDS), Secondary Ion Mass Spectrometry (SIMS), Laser Ablation Inductively Coupled Plasma Mass Spectrometry (LA-ICP-MS), X-Ray Diffraction (XRD), Computer Tomography (CT) Scans were all employed in analyzing the geochemical components of the three topics.

Manson Impact and the Black Hills

The Manson Impact was a bolide which hit the area of what is now Manson, Iowa., in the Campanian Stage of the Late Cretaceous. It impacted along the eastern shore-line of the Western North American Inland Sea-Way (Anderson & Witzke, 1994) Figure 1.1). Whether it impacted the sea-way directly or was merely close-by is still a matter for debate, as the eastern margin of that sea has been eroded away. In any case the impact certainly affected the sea-way with tsunamis, seiches, (Stein & Shoemaker, 1996;

Weber, 2006) fires, and apparently acid fall-out from the impact (Nelson, 2012). These effects stretched all the way into Montana and North Dakota, yet apparently spare the area directly behind (from the impact) the Black Hills (Varracchio, et al., 2009, 2010). The acid fall-out impacted both the formation of clays (leading to increased formation) and the dissolution of calcareous fossils, especially ammonites such as *Excitelocerasjennyi* (Figure 1.2).

The Black Hills were created by an up-doming during the Laramide orogeny. The timing is estimated at late Cretaceous based on the Cretaceous deposits which came from the erosion of these hills in the Powder River basin (Larson et al.1997), though some (Lisenbee, 1988) put the event in the Tertiary. Since the uplift, the Black Hills have been affected by the weathering and erosion of the Mesozoic (and some Paleozoic) sediments. In their younger days they would have been significantly higher and presented a barrier to the Manson effects. The sedimentary Formation known as the Pierre Shale lies on both sides (east and west) of the Black Hills, but the rock units (members) differ. The member deposited at the time of the Manson impact is known as the Crow Creek Member and it is quite different geochemically (Joliff, et al., 1996; Jones, et al., 1996; Katango, et al., 2004), lithologically, (Bretz, 1979) and fossiliferously (Watkins, 1995; Larson, et al., 1997) to the Red Bird member (Gill & Cobban, 1966) found on the western side of the Black Hills. This study will attempt to delineate some of those differences and provide a hypothesis for their existence. Today the latitude of South Dakota, Iowa, Montana, and upper Wyoming are influenced strongly by the Westerlies (a flow of wind and weather from the west to the east), but in Cretaceous time, this was not the case. Due to warmer climates and a smaller temperature gradient between the poles and the equator, those latitudes would be within the Hadley Cell high pressure system and would experience the equivalent of winds (or lack there-of) as are now found in the horse latitudes (Jiang, et al., 2001; Hasegawa, et al., 2012).

It is hypothesized that the Manson Impact created a time of great environment stress on the Inland Seaway, mainly through acid rain and tsunamis. It is believed that these stress factors are recorded in the geological record. Furthermore, it is hypothesized that the Black Hills were much larger then and acted as a mitigating, atmospheric barrier to the acid rain and a physical barrier to the tsunamis caused as well.

Campanian Dinosaur Eggs

This study examines six dinosaur eggs found in the Judith River Formation in southern Montana. The matrix, fossilized wood, egg-shells, volcanic ash and embryos were examined in the hope that the genus and species of the dinosaur in question (or at least the oo-genus and species) can be determined which will give us more data on the range and habitat of such organisms (Jackson and Varracchio, 2010). It is also hoped that a clearer picture of the habitat where these organisms nested will be better established as well as any changes in ocean level which might be reflected in the geochemical composition of the egg-shells (Deckker, et al., 1988). Several methods and techniques were used to evaluate the geochemistry of the eggs. Several different methods were utilized and these included XRD on the matrix and ash, SEM and EDS on the egg-shell, matrix, and ash. Thin sections of the matrix, fossilized wood, ash, and egg-shell were used to examine components and the mineralogy. The embryos were viewed using a CT scan. It is hypothesized that these eggs are from a species of Hadrosaur, that they nested in a fluvial flood-plain, were affected by volcanic fallout, and that a transgressive event of the Western North American Seaway took place sometime after the eggs fossilized.

Study on oxygen isotopes and Element:Calcium ratios in reef-building corals

Corals have long been used as temperature proxies in oceans and seas based on their $\delta^{18}O$ value, which is (define it as [$^{18}O/^{16}O$ (sample)- $^{18}O/^{16}O$ (std.)]/($^{18}O/^{16}O$ (std.))x1,000 (Land, et al., 1975; Watanabe, 2001). Higher $\delta^{18}O$ corresponds to colder seawater and vice versa. It appears that inconsistencies between $\delta^{18}O$ and element/Ca ratios further complicate reconstruction of paleo-environments. Corals are also composed of various architectural structures (Figure 1.3). The various architectural structures include the theca, which houses the body of the polyp, the septa, which divide the theca vertically, the costae, which are the upper-most growth on the theca wall, endothecal dissepiments which are built by the polyp below itself as the theca grows upward towards the surface, and exothecal dissepiments which connect one septa to another in colonial corals. These structures vary among themselves with their oxygen ratios (Leder, et al., 1996). By determining and correlating which architectural structure is best suited as a temperature proxy, one should be able to improve the use of corals by sampling only those structures which represent a true correlation to temperature. Element:Calcium (B/Ca, Mg/Ca, Sr/Ca, Ba/Ca, and U/Ca) ratios also reflect different aspects of environment such as temperature, sunlight, and water composition, pH, and continental weathering(Hayashi, et al., 2013; Giry, et al., 2010; Cohen, et al., 2004). An examination of how these ratios vary among architectural elements will provide a more accurate proxy as well.

By using high resolution beam techniques such as SIMS and LA-ICP-MS it was possible to analyze the individual architectural elements for $\delta^{18}O$ and elemental composition. These techniques have the advantages of being able to sample very small amounts ($6.2832 \cdot 10^5 \mu m^3$ or 1.7033g) compared to 12.5g-67.5g for gravimetric analysis) at high resolution without extensive sample preparation. The corals were collected alive in the Gulf of Mexico off-shore of Veracruz (Figure 1.4), a warm, shallow marine area much like the inland Cretaceous Seaway discussed earlier.

Commonalities

All three of these projects deal with calcium carbonate minerals. The first project is focused on fossil mollusks in the Inland Cretaceous Seaway during the Campanian to estimate the effects of a bolide impact on the shore of that seaway. The second deals in part with measuring calcitic egg-shells laid during the Campanian, the volcanic orogenies taking place at the time of egg-laying, and the effect of the Inland Seaway transgressing over them. The third measures isotopic, and elemental ratios of aragonite ($CaCO_3$) in modern, scleractinian corals of a warm sea-way (Gulf of Mexico).

The first two projects are very close (within a few million years) of each other, both placed in the Campanian Stage. The third project deals with modern scleracintian corals. These corals evolved in the Triassic period and there have been paleo-environmental studies on them using stable isotopes (Stanley & Helme, 2010). These coral types were also present in the Cretaceous and in a habitat which existed, essentially unchanged (Gulf of Mexico) during the Cretaceous. Most importantly all three projects demonstrate the use of geochemistry to investigate and explain paleo-environments and the changes these environments undergo.

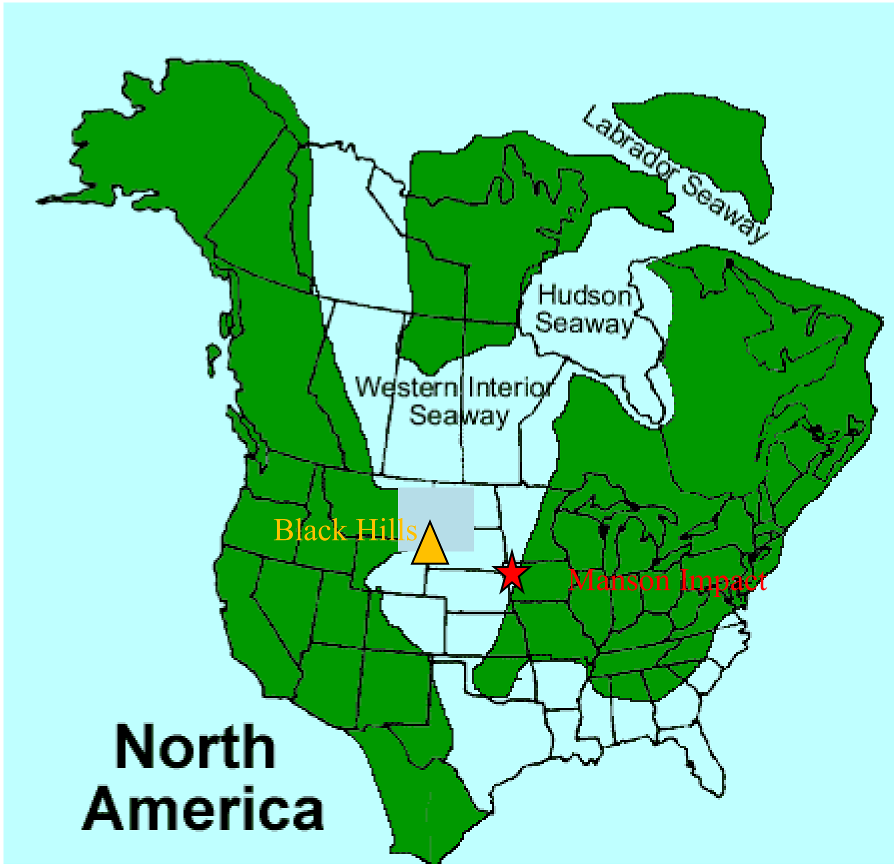

Figure 1.1 Manson Impact and position of Black hills during Campanian

Adapted from discoverfossils .com

Figure 1.2 *Exciteleceros jennyi*

Paleoportal.com

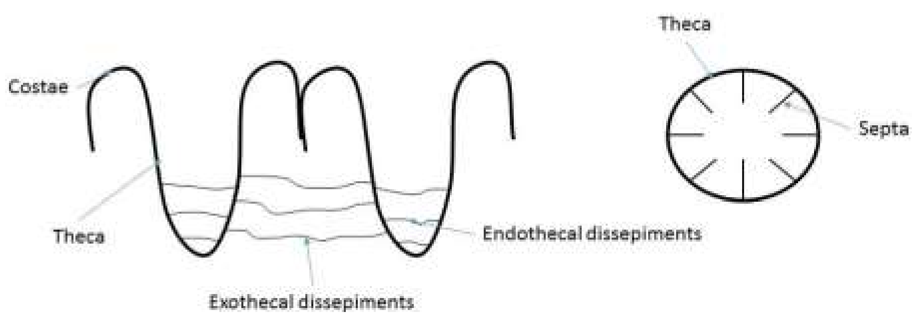

Figure 1.3 Architectural structures of coral

Drawing by Jeremy Weremeichik and John Paul Jones

Figure 1.4   Location of coral sampling site (Red

References

Anderson, R. and Witzke, B., (1994) The terminal Cretaceous Manson Impact Structure in north central Iowa: A window into the Late Cretaceous history of the eastern margin of the Western Cretaceous Seaway. *Geological Society of America Special Paper,* Vol. 287, pp. 197-211

Barnes, D., Lough, J. (1993) On the nature and causes of density banding in massive coral skeletons. *Journal of Experimental Biology and Ecology* Vol. 167, pp.91-108

Bretz, R., (1979) Stratigraphy, Mineralogy, Paleontology and Paleoecology to the Crow Creek Member, Pierre Shale (late Cretaceous), south central South Dakota. *Master's Thesis. Fort Hayes State University, Kansas*

Deckker, P., Chivas, A., Shelley, J., Torgersen, T. (1988) Ostracod shell chemistry: A new paleoenvironmental indicator applied to a regressive/transgressive record from the Gulf of Carpentaria, Australia. *Palaeogeography, Palaeoclimatolgy, Palaeoecology* Vol. 86, pp.231-241

Gill, J. and Cobban, W., (1966) Red Bird Section of the Upper Cretaceous Pierre Shale *U.S. Geological Survey Professional Paper,* 393-A, pp. 73-85 and stable isotopic ($^{13}C/^{12}C$ and $^{18}O/^{16}O$) composition in response to several environmental variables in the Caribbean reef coral *Siderastrea sidereal. Marine Ecology Progress Series*, Vol. 166, pp. 109-118

Guzman, H., Tudhope, A. (1998) Seasonal variation in skeletal extension rat

Hasegawa, H., Tada, R., Jiang, X., Suganuma, Y., Imsamut, S., Charosiri, P., Ichinorou, N., Khand, Y. (2012) Drastic shrinking of Hadley circulation during mid-Cretaceous supergreenhouse. *Climate of the Past* Vol. 8 pp1323-1337

Hayashi, E., Suzuki, A., Nakamura, T., Iwase, A., Ishimura, T., Iguchi, A., Sakai, K., Okai, T., Inoue, M., Araoka, D., Murayama, S., Kawahata, H. (2013) Growth-rate influences on coral climate proxies tested by a multiple colony culture experiment. *Earth and Planetary Letters* Vol. 362, pp.198-206

Jackson, F., Varricchio, D. (2010) Fossil Eggs and eggshells from the Lowermost Two Medicine Formation of Western Montana, Sevenmile Hill Locality. *Journal of Vertebrate Paleontology* Vol. 30, Issue 4, pp. 1142-1156.

Jiang, X., Pan, Z., Fu, Q. (2001) Primary study on patterns of general circulation of atmosphere before uplift of Tibetean Plateau in eastern Asia. *Science in China* (Series D) Vol. 44, Issue 8, pp 600-688

Joliff, B., Rockow, K., Korotev, R., Haskin, L., McCarville, P., Crossey, L., (1994) Geochemical study of cores from the Manson impact structure. *Proceedings of the VIIth International Symposium on the Observation of the Continental Crust through Drilling. April 25-30, 1994, Santa Fe, NM.,* pp. 215-218

Jones, M., McCormick, G., Anderson, R., (1996) Preliminary clay-mineral investigation of some impactites recovered by core drilling in the Manson impact structure. *Geological Society of America Special Paper,* Vol. 302, pp.341-346

Katongo, C., Koeberl, K., Witzke, B.J., Hammond, R.H., (2004) Geochemistry and Shock Petrography of the Crow Creek Member. *Meteoritics and Planetary Science,* Vol. 39, pp. 31-51

Land, L., Lang, J., Barnes, D. (1975) Extension rate: A primary control on the isotopic composition of West Indian (Jamaican) Scleractinian reef coral skeletons. *Marine Biology* Vol. 33 pp. 221-233

Larson, N., Jorgensen, S., Farrar, R., Larson, P., (1997) Ammonites and the other Cephalods of the Pierre Seaway, Geoscience Press, Tucson, AZ

Leder, J., Swart, P., Szmant, A., Dodge, R. (1996) Origin of variation in the isotopic record of scleractinian corals. I Oxygen. *Geochimica et Cosmochimica Acta* Vol. 60, No. 15, pp2857-2870

Lisenbee, A. (1988) Tectonic History of Black Hills Uplift. *AAPG Data Pages, Wyoming Geological Association 39th Annual Field Conference Guidebook* pp.45-52

Nelson, S. (2012) Meteorites, Impacts and Mass Extinctions *Natural Disasters, Tulane University* www.tulane.edu/snelson/natural_disasters/htm

Stanley, G., Helmle, K. (2010) Middle Triassic coral growth bands and their implications for photosynthesis. *Palaios*, Vol. 25, No. 12, pp.754-763

Stein, M., and Shoemaker, E., (1996) A Hypothesized Manson Impact Tsunami: Paleomagnetic and Stratigraphic Evidence in the Crow Creek Member, Pierre Shale. *Geological Society of America Special Paper* 302 pp. 419-431an Scleractian coral for reconstruction of climate variability in the Northwestern Indian Ocean. *Palaios,* Vol. 28, pp. 42-55

Storz, D., Gischler, E., Fiebig, J., Eisenhauer, A., Garbe-Schönberg, D. (2013) Evaluation of oxygen isotope and Sr/Ca ratios from a Maldiv

Suzuki, A. (2012) Paleoclimate reconstruction and future forecast based on coral skeletal climatology. *Synthesiology* Vol. 5, No. 2, pp.80-88

Varricchio, D., Raven, R., Wolbach, W., Elsik, W., Witzke, B., (2009) Soot and palynologic analysis of Manson impact-related strata (Upper Cretaceous) of Iowa and South Dakota, USA. *Cretaceous Research*, Vol. 30, pp. 127-134

Varracchio, D., Koeberl, C., Raven, R., Wolbach, W., Elsik, W., Miggins, D., (2010) Tracing the manson impact event across the Western Interior Cretaceous Seaway. *The Geological Society of America Special paper.* Vol. 465, pp. 269-299

Watanabe, T., Winter, A. Oba T., Anzai, R., Ishioroshi, H. (2002) Evaluation of the fidelity of isotope records as an environmental proxy in the coral *Montastraea. Coral Reefs* 21, pp.169-178

Watkins, D.K., (1995) Biostratigraphical and Sedimentological Implications of Calcareous Nanno-fossil Assemblages From the Crow Creek Member of the Pierre Shale (Upper Cretaceous) *Geological Society of America Abstracts with Programs*, Volume 27, No. 3 pp. 93-94

Weber, R. (2006) Evidence for an impact-induced resuspension event in the Late Cretaceous Western Interior Seaway from the Crow Creek member (Pierre Shale) Thesis, University of Nebraska, Lincoln.

CHAPTER II

THE MANSON IMPACT, ACID RAIN, TSUNAMIS, AND THE EFFECT OF THE BLACK HILLS: AN EXAMINATION OF PALEO-ENVIRONMENT IN THE CAMPANIAN MITIGATED BY THE MANSON IMPACT

Introduction

The Manson Meteor Impact took place mainly in a marine environment, namely the Western North American Inland Seaway (WNACIS) (Figure 2.1), Estimated extent of North American Western Cretaceous Inland Seaway around 74.1 mya, in present day western Iowa. This corresponds with the Campanian Stage. The presence of shock quartz crystals in the crater peak is diagnostic (Short and Gold, 1996). Meteor impact craters can be divided into two categories, complex and simple. Simple craters generally are created from smaller, slower bolides. These simple craters lack a central peak and their rim is overturned. An example of such a simple crater is the Barringer Crater in Arizona (Figure 2.2).

Complex craters have a central peak and exhibit signs of fault slumping along their rims (Figure 2.3). They are formed by larger bolides traveling at higher velocities. The crater created is a complex one rather than a simple crater such as the Barringer Crater of Arizona exhibits. The crater is asymmetrical, being slightly oval, showing an impact of 20-30 degrees from the horizontal from the direction of the southeast (Schultz & Anderson, 1996) (Figure 2.4).

The distinctive "inverted sombrero" shape of the crater denotes not only the size of the object, classifying it as a complex crater, but also the velocity of the bolide. Furthermore the sombrero feature in the center is distinctive of those seen in other shallow impacts such as the Alamo, Nevada, from the Devonian; Chesapeake, Maryland, from the Eocene; Mjolnir in the Barents Sea, dating to the Volgian-Berriasian Age or 141-149 mya; and Lockne, Sweden impact dating from the early Late Ordovician (Horton et al., 2008) (Figure 2.3). Other features of this complex crater include the broad central peak of Pre-Cambrian rock, an outer terrace of down-dropped Cretaceous sediment and an intermediate moat structure (Anderson & Hertung, 1992). The complex shape of the crater indicates a larger bolide traveling at a much higher rate. This bolide is thought to have released 2.2 x 10^{21}Joules of heat energy.. This would have ignited flammable material within 200 km^2 and killed most terrestrial organisms in over 1000 km^2 (Anderson & Hartung, 1992). The relatively shallow rim is a result of the sediment being more water-saturated and less consolidated rather than a steeper rim from an impact which would have impacted more crystalline rocks (Dypvik and Jansa, 2003). Stratigraphic column of the Manson Site at time of impact is in Figure 2.5. The impact likely set off a series of mega-tsunamis and subsequent seiches, which resulted in local extirpations in, and possibly along the shores, of the WNACIS (Stein and Shoemaker, 1996).

There is an absence of ammonite and other calcareous fossils in the upper portion of the Crow Creek Member, east of the Black Hills. These absences are also accompanied by evidence of high levels of chemical weathering in the form of clays. Soot deposits, impact sphericales and shocked quartz are also present in the Crow Creek

Member sediment. Stratigraphic column for the Red Bird Member, west of the Black Hills is Figure 2.6, and the Stratigraphic column for the Crow Creek member, found east of the Black hills is given in Figure 2.7

The Black Hills resulted from a domal uplift caused during the Laramide Orogeny (Larson, et al., 1997) (Figure 2.8). The exact timing of this is unclear, but according to Jarrett (1994) weathering and erosion brought the Black Hills down from their high point to almost their present height about 40 million years ago. Thus, in the Campanian the Black Hills were of significant height and could present a substantial barrier. The North American Continent has remained at roughly the same latitude since the Cretaceous, however, due to the significant warming of the atmosphere during the Cretaceous, the Hadley Cell configuration and heat gradient was significantly different. Instead of the high pressure cell forming along the 30^{o} N latitude North and South of the equator (figure 2.9), the Hadley Cell formed at 46^{o} N (Figure 2.10), at least in the Northern Hemisphere. This would have caused an area from Texas to Montana to fall, not under the Westerlies as they do today, but in an area of light winds, which today is known as the horse latitudes (Hasegawa, et al., 2012; Jiang, et al., 2001) (Figure 2.10).

Hypothesis

The absence of mollusk and other carbonate fossils in the Crow Creek Member (Figure 2.8) east of the Black Hills was caused by the lowering of the pH resulting from the fallout caused by the Manson Impact. The evidence of fossils existing on the western side of the Black Hills would seem to indicate that the Black Hills served as a mitigating factor in preventing some of the effects of the Manson Impact.

Since the general wind pattern was not out of the west at that latitude as it is today there would have been little resistance to a rapid ejecta blanket spreading westward from the Manson Impact Structure and a resulting acid and soot fall-out. The presence of the Black Hills served to mitigate many of these effects on the western side of the emergent Black Hills away from the impact.

The examination of soot, trace elements, sedimentary structures such as cross-bedding and inclusions, fossil evidence and types of lithologies; shale, sand, shocked quartz can all give us an in-sight into the paleo-environment which existed prior and was created as a result of the Manson Impact east of the Black Hills. Examination of these same structures can give us a picture of the paleo-climate to the west of the Black Hills. Further inferences were made as to how these mountains affected the paleo-environment and climate on the western side of the Black Hills after the bolide strike.

The Manson impact, in addition to creating fires, tsunamis, and shock waves (Anderson & Hartung, 1992) usually associated with large bolide impacts, also created a significant acid rain and subsequent lowering of the pH in the WNACIS, at least the eastern half. The increased Y1 temperature of the bolide impact would have led to the decomposition of sediments and vaporization of their volatile components including sulfates and sulfides, (especially pyrite in a marine setting), these sulfur containing compounds would have been converted into sulfuric acid with atmospheric moisture. The heat necessary for this formation of sulfates into acid is roughly 1300°C, temperatures easily reached in the described impact. This has been documented by the inclusion of elevated levels of SO_3 in glass sphericals formed during the Chixculub impact (Sigurdsson, et al., 1992). Research and simulations suggest that most of sulfur was converted into SO_3, not SO_2. This would mean that the aerosol would have been in the troposphere rather than the stratosphere and more easily converted into acid rain by moisture (Ohno, et al., 2004), $SO_3 + H_2O \rightarrow H_2SO_4$. The fires and soot that has been found associated with this impact would have elevated the carbon dioxide, which would have been converted into carbonic acid by atmospheric moisture, $CO_2 + H_2O \rightarrow H_2CO_3$. Finally the heat generated by the impact probably converted atmospheric nitrogen into nitrates (a similar process takes place in automobile engines) which converted into nitric acids with atmospheric moisture. Prinn and Fegley (1987) have developed a formula for estimating NO_x production from an asteroid strike:

$$P \sim [€_1(Y_1)+(1-€_1)€_2 x V_2] 1/2\ mv^2 \text{ (Prinn \& Fegley, 1987)} \qquad (2.1)$$

Where P=moles of NO_x, m=bolide mass, v=velocity of bolide, $€_1$=incoming energy of bolide, and $€_2$=fraction of kinetic energy returned as high speed ejecta, V_2=velocity of the shock wave moving out from the impact (roughly 5 times the bolide velocity, and Y_1 is a value assigned to either cometary or asteroid/meteoric bolides. $€_1 = \pi r^2 P_{(surface)}/mg$(cosine of the angle of impact). According to Anderson and Hartun(1996), $2.2 \cdot\cdot 10^{21}$Joules were released. The Manson impact bolide was approximately 2.2×10^{13} kg, radius of 2.1 km, an angle of 20° -30° and traveling at a speed of 72,000 km/hr (Anderson and Hartung, 1992). The ejecta is estimated to be between 600 and 1200 km^3 of which about 15% is estimated to have escaped from the troposphere, and distributed on a global trajectory rather than remaining in the Inland Seaway. (Witzke & Anderson, 1993). From these calculations it is possible to calculate how much nitric acid was released into the area. $€_2 \sim 2.25 \cdot 10^{15}$ J, $€_1 = 5.4 \cdot 10^{-11}$ J,

Y_1~$2.0 \cdot 10^{17}$, which roughly equals $1.92 \cdot 10^{26}$ moles of nitric acid. This is not an exact figure as many of the variables are estimated, yet it is close enough to give an idea as to the great quantity of acid produced. The total amount of acid (sulfuric and carbonic) from all sources is more difficult to calculate, but is definitely more than that of just the nitric acid released. Since the impact took place in a marine setting (judging from the shale deposits in the crater and the shape of the rim) (Anderson & Witzke, 1994; Dypvik & Jansa, 2003), abundant moisture would have been vaporized as well. This moisture would have supplied the necessary water vapor for conversion of sulfates, carbon dioxide, and nitrates into acids.

By examining the chemical weathering signature in the zone of acid-rain fall-out, it is possible to delineate the effects of the bolide and lowering of pH in the affected area of the inland sea. An examination for the number and age of calcareous fossils both east and west of the Black hills will likewise be helpful in detecting the effects of any fall-out.

Background

There has been much discussion as to the eastern margin of the Inland Seaway (Fig. 2.4) due to the erosion which has taken place on the continent. However the Manson crater itself, which was buried during the last glaciations is surprisingly intact. An examination of the crater and a comparison of it to other marine impacts are revealing. At the time of impact, the top layer of consolidated sediment was Cretaceous marine rock, specifically: Graneros Shale, Carille Shale, Pierre Shale, the Greenhorn and the Niobrara Formations (Anderson & Witzke, 1994) (Figure 2.5). The Manson impact has been correlated as taking place during the Bearclaw transgression (Verracchio, et al., 2010).

Other features of shallow marine impacts are that the crater rims tend to collapse more in fluid rich sediments than those impacts in crystalline targets (Dypvik & Jansa, 2003). Also because of deposition of later sediments; the craters tend to become buried and preserved, as the Manson Impact certainly was (Dressler and Sharpton, 1999). There is certainly evidence of widespread fires by the presence of large amounts of soot which appears to have been preserved by the anaerobic conditions of the bottom of the Inland Seaway (Varricchio et al., 2009). From the examination of the crater, the Impact Object impacted from the south-east as evidenced by the offset of the central uplift, shape of the diameter of the crater, and the down-range rim of the crater being shallower (Schultz and Anderson, 1996) (Figure 2.3) (and thus the ejecta, including any acid rain was thrown to the north-west across South Dakota, Wyoming and Montana (Figure 2.11). From looking at soot and shocked quartz analysis (Izett, et al., 1993; Varricchio et al., 2009) through-out the Crow Creek Member of the Prairie Shale Formation and associated lithologies one may estimate a fall-out zone from the impact (Figure 2.11). Soot and shocked quartz were also found in an investigation of the area during a 2013 expedition in the Crow Creek member to the east of the Black Hills (Figures 2.16-2.17). No soot or shocked quartz was found to the west of those hills (Figures 2.18). Calcareous microfossils such as foraminifera and broken ammonite shells are found in the lowermost area of the Crow Creek Member but are absent from the upper portion which is believed to correspond to the Manson Impact (Weber & Watkins, 2007). To the west of the Black Hills there is no break in the calcareous fossil record found in the Red Bird Formation.

Methods

Samples of the Crow Creek Member of the Pierre Shale Formation were taken, the first sample was taken just north of the Yankton area, along the Missouri River (Figure 2.12). Another sample from an out-crop on the Missouri River; 43°48' 35" N, 99°22' 48" W along I-90 (Figure 2.13) as well as a sample on an outcrop along I-90 and highway 83 Figure 2.14). These were examined for soot, clast size, shocked quartz and clay content by XRD and thin section petrographic microscopy.

In addition, numbers and types of marine fossils especially the index ammonite, *Exiteloceras jennyi,* were examined and compared from one side of the Black Hills to the other. Signs of chemical weathering (especially the presence of clays) were compared through examination of samples from both the Crow Creek Member and the Red Bird Member using petrographic microscopes (Nikon Eclipse E400).

Three samples of the Red Bird Member were taken from just west of the Black Hills in Wyoming to as far away as the Devil's Monument area (Figure 2.8) for soot, shocked quartz and clay.

Results

The examined sites in which the Crow Creek Member of the Pierre Shale Formation is exposed exhibited particles of soot (Figures 2.16 &2.17). These results agree with Varricchio, et al., (2010). Clasts of shocked quartz were also found east of the Black Hills in this study. These soot particles also showed up in the thin sections. No shocked quartz or soot was present in the Red Bird Member directly to the west of the Black Hills based on petrographic examinations (Figure 2.18). Shocked quartz crystals, while present in the South Dakota samples, were absent in the Red Bird Formation sample just to the west of the Black Hills. The Red Bird Formation contained quartz as shown by an XRD scan (Fig 2.19), but there was no shocked quartz or soot visible in thin sections in Fig 2.18. This lack is in contrast to the Crow Creek Member which is contemporaneous in deposition. There is soot and shocked quartz (though not in as much quantity) northwest of the Black Hills, even as far away as Montana (Varracchio,et al., 2009). Carbonaceous fossils, especially mollusks are absent from the eastern side in the Crow Creek member, but present in layers both above and below it. There are also fossils present from the same time period in the Red Bird section, (a mostly sandy marine deposit) especially the index ammonite *E. jennyi* (Figure 2.20). There was little if any clay found in the Red Bird sediment. In-bedded Niobrara Member clasts found with-in the Crow-Creek contained fossils, especially diatoms (which has a siliceous skeleton) dating from this earlier time (Figure 2.12).

Discussion

An impact the size of the Manson Impact Structure (roughly 2 km in diameter) (Anderson et al., 1996), either in the Inland Sea-way, or very close to the land could have set off tsunamis. These tsunamis would have been caused through several different methods. As the sediment and water are vaporized by the extreme heat of impact, the water from the Inland Seaway would have rushed in to fill the void. Massive displacement of water is the cause of tsunamis. This was witnessed when Krakatau and Thera both erupted and destroyed their islands, and in the process created large tsunamis (Kasten & Cita, 1981). The paleo-depth of the inland Seaway is reported as having been between 200 m and 400 m across the sea-way (Ericksen & Slingerland, 1990). It is thought to have been quite shallow, only several hundred meters at its deepest (Redfern, 2000). This would have limited the total wave height of the tsunamis, as he longer wave-length tsunamis would have experienced interference with the bottom of the Inland Seaway, but not prevented them. Indeed it might have even encouraged more of a seiche action and there is quite a bit of evidence of both a massive destructive tsunami and several accompanying seiches (Stein & Shoemaker, 1996). Among the evidence for the tsunamis and seiches are the observable in-bedded clasts of the Niobrara Member within the Crow Creek member from earlier and lower in the stratigraphic column, Niobara member clasts (Figure 2.12) and micro-fossil (especially diatom) assemblages which pre-date the Manson Impact Structure. The Crow Creek Member, which is part of the Pierre Shale Formation (which stretches widely across the mid-west and present day Canada), has many sedimentary oddities in it. These sedimentary features include hummocky cross-bedding, breccias, terrestrial sands mixed with shale, in-bedded earlier members which contain micro-fossils dating from an earlier stage, and hummocky formations. This suggests that some of this earlier material was taphonomically redeposited (Watkins, 1989), possibly by the same heavy, large wave action which deposited the inclusions of rip-up shale clasts from the lower Gregory Member (Crandell, 1952). There are unusual deposits of sand grains within the Crow Creek Member. These grains decrease in size away from the direction and distance of the Manson Impact Structure both in size and number (Crandell, 1952). These grains are angular to sub-angular and are poorly sorted. This type of sand deposit is missing from the stratigraphic layers above and below the Crow Creek Member. These deposits have been dated using Argon/Argon methods which were applied to the Manson impact time of 74.1 m.y.a (Izett, et al., 1993). Also present within the Crow Creek Member are impact sphericules and shocked quartz which suggest a bollide impact, probably a large meteor or asteroid. Comparisons of trace elements in the Crow Creek Member across South Dakota, outward from the ejecta trajectory of the Manson Impact Object demonstrate a commonality with trace elements (especially rare earth elements (REE) on the eastern side of the Black Hills towards the Manson Impact Structure (Blum, et al., 1996; Koerberl & Shirley, 1996). A comet has generally been eliminated from discussion since the rocks associated with the Manson Impact are relatively high in iridium, osmium, and REE. The level of trace metals is more consistent with a metallic or stony/metallic meteorite (Hartung and Anderson, 1996). Once again these deposits increase in both number and size the closer to the Manson Impact Structure that the Crow Creek Member is surveyed.

It has been suggested that the above deposits and cross-bedding were caused not by tsunamis and seiche action but by a series of severe storms (Izett et al., 1998). It is possible that severe category 4 and especially Category 5 hurricanes can disturb the underlying sediments, create cross bedding and even deposit the terrestrial sand in marine deposits. However, the study area latitudes of 40-50 degrees, are a bit far north for storms that strong, even in the warmer Cretaceous times. This is even more evident given the constricted surface area and shallow depth of the Inland Sea which would have disturbed circulation patterns and the constricted area would inhibit the time needed for storm development. Furthermore, we can see evidence of this great disturbance as far south as Nebraska (Mendenhall, 1954) as well as the South Dakota sediments, all confined within the same time frame of the Manson Impact. If great storms were so prevalent during the Cretaceous in the Inland Sea, then one might reasonably ask why similar deposits aren't found in the other stratigraphic layers through-out the age of the

Inland Sea. Indeed the marine deposits found in Crow Creek Member and other locations dating to this time are remarkably similar to deposits found in the eastern Mediterranean resulting from the Santorini (Thera) eruption and tsunami (Kastens and Cita, 1981). Asymmetric ripple marks, hummocky cross-stratification and locally large ripple marks (Izett et al., 1998) can be representative of a tsunami as well as a mega-storm. Researchers have interpreted the Crow Creek Member as a deposit resulting from a tsunami caused by the Manson impact (Bretz, 1979; Steiner and Shoemaker, 1996). Further comparisons of the Crow Creek Member compare it with similar structures near the Brazos River in Texas caused by the tsunami set off by the Chixculbub Impact 65 m.y.a. (Hanczaryk and Gallagher, 2007).

One very unusual facet about the Crow Creek Member is the dearth of fossils, especially nautiloids, ammonites, bivalves, and gastropods considering that these are found in relative abundance both above and below the layer in question (Steiner and Shoemaker, 1996). There is a relative abundance of some micro-fossils such as radiolarians, sponge spicules, which are common along with gastropods and other fossils through much of the WNACIS. The Inland Seaway was a shallow epeiric ocean with exchange of water at three points, the present day Gulf of Mexico, the Hudson Seaway and the Northern coast of Alaska, because of the multiple exchange with the larger global ocean, the change in prevailing winds during the Cretaceous, and the uncertainty of river input, the circulation pattern and tidal flows were uncertain. The current flow of the whole of the WNACIS is still being studied and debated, however, there is evidence that in most places, especially on the Eastern shore, the current was weak. This is revealed in the deep deposits of shale and evidence of anoxic conditions resulting from a weak current and not much input from streams up in the mid-to northern part of the sea-way. These organisms have silica skeletons and are thus not as susceptible to acid as the carbonates such as mollusks and foraminifera. It is believed that an impact of an asteroid would have reduced the pH to level of 0-1 near the zone, out-ward from Manson, and possibly as much as 4-5 in the upper-levels of oceans globally. This would have had profound and catastrophic effects on calcite formation, which in turn would have affected the calcareous organisms living there (Prinn & Fegley, 1987). Some foraminifera are found in the Crow Creek, but these foraminifera date from the earlier Gregory formation and are believed to be allochthonous (Weber, 2006), already fossilized, largely covered by sediment and have probably been redeposited there, perhaps by a tsunami (Izett et al., 1998). Most of the microfossils are diatoms (Varracchio, et al., 2007) and these dominate considerably over what few foraminifera there are. It is my hypothesis that due to the Manson Impact, the resulting fallout of ejecta and rain caused a significant, if only temporary drop in pH (down to at least 1-2) in the Inland Sea, at least for a large area down range of the strike. There is also some corroborating evidence for a pH drop and massive tsunami found further away. Researchers have found that much of the Manson impact debris, especially soot, "has indications of being reworked" (Varracchio et al., page 132, 2009), possibly as a result of a tsunami and seiche action. In the Red Bird Member section of eastern Wyoming, areas south of the Black Hills show an absence of the fossil ammonite *E. jennyi*as well as other carbonaceous fossils (Izett et al., 1993). The area directly to the west of the Black Hills show these fossils in abundance. A drop in pH would have caused dissolution of the above creatures' calcium carbonate shells, leaving little to fossilize. It has been determined that during this time (74.1 m.y.a.) a low pH was prevalent through the Pierre Sea in much of the Cretaceous Inland Waterway. The main evidence for this is the chemical weathering of the sediments into various clays and the dissolution and weathering of many mollusks east of the Black Hills (Gill and Cobban, 1966). Further evidence of a lowering of pH can be seen from the rocks themselves. The rocks and minerals of the Crow Creek Member show signs of severe chemical weathering (Katongo, et al., 2003). Much of this weathering is evident as clay minerals such as kaolinite and smectite. We are seeing some dissolution of corals and other creatures today with a very modest decrease in pH due to increased acidification of the oceans due to climate change and other man-induced effects (Beauregard, 2010). The more significant drop in pH from the Manson impact would have had a much more profound impact on calcareous organisms in the sea-way. Additionally, the emergent Black Hills of South Dakota would have been expected to have provided some buffer from both the cloud of acid rain and the tsunamis. That interpretation appears to be true. There are deposits of ammonites on the lee (Western side), away from the impact zone, but none in the same time period (74.1 mya) on the windward side (Larson, Jorgensen, Farrar, Larson, 1997; Verracchio, et al., 2010).

Conclusion

The imbedded clasts of an earlier geological member, the soot, shocked quartz, extensive weathering (represented by the presence of clays and the lack of calcareous fossils in the Upper Crow Creek Member all point to a bolide impact at the Manson site which produced a significant amount of acid fall-out. This acid fallout and tsunamis caused many local extinctions.

The presence of these features east of the Black Hills and the absence of the same features west of the Black Hills in the Red Bird Member supports the hypothesis that the Black Hills acted as a mitigating and substantial barrier to the fact. The one, two punch of a tsunami and accompanying seiche waves with a drastic and rapid lowering of the sea's pH would be enough to ensure many local extinctions. It is also apparent that the Black Hills acted as a buffer to the fallout and prevented much of the devastation which occurred east of the Black Hills from happening to the west. Given the relatively restricted flow of the Inland Sea, its small volume and limited access points, it may have taken a significant amount of time, at least as long as the Crow Creek Member depositional sequence represents, to have recovered from this catastrophe. Further studies and sampling to the north and to the south of the area directly to the west of the Black Hills should be informative as to the extent of the fall-out and ejecta cloud. It was possible to reconstruct this catastrophe by examining the various paleontological and sedimentary evidence and disseminating the paleo-environment of the time. Once the paleo-environment has been established, it only remains to find out what events, or climates caused such a paleo-environment and the changes it underwent.

Figure 2.1 Extent of Cretaceous Inland Seaway

Eastern and Western margins are approximate and varied with time. Adapted from discoverfossils.com

Figure 2.2 Barringer Crater, AZ, USA

A simple impact structure, author as scale

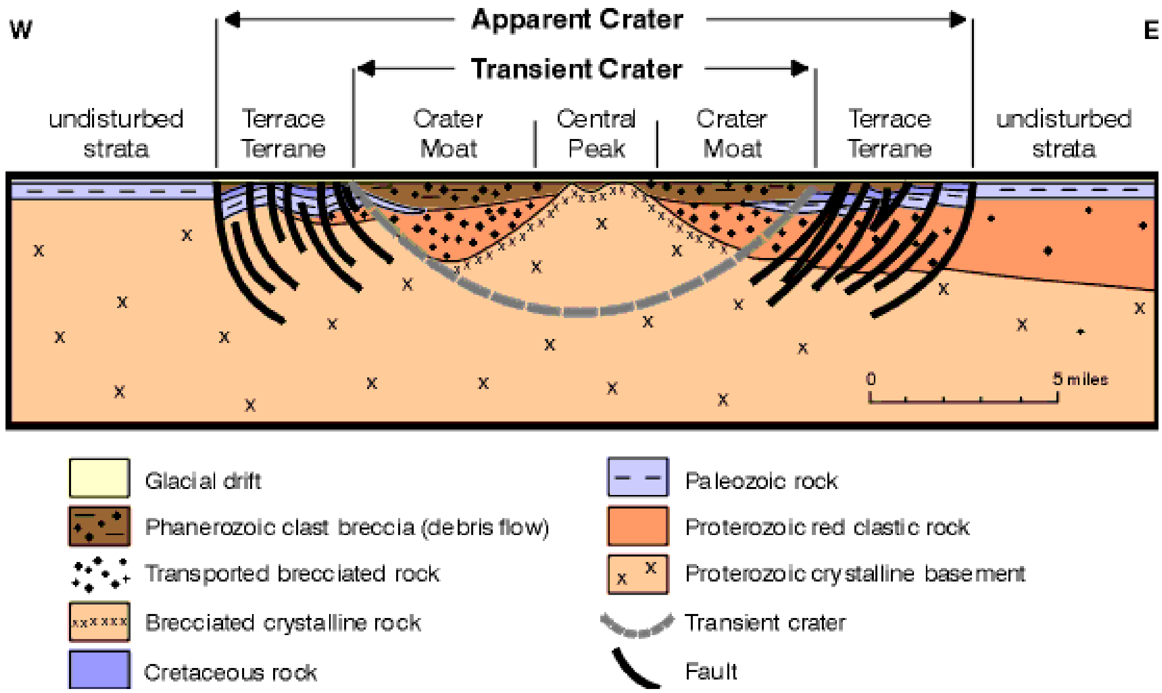

Figure 2.3 Cross section of a complex impact crater www.igsb.uiowa.edu

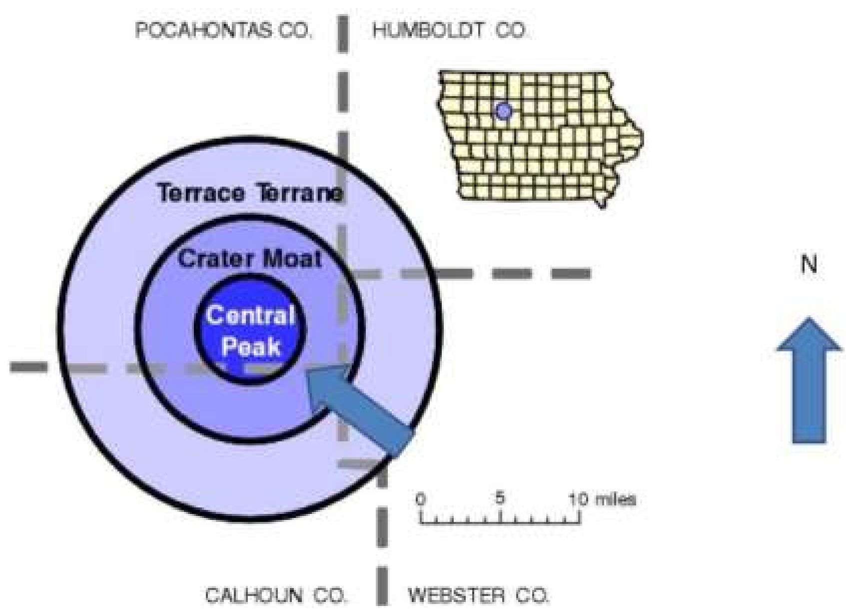

Figure 2.4 Location of Manson Impact and direction of bolide

http://www.igsb.uiowa.edu/browse/manson99/Mansnloc.gif&imgrefurl

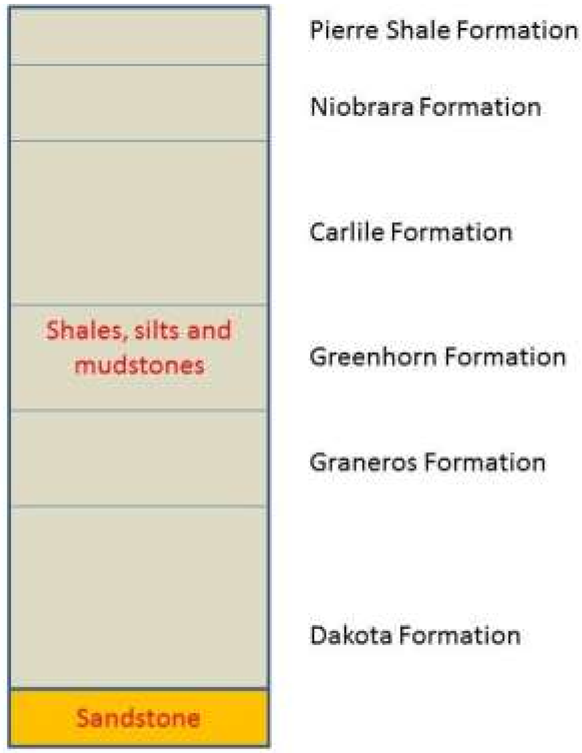

Figure 2.5 Stratigraphic column at time of impact

Figure 2.6 Stratigrpahic column from west of the Black Hills

Figure 2.7 Stratigraphic column east of the Black Hills

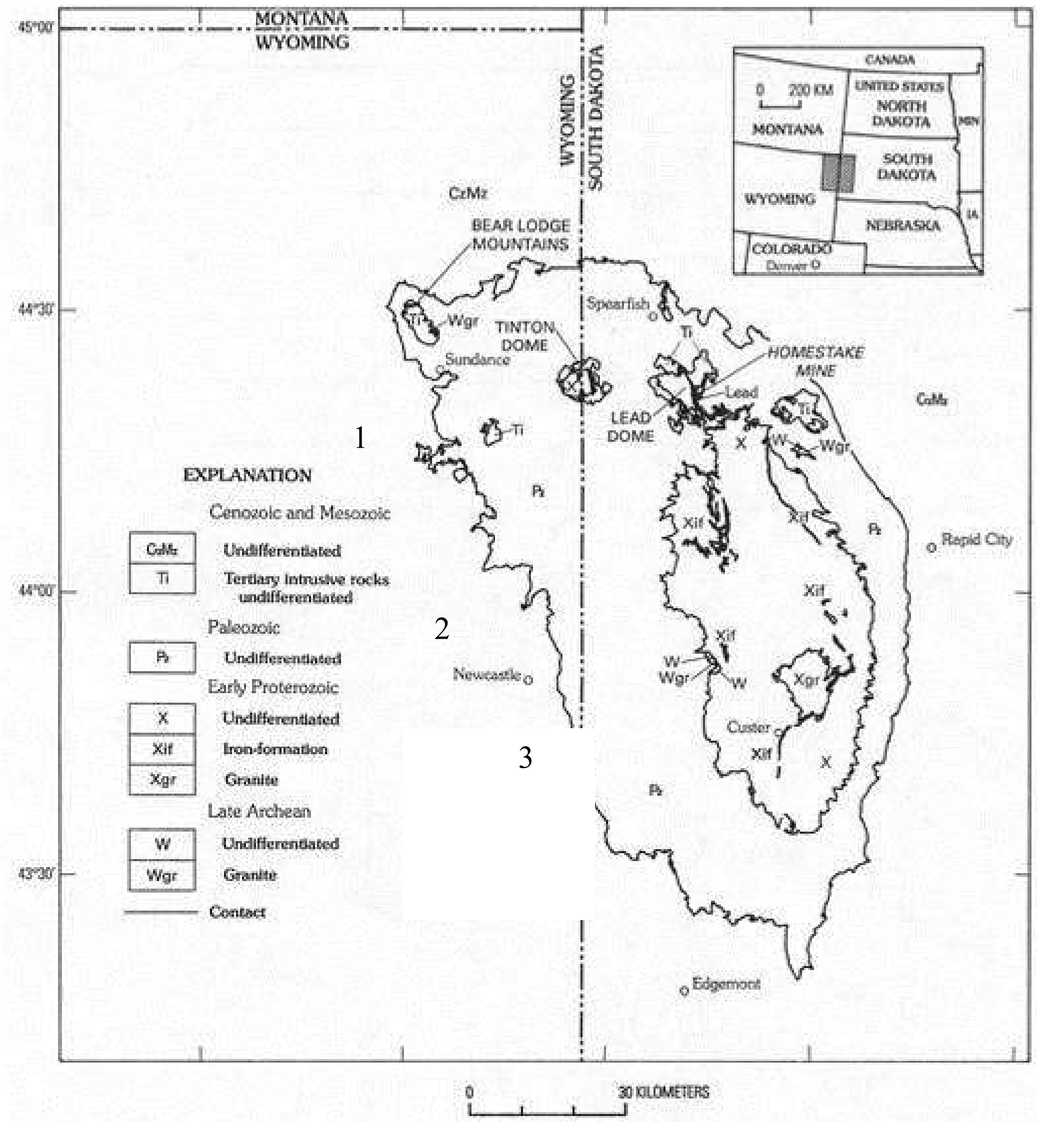

Figure 2.8 Location, type and age of rock in the Black Hills

Numbers correspond to sample sites
http://homestke.sdmt.edu/Geology

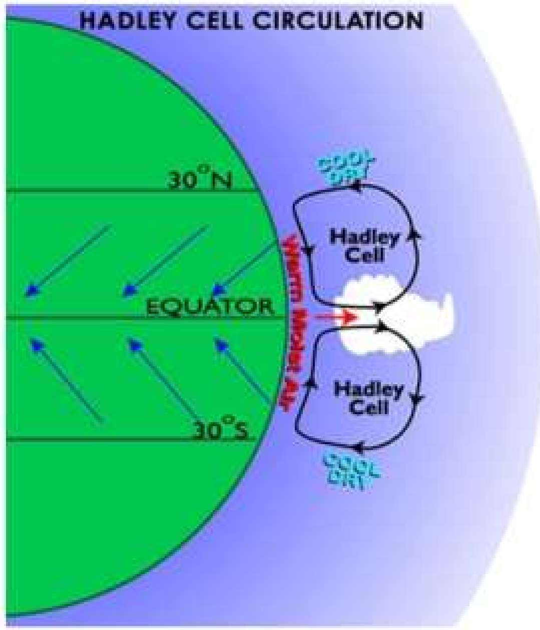

Figure 2.9 Modern Hadley Cell configuration

www.windows2universe.org

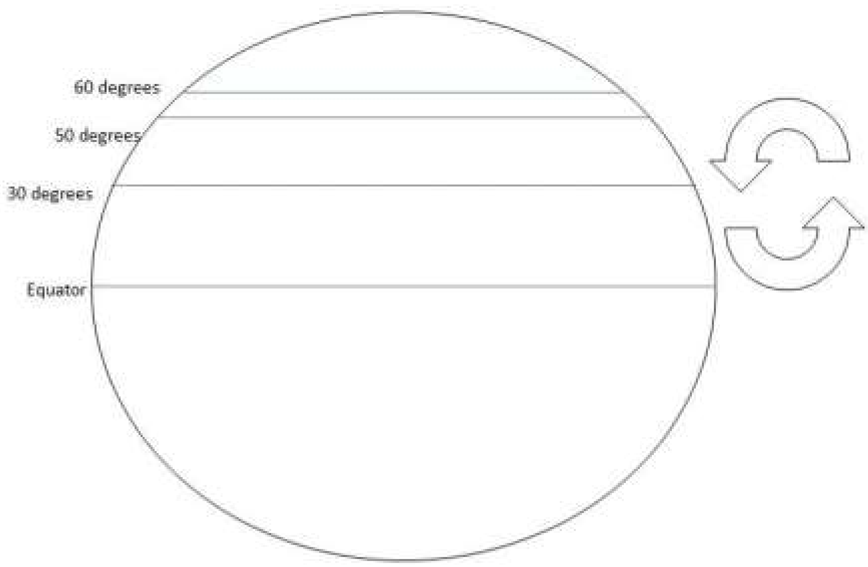

Figure 2.10 Cretaceous Hadley Cell configuration

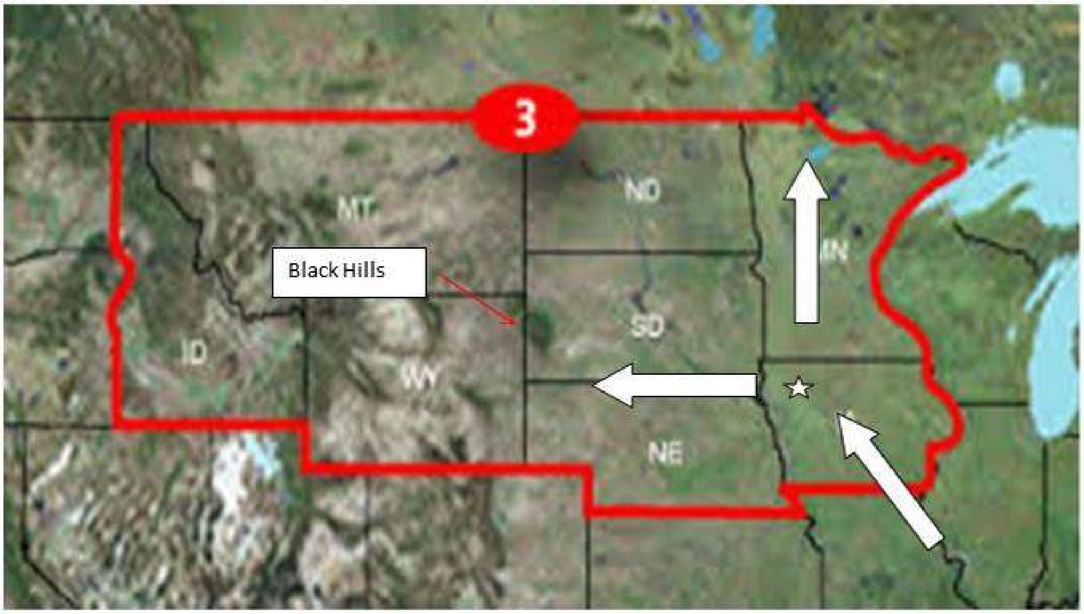

Figure 2.11 Bolide direction from SE and fallout to N and W

Modified from www.software.maps.com

Figure 2.12 Crow Creek outcrop near Yankton, showing ripped up, imbedded sediments

Photo by Tracy Frank

Figure 2.13 Crow Creek further west along Missouri River

Figure 2.14 Crow Creek south of Pierre S.D. off I-90

Figure 2.15 Red Bird Member west of Black Hills in Wyoming

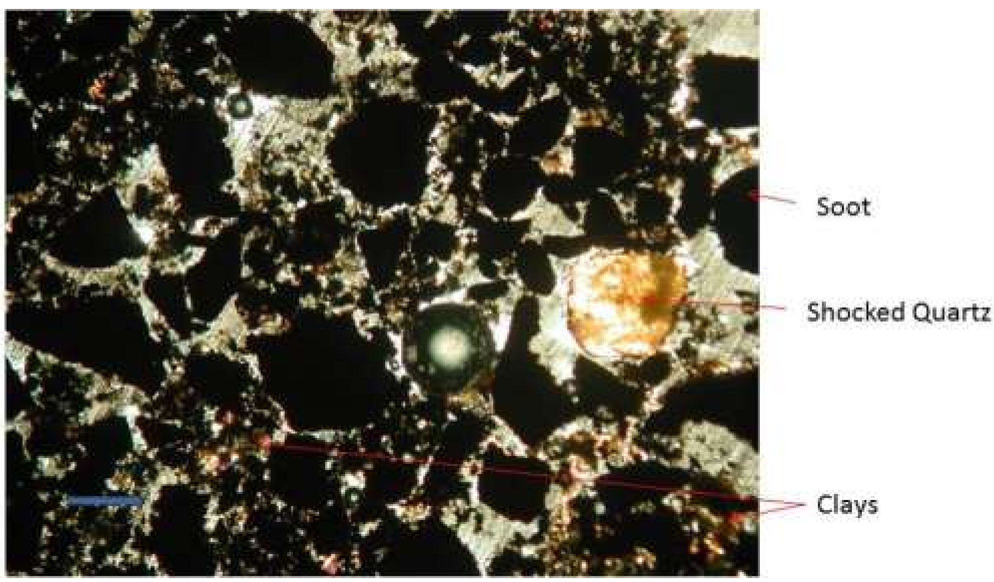

Figure 2.16 Thin section of Crow Creek from Yankton showing soot and shocked quartz

Blue bar is 0.25mm for scale

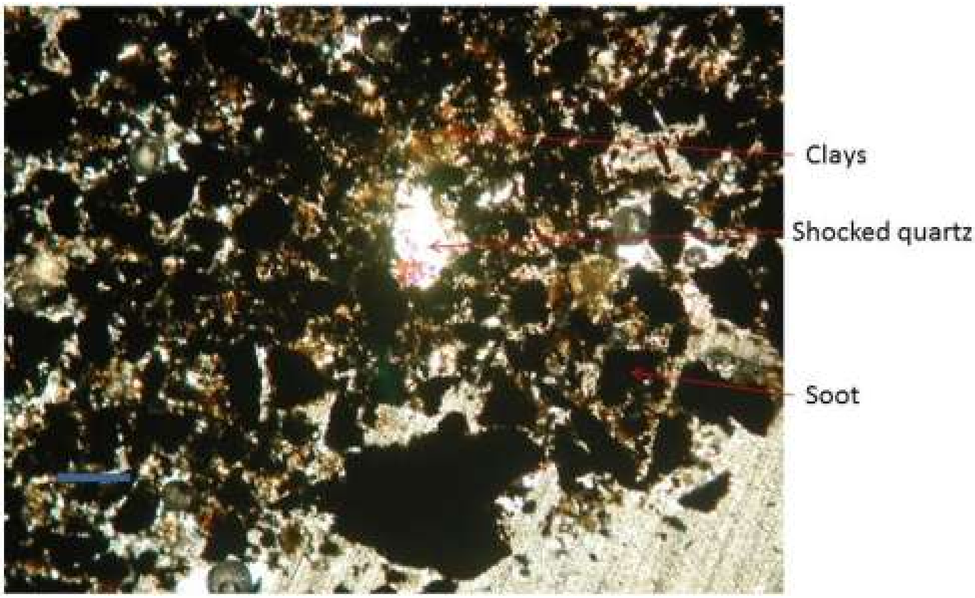

Figure 2.17 Thin section of Crow Creek farther west along the Missouri

Note shocked quartz, soot, and clays. Blue bar is 0.25mm

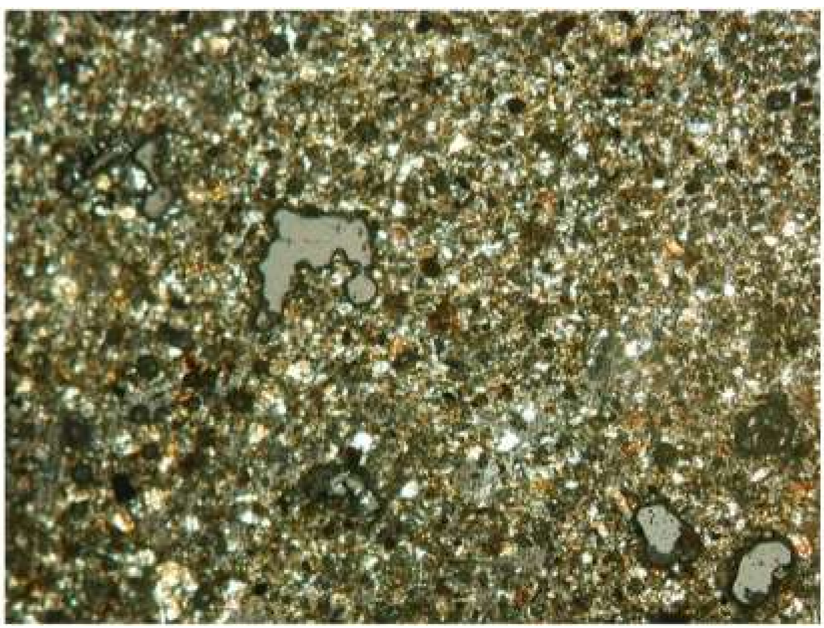

Figure 2.18 Thin section of Red Bird Member

From west of the Black Hills; no soot, clays, and just normal quartz

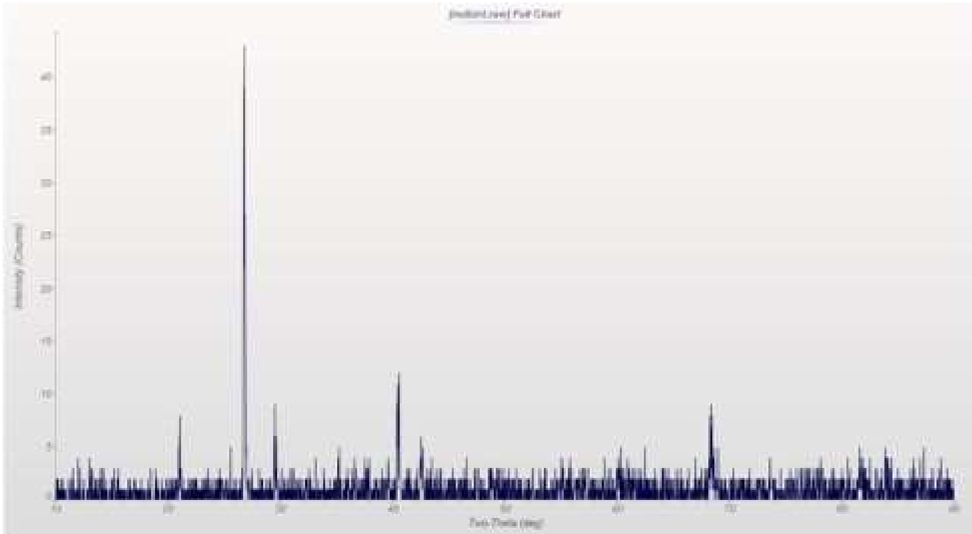

Figure 2.19 XRD of Red Bird indicating silicon and oxygen peaks only

Figure 2.20 Photo of *Exitelceros jennyi*

www.paleoportal.com

References

Anderson, R. and Hartung, J., (1992) The Manson Impact Structure; Its contribution to impact materials observed at the Cretaceous/Tertiary boundary. *Proceedings of Lunar and Planetary Science,* Vol. 22, pp.101-110

Anderson, R. and Hartung, J. (1996) A brief history on investigations of the Manson Impact Structure. *Geological Society of America, Special Paper* Vol. 302, pp. 31-44

Anderson, R. and Witzke, B., (1994) The terminal Cretaceous Manson Impact Structure in north central Iowa: A window into the Late Cretaceous history of the eastern margin of the Western Cretaceous Seaway. *Geological Society of America Special Paper,* Vol. 287, pp. 197-211

Anderson, R., Hartung, J.B., Witzke, B.J., Shoemaker, E.M., and Roddy, D.J., (1994) Preliminary results of the U.S. Geological Survey-Iowa Department of Natural Resources Geological Survey Bureau Manson Core Drilling Project *Large Meteorite Impacts and Planetary Evolution: Geological Society of America Special Paper* 29

Anderson, R. and Witzke, B., (1996) The drilling of the 1991-1992 Geological Survey Bureau and U.S. Geological Survey Manson Impact Structure cores. *Geological Society of America Special Paper,* Vol. 302, pp.45-88

Blum, J., Chamberlain, C., Hingston, M., Koerbel, C., (1996) Neodymium, strontium, and oxygen isotope investigation of the target stratigraphy and impact melt rock from the Manson Impact Structure. *Geological Society of America, Special Paper* , Vol. 302, pp. 317-324

Bretz, R., (1979) Stratigraphy, Mineralogy, Paleontology and Paleoecology to the Crow Creek Member, Pierre Shale (late Cretaceous), south central South Dakota. *Master's Thesis. Fort Hayes State University, Kansas*

Crandell, D., (1952) Origin of the Crow Creek Member of the Pierre Shale of central South Dakota. *American Association of Petroleum Geologists Bulletin,* Volume 36, pp. 1754-1765

Dypvik, H., & Jansa, L. (2003) Sedimentary signatures and processes during marine bolide impacts: A review. *Sedimentary Geology* Vol. 161, pp. 309-337

Erickson, M., and Slingerland, R. (1990) Numerical simulation of tidal and wind driven circulation in the Cretaceous Seaway of North America. *Geological Society of America Bulletin* Vol. 102, no. 11, pp. 1499-1516

Gill, J. and Cobban, W., (1966) Red Bird Section of the Upper Cretaceous Pierre Shale *U.S. Geological Survey Professional Paper,* 393-A, pp. 73-85

Hanczaryk, P.A., and Gallagher, W.B., (2007) Stratigraphy and Paleoecology of the Middle Pierre Shale along the Missouri River, central South Dakota. *The Geological Society of America Special Paper,* Vol. 427, pp. 51-69

Hasegawa, H., Tada, R., Jiang, X., Suganuma, Y., Imsamut, S., Charosiri, P., Ichinorou, N., Khand, Y. (2012) Drastic shrinking of Hadley circulation during mid-Cretaceous supergreenhouse. *Climate of the Past* Vol. 8 pp1323-1337

Horton, J., Cohn, G., Powars, D., and Edwards, L., (2008) Impactites in the Chesapeake Bay Impact Structure Virginia U.S.A.. *Sedimentary Record of Meteorite Impacts: Geological Society of America Special Paper* 437, pg.92

http://www.igsb.uiowa.edu/browse/manson99/Mansnloc.gif&imgrefurl

Izett, G.A., Cobban, W.A., Obradovich, J.D., and Dalrymple, G.B., (1998) Age of Manson Impact Structure, Iowa. *The Geological Society of America Bulletin.* Volume 110, No.3, pp. 361-375

Izett, G.A., Cobban, W.A., Obradovich, J.D., Kunk, M.J., (1993) The Manson Impact Structure Ar/Ar Age and Its Distal Impact Ejecta in the Pierre Shale in Southeastern South Dakota. *Science,* Vol. 262, pp. 730-731

Jarrett, M. (1994) www3.northern.edu/natsource/EARTH/Geolog1.htm

Jiang, X., Pan, Z., Fu, Q. (2001) Primary study on patterns of general circulation of atmosphere before uplift of Tibetean Plateau in eastern Asia. *Science in China* (Series D) Vol. 44, Issue 8, pp 600-688

Joliff, B., Rockow, K., Korotev, R., Haskin, L., McCarville, P., Crossey, L., (1994) Geochemical study of cores from the Manson impact structure. *Proceedings of the VIIth International Symposium on the Observation of the Continental Crust through Drilling. April 25-30, 1994, Santa Fe, NM.,* pp. 215-218

Jones, M., McCormick, G., Anderson, R., (1996) Preliminary clay-mineral investigation of some impactites recovered by core drilling in the Manson impact structure. *Geological Society of America Special Paper,* Vol. 302, pp.341-346

Kastens,K., and Cita, M.,(1981) Tsunami-induced sediment transport in the abyssal Mediterranean Sea *Geological Society of America Bulletin* 1 pp. 845-857

Katongo, C., Koeberl, K., Witzke, B.J., Hammond, R.H., (2004) Geochemistry and Shock Petrography of the Crow Creek Member. *Meteoritics and Planetary Science,* Vol. 39, pp. 31-51

Koeberl, K. and Anderson, R., (1996) The Manson Impact Structure, Iowa: Anatomy of an Impact Crater. *Geological Society of America Special Paper,* 302, pp. 145-219

Koeberl, C., and Hartung, J., (1992) Geochemistry of Manson Impact Structure rocks: Target rocks, impact glasses, and microbreccias. *Proceedings of Lunar and Planetary Science,* Vol. 22, pp.111-126

Koeberl, C. and Shirley, S., (1996) Re-Os isotope study of rocks from the Manson impact structure. *Geological Society of America Special Paper,* Vol. 302, pp.331-339

Korotev, R., R*ockow, K.,* Jolliff, B., Haskin, L., McCarville, P., Crossey, L., (1996) Geochemical comparison of four cores from the Manson impact structure. *Geological Society of America Special Paper,* Vol. 302, pp. 275-315

Kulp, T. and Pratt, L., (2004) Speciation and weathering of selenium in Upper Cretaceous chalk and shale from South Dakota and Wyoming, USA. *Geochimica et Cosmochimica Acta,* Vol. 68, No. 18, pp. 3687-3701

Larson, N., Jorgensen, S., Farrar, R., Larson, P., (1997) Ammonites and the other Cephalods of the Pierre Seaway, Geoscience Press, Tucson, AZ

Lindstrom, M. Ormo, J. Storker E., (2008) Water-blow and resurge breccias at the Lockne Marine Target Marine Impact Structure. *Geological Society of America Special Paper,* 437 pp.

Mendenhall, G., (1954) Distribution of Crow Creek Member of Pierre Shale in Northeastern Nebraska Geological Notes. *Bulletin of the American Association of Petroleum Geologists* Vol. 38, No. 2 , pp. 333-334

Nelson, S. (2012) Meteorites, Impacts and Mass Extinctions *Natural Disasters, Tulane University* *www.tulane.edu/snelson/natural_disasters/htm*

Ohno, S., Sugita, S., Kadono, T., Hasegawa, S., Igarashi, G. (2004) Sulfur chemistry in laser-simulated impact vapor clouds: implications for the K/T impact event. *Earth and Planetary Science Letters,* Vol. 218, issues 3-4, pp. 347-361

Prinn, R. & Fegley, B. (1987) Bolide impacts, acid rain, and biospheric traumas at the Cretaceous-Tertiary Boundary. *Earth and Planetary Letters* Vol. 83 pp.1-15

Redfern, R., (2000) Origins: The evolutions of continents, oceans and life. University of Oklahoma Press, Norman, Oklahoma, pp.191-192

Russell, D., (1993) Manson Crater Extinctions. *Science New Series* Volume 262 No. 5142, pp. 1956-1957

Schultz, P., and Anderson, R. (1996) Asymmetry of the Manson impact structure: Evidence for impact angle and direction. *Geological Society of America Special Papers* Vol. 302, pp. 397-417

Short, N., Gold, D. (1996) Petrography of shocked rocks from the central peak at the Manson Impact Structure. *Geological Society of America Special Paper* 302, pp. 245-265

Sigurdsson, H., D'Hondt, S., Cavey, S. (1992) The impact of the Cretaceous-Tertiary bolide on evaporate terrane and generation of major sulfuric acid aerosols. *Earth and Planetary Science Letters* Vol. 109, No. 3-4, pp.543-559

Stein, M., and Shoemaker, E., (1996) A Hypothesized Manson Impact Tsunami: Paleomagnetic and Stratigraphic Evidence in the Crow Creek Member, Pierre Shale. *Geological Society of America Special Paper* 302 pp. 419-431

Tsikalas, F., Gudlaugson, S., Faleide, J.I., Eldholm, O., (1999) Mjolnir Structure, Barents Sea: A Marine Impact Crater Laboratory. *Large Meteorite Impacts and Planetary Evolution II: Geological Society of America Special Paper* 339 pp.193-204

Varricchio, D., Raven, R., Wolbach, W., Elsik, W., Witzke, B., (2009) Soot and palynologic analysis of Manson impact-related strata (Upper Cretaceous) of Iowa and South Dakota, USA. *Cretaceous Research*, Vol. 30, pp. 127-134

Varracchio, D., Koeberl, C., Raven, R., Wolbach, W., Elsik, W., Miggins, D., (2010) Tracing the manson impact event across the Western Interior Cretaceous Seaway. *The Geological Society of America Special paper.* Vol. 465, pp. 269-299

Watkins, D.K., (1995) Biostratigraphical and Sedimentological Implications of Calcareous Nanno-fossil Assemblages From the Crow Creek Member of the Pierre Shale (Upper Cretaceous) *Geological Society of America Abstracts with Programs*, Volume 27, No. 3 pp. 93-94

Weber, R. (2006) Evidence for an impact-induced resuspension event in the Late Cretaceous Western Interior Seaway from the Crow Creek member (Pierre Shale) Thesis, University of Nebraska, Lincoln.

Weber, R. and Watkins, D. (2007) Evidence from the Crow Creek Member (Pierre Shale) for an impact induced resuspension event in the Late Cretaceous Western Interior Seaway. *Geology* Vol. 35, No. 12, pp.1119-1122

Witzke, B., Anderson, R. (1993) Terminal Cretaceous Manson impact structure of Iowa and its possible influence on Cretaceous/Tertiary events in the Western Interior Seaway of North America. *Marshall-Lambert Symbosium, from AAPG 1993,* pp.13-16

www.igsb.uiowa.edu (2013)

www.paleoportal.org (2013)

CHAPTER III

AN EXAMINATION OF CAMPANIAN DINOSAUR EGGS

Abstract

A clutch of four dinosaur eggs, from the Late Cretaceous (Campanian) and originating in the Judith River Formation of South-Central Montana were investigated with the goal of determining their species. They were found in an outcrop along an intermittent stream where the visible lithological layer was roughly 5 meters in a unit which generally has a thicknesses range from 50-65 meters thick in 2002. Later in 2013, two more eggs were found in an active stream on the same ranch, where they had apparently been recently eroded to. The eggs were cleaned of much of their matrix, which was examined for petrified wood, soil type, and volcanic ash. They were then measured, photographed and subjected to a series of C-T images which showed many of the embryonic features which suggest that the eggs are likely from a Hadrosauroid. Next, the egg shell, matrix, interior of the egg and volcanic ash were examined in thin section. This analyses produced diagnostic information based on the pore shape, size and pore density for the egg shells and revealed that the surrounding matrix is largely mudstone and clay. The ash was examined for potassium feldspar to initiate radiometric dating. Scanning Electron Microscopy (SEM) was used to examine the accompanying ash as well as the egg-shell surface and cross-section. The interior of the egg is largely

silicon dioxide.   The matrix consisted mainly of mudstone mixed with sand, clay, and some 1-5 mm clasts of petrified wood were found at the ventral portion of the nest.

The egg-shell was examined as an oolithic genus/species, and while there were similarities to some described eggs, for the most part these appeared to be undescribed. It did appear that the eggs underwent a transgressive event based on the higher levels of magnesium found in the upper levels of the egg-shell. The crest which appears in the CT scan would seem to indicate that these structures had a communicative function as opposed to a sexual display.

Introduction

Several dinosaur eggs of various species; Maiasaurs, Hadrosaurs, Troodons and others have been found in the Montana/Wyoming area (Figure 3.2). Identification of these species was made possible by the location of either nestlings among the eggs or embryos inside the fossilized eggs. In previous studies eggs have been identified by their "egg species nomenclature", mainly due to the shell structure, pore size, surface area, and pore density.

Since the first discovery in the 1920's in Mongolia (Andrews, 1935), dinosaur eggs have become much less rare and have now been found on almost every continent. Most eggs are described by the shape of the egg, pore shape and density rather than the species which is often difficult, if not impossible, to determine (Vila, et. al., 2010). The classification of eggs has evolved from merely their shape, to a combination of the shape and shells, especially pores and associated structures. There are many different types described today including *Continuoolithis*, which is assumed to be an theropod based on their shape. This particular type has a highly complex series of pores and obvious mammilaries (bulges extending up from the surface of the shell) (Jackson & Varracchio, 2010). Only when juvenile and adult fossils are found alongside the nests, as in the case of Jack Horner's Maisasaur find (Horner, 1984), or C-T scans and other imaging is performed on intact eggs which are then compared to previously confirmed samples can such identification be confirmed (Liang, et. al., 2009).

The shape of the dinosaur eggs is important and unique. Dinosaur eggs come in only a few shapes: spheroid, prolate-spheroids, oblate spheroids, and semi-conical. All of these shapes are diagnostic. The spheroids belonged to the saunropods, the prolate-spheroids to the therapods, the oblate-spheroids to hadrosaurs or orithischians, and the semi-conical to marginocephalians (Martin, 2006). The oblate-spheroid shape and size of the eggs suggest strongly that these are Hadrosaur eggs (Liang, et. al., 2009) (See Figure 3.1 & 3.3). The shape, size, placement within the nest, egg-shell morphology, and nesting sites are all diagnostic tools used in identifying the type of eggs and possibly the type (genus and species) of dinosaur which laid them.

The objective of this study is to determine the type of dinosaur, if not the actual species or genus which produced the eggs. A variety of non-destructive methods, including C-T scans, the size, shape of the eggs, and their positioning in the clutch as well as the location of the find were used to help identify the eggs. Furthermore thin sections of the matrix, ash, petrified wood and egg-shell were taken and examined by petrographic microscopy, Scanning Electron Microscopy, X-Ray Diffraction, and Elemental Dispersive Spectroscopy, all of which used minimally destructive methods of sampling. These tests were done in order to test the hypothesis that these eggs are Hadrosaurs, and perhaps even *Parasaurolopus,* a type of Hadrosaur with a long-tubed crest, whose eggs have never been found, the eggs were subjected to a series of C-T scans, to visualize the embryos contained within.

Methods

Two sets of eggs have been found in south-central Montana (Figure 3.3) which, while previously yielding dinosaur remains, had not produced any eggs until recently. The first set was found in a group of ten, with one just starting to weather out of a gully in 2002. The second set was found as a group of two and had already been weathered out and was currently in a flooded gully (rain was heavy that year) in 2013. Egg positions of both sets of eggs are referenced by Figure 3.1 and Figure 3.3 respectively. Both sets were found in a mud-stone/sandstone bed of the Judith River Formation in Montana (Figure 3.4). This formation has been described as having been formed by a meandering fluvial system(s) (Wasser, 1988).

The surrounding area in Montana, Wyoming, and South Dakota has been extensively mapped and the out-crops of this notable formation are well indicated on most geologic maps, even road-side geology maps.

The four oblate spheroid eggs were encased in a reddish-brown coarse mudstone, as was the two egg clutch found in 2013. The mudstone matrix was removed from the clutches with the exception of enough stone to hold the eggs together at what was thought to be the ventral side of the specimens. This was done with a combination of cold chisels, hammers, and finally a “jack-rabbit” foot pump dental drill. The size differentials and measurement of the egg are given in Table 3.3.

Portions of the ash were removed by using the dental drill as well. The individual grains were separated into quartz, orthoclase, plagioclase, and mica. This separation was accomplished using a spectrographic microscope and a pair of fine tweezers. Using denatured ethanol to wash the samples, they were then placed in a sonic applicator and ran for a minute. The solution was allowed to settle and then the ethanol was drawn off with a syringe and discarded. The vial containing the cleaned crystals was placed in an oven for drying and then imaged by SEM using secondary electron detector. Electron Dispersive Spectroscopy (EDS) was applied to identify chemical composition of the minerals found in the ash.

The shape, size, placement within the nest, egg-shell morphology, and nesting sites are all diagnostic tools used in identifying the type of eggs and possibly the type (genus and species) of dinosaur which laid them.

Two different Computed-Tomography (C-T) scanning instruments were used to produce the images of the interior of the eggs. The first scanning session was performed at the White Wilson Clinic in Fort Walton beach, Florida. The eggs were placed on the C-T table axially with the long axis length-wise down the table. This left two eggs side by side and too thick to be scanned. Therefore due to the thickness and density only the end two eggs were scanned, eggs number one and three (Figure 3.1 & Table 3.1). In the first session C-T Model Somatom Definition 64 Slice 2009 Brand Siemans scanner was used. In order to view the results Siemans Synga fastView Standalone software for viewing the DICOM images 2004-2005 was applied. . The settings on the instruments were as follows: DST Specials Poly Trauma Skull AF - 13.12.2.1107.5.1.4.64.343 Spino T.IT-91, Time=3 hr., 16 min., 54 s. The “Skull” category was used as a model due to its approximate size, shape, and similarity to an egg. Since this was a medical C-T imager, the setting for the human skull was the closest that could approximate the eggs;

the size, general shape are both similar and the skull is dense as are the eggs. Follow-up C-T scans were done at Mississippi State University through the donated services of I2AT with LightSpeed VCT 64 Slice CT imager instrument.

Thin sections of the egg shell, matrix, ash, and petrified wood were commercially prepared by Spectrum Petrographics. These thin sections were of special use in calculating pore density, percentage of different crystals. By counting the pore density and calculating the number of pores along with the surface area of the egg obtained by examining the thin sections, an egg-species and egg-shell morphotype can be found (Deeming, 2005). SEM images of the egg shells and the internal matrix of the eggs were collected at I2AT at Mississippi State University.. Two instruments were used, a Zeiss EVO-50 Variable pressure SEM run at 5.0 kV, and a Hitachi TM-1000 Table top, also run at 5.0 kV. The Zeiss instrument allowed for EDS measurements to be done, while the Hitachi allowed for an examination of the layering of the egg-shell. Samples were prepared showing raw cross-section, raw surface with special care to examine the pores. Cut and polished cross-sections of the egg shells were also examined. Elemental analysis was done by EDS with a precision of ~5% on all sites in order to determine the degree of diagenesis and the chemical composition of the egg shell and internal matrix when possible, in hopes of exploring the eggs' taphonic history.

Results

All eggs are aligned in the same direction, in parallel rows, (Figure 3.1 & 3.2) and are fully inflated. The axial length, or x-axis, is consistently longer than the y-axis on all the eggs (Table 3.1). The first four eggs are close to each other in both length and width with the following variations (see Table 3.1). The other two eggs (5 & 6) are slightly larger in all dimensions (Figure 3.2 & Table 3.1).

A total of 52 images were collected by the C-T scan procedure from Ft. Walton Beach. These images were collated to run as a video loop as the scan moves through the eggs. A C-T scan (number 46) is presented in Figure 3.5 showing bones (see arrows) on egg number one and egg number 3. The bones revealed by the C-T scan were clustered at the dorsal surfaces of the eggs (see Figure 3.6). These scans were viewed in a continuous loop as the CT "sliced" the egg into thin parts one after another. Thousands of individual scans were done by I2AT at Mississippi State. These revealed that one egg, (#4) is partially hollow yet contains some disarticulated bone, another egg, (#2) shows an articulated embryo with the skull, tail, pelvis and ribs all intact (Figure 3.7). Some of the scans showed no results, these were often the "slices" were of the matrix or of an unoccupied egg. The other two eggs showed partial bones, mainly due to poor resolution. This was the first time the instrument was used for this purpose and the settings may not have been ideal. Up to three thin layers were found in egg shells. The outermost layer measured 0.25mm, the middle layer containing the pore structure was 1.25 mm, and the inmost layer was 0.50 mm (Figure 3.8). The pore structure stretches from the surface down to, but not through, layer three. The shells show signs of porosity under both 4X optical microscope and more clearly at SEM images, preserving the small holes which allowed the embryo to breathe while within the egg. Egg #3 has some damage done to it from a slipped chisel (a long gouge out of one side), other-wise the eggs are in remarkably good condition.

The sedimentary matrix which surrounds all the eggs, is reddish-brown in color and heterogeneous in composition. There are many small angular rock fragments, along with small pieces of petrified wood (which was concentrated on the underside of the nest), mica, quartz, lithified mud, and streaks of rhyolitic ash. The ash is identified as rhyolitic based on its composition of quartz (10%), mica (25%), and mixed feldspars (25% potassium feldspar by EDS, and it appears to be microcline under a thin section observation, and 40% plagioclase) in the main and the noticeable absence of iron and manganese. This was further confirmed by thin section examination (Figures 3.9-3.10). The microcline stands out very distinctly by its characteristic extinction pattern, whereas the matrix shows a lot of heavily weathered clay, approximately 30 percent (Figure 3.11-3.12).

Small micro-dendritic structures were observed on some of the plagioclase from the ash. Under EDS, these were revealed as iron and tungsten deposits in a micro-dendritic pattern (Figures 3.13, 3.14 & Table 3.2). This is important because this is added evidence as to the origin of the eggs, tungsten being relatively common in that area of the country.

Thin Sections

Examinations of the various thin sections are informative. This analysis indicates that the ash was deposited after the chemical weathering of the matrix and subsequently covered up, perhaps by a flooding or even a transgressive event. Figure 3.8 shows some three tiered layering. Mammillary structures (small bumps on the surface of the egg shell) were not present on the study eggs in either thin sections or SEM. The pore diameter for the first set of eggs (collected in 2002 and measured with thin section) are

0.125mm, those of the second set of eggs (collected in 2013) range from 0.075 mm to 0.100 mm, with most of them in the 0.075 mm diameter. On the bottom of the nest reside clasts of what appear to be petrified wood, now largely turned into quartz, according to thin section examination.

SEM, EDS, and CT scans

SEM's were conducted on samples of the ash and the following are images from the ash and elemental dispersive spectrometry (EDS) of a representative potassium feldspar crystal (Figure 3.14, 3.15, and Table 3.5). Further SEM studies were conducted on the egg shells, both unpolished and in polished thin sections. These presented an even clearer analysis of the pore structure, surface features, and diagenetic changes which have occurred through-out the egg-shell (Figures 3.16-3.19). These changes included the in-filling of the pores, the substitution of magnesium for calcium at the surface features of the egg, and the relative uniformity of the pore size and shape despite their age (Campanian Stage).

The elemental EDS from SEM analysis shows some magnesium replacement of calcium in the upper portion of the raw egg cross-section but almost no magnesium replacement of the calcium towards the interior of the shell (Figures 3.20-3.23 & Tables 3.6 & 3.7). No potassium was present in the egg-shell. The SEM analyses allow for a close examination of the surface of the eggs, especially their pore structure and depth (Figures 3.22 & 3.24) (blue stars are sampling sites to differentiate Mg concentrations).

The first C-T scans at the White-Wilson Clinic, located in Ft. Walton Beach Fl., showed what appear to be skulls, pelvis, vertebrata, and long bones. The bones and egg-shell show up as a lighter color due to their higher density than the silica matrix within the egg. The lower resolution and limited number of scans reduced the effectiveness of these images, but the images provided needed evidence that embryos existed inside the eggs. This information was imperative in order to get more, higher resolution imaging done at Mississippi State University follow-up CT scans were done at Mississippi State University through the donated services of I2AT. These images were of superior quality and in much greater quantity than the ones done at Ft. Walton Beach, Florida. In addition to detecting the unusual density of the egg-shell and embryo bones, providing clues to the degree of diagenesis which has taken place, features of the embryos such as their skulls, vertebrae, pelvis and long bones were now more distinct.

With the higher resolution scan of the I2AT instrument at Mississippi State University, more of the embryos were revealed, including what appears to be one intact and mostly articulated embryo in situ (Figure 3.7). Furthermore the image shows what appears to be a crest on the skull of the embryo. This may (if further scans confirm this) narrow the search down to only several species and help resolve the questions as to the function of these crests. In the future I hope to further resolve these images by use of a synchrotron CT, which has much high resolution.

Discussion

The eggs are aligned in a characteristic manner. This alignment is consistent with those eggs previously found in sites known to be from Hadrosaur groups such as *Hadrosaurs*, *Maiasaurs,* and *Edmontosaurs* (Carpenter, 1999; Dingus and Norell, 2008*).* These eggs are laid end to end in parallel rows. Other dinosaurs laid their eggs in many other variations: rows, circles (raptors), layers, or sometimes in no apparent order or arrangement. Each of these signature nesting techniques helps describe the family, if not the genus and species of dinosaur (Liang, et. al., 2009, Carpenter, 1999).

The sediment is interpreted as having been deposited in a fluvial facies following a flooding event based upon the thick mud deposit, the clasts of rock within the mud, poorly sorted sediment, and bits of petrified wood. Previous locations of similar and dissimilar nests have been found on ancient flood-plains (Dingus and Norell, 2008; Carpenter, 1999;). The matrix itself is a wealth of information. The majority of the matrix is a poorly sorted reddish-brown clay-like mudstone. Within it occur quartz clasts, streaks of rhyolitic ash, and bits of petrified wood. These materials are consistent with the environment in which the Hadrosaur lived and nested. Vulcanism was prolific during the late Cretaceous, and was probably the source of the ash, which is high in potassium feldspar (microcline) (based upon the crystal's distinctive extinction pattern) (Figures 3.9 & 3.10). The ash is present at the bottom of the nest, on the egg-shell itself and in-between the eggs, indicating that volcanic eruption(s) were on-going through-out the nesting process. The Hadrosaurs were known to nest on floodplains near rivers (Carpenter, 1999; Carpenter, et al., 1994) and to cover their nests with foliage. The petrified wood present is consistent with the known and documented nesting habits of Hadrosaurs and other similar dinosaurs (Carpenter, 1999). The petrified wood is concentrated, indeed present only in the bottom of the nest beneath the eggs, indicating the use of foliage as a nest lining material. This has been found in other Hadrosauroid species (Carpenter, et al., 1994) The presence of magnesium in the upper portion of the egg shell, but lacking in the lower layers seems to suggest that a transgressive event took place after their deposition in which they were soaked for a while in sea-water (which is high in magnesium) Deckker, P., et al., 1988; Bennett, C., et al., 2011). This corresponds well with their date and location, which was on the paleo-shoreline during the Campanian stage, but would have been submerged during the later Maastrichian stage of the Cretaceous. This also corresponds with known hadrosaurs nesting habits along river-banks and shore-lines. This age can probably be confirmed with Potassium/Argon or Argon/Argon radiometric testing.

SEM scans and petrographic microscopy of the egg shell show three distinct layers, extensive pore structure with branching, and a distinct lack of mammillaries. The thin sections of the egg shell shows pore structures and layering not previously found in any of the existing literature (Figure 3.15 & 3.16). This is closest to the oolithius species *Continoolithus candadensis*. *Continoolithus candadensis* appears to have only two layers, while three distinct layers are present in both sets of the study eggs (Figure 3.8). While some of the interior pores are vaguely similar to *Continoolithus candadensis,* these eggs lack the mammillary (bump like structures on the surface of the egg, like mammillary glands) structures and the egg shells themselves do not exhibit the two definite layers which *C. candadensis* shows (Jackson & Varricchio, 2010) (Figure 3.8). That described species (Jackson and Varracchio, 2010) has only two described layers and extensive mammillary structures. As a result of these differences, and the fact that they are larger than normal dinosaur eggs (except for sauropods, which have an entirely different shape), the eggs appear to not truly belong to any described oolithic species. Further studies and a resolution/new C-T scans are vital for identification of this species which does not seem to fit neatly into any of the oolithic species based on the number of layers, pore structures and lack of mammillaries. Many known species of dinosaurs have been described that do not have eggs or nests associated with them. Part of the reason for the lack of eggs and nests is the nature of nesting, in which the nest and eggs are often destroyed by the hatchlings soon after hatching, through trampling. Another aspect is the difficulty in which it is to preserve and then fossilize objects as fragile as eggs. So, it is quite possible that these embryos are known as adults but have never been described as eggs and young.

Other branches of this research are the study of elemental replacement in the bones of the embryos, which according to the C-T scans done by I2AT are much denser than any of the surrounding material by several magnitudes. Diamond Light Source, located in Wales is considering a joint proposal to examine the eggs and embryo(s) with a synchrotron which will provide a high resolution 3-D image of the features in question. The synchrotron has been used in the past to examine Jurassic age egg shells and remains (Martins, et al., 2010).

Conclusion

1. Size, shape, and position of the eggs found in the nest suggest that the eggs were laid by members of the Hadrosaur family.
2. The texture and shape of the egg shell pores are similar to the oolithius species *Continoolithus candadensis.* however, there are several major and minor differences in the structural components; mammillaries, layers, pores and the size of the eggs. Based on all these factors it is quite likely that these eggs are from an un-described genus and species, but probably related to the Hadrosauroids.
3. The mudstone had a large amount of clay, probably from the chemical weathering of potassium feldspars originally derived from the volcanic ash

in the region. The volcanic ash yielded enough potassium feldspar to radiometric date the eruption and by extension the eggs. In addition the unusual signature of the ash (tungsten traces) may allow for the individual volcano responsible to be identified.

4. The presence of magnesium in the upper portion of the egg shell, but lacking in the lower layers seems to suggest that a transgressive event took place after their deposition in which they were soaked in sea-water.. This corresponds well with the egg's date and location, which was on the paleo-shore-line during the Campanian stage, but they would have been submerged during the Maastrichian stage of the Cretaceous. This also corresponds with known hadrosaurs nesting habits along river-banks and shore-lines. This can probably be confirmed with argon/argon radiometric testing. Further studies and a resolution/new C-T scans are vital for identification of this species which does not seem to fit neatly into any of the oolithius species. Other branches of this research are the study of elemental replacement in the bones of the embryos, which according to the C-T scans done by I2AT are much denser than any of the surrounding material by several magnitudes.
5. Nesting habitat and the surrounding sediments of poorly sorted sandstone and mudstone suggest that the nesting site experienced at least one flooding event. While we were unable to ascertain the type of foliage lining the nest, we do know that many dinosaurs lined their nests with foliage. Due to the ash, below, and with-in the nest we conclude that there

was at least one active volcano in the vicinity and that the nest was down-wind of the ash-fallout.

6. The newest C-T scans from Mississippi State and I2AT show an intact embryo, still articulated which promises much hope for identification of the genus and species (Figure 3.29). The perceived crest may narrow the candidates for identification to a species of *Parasaurolopus* or perhaps *Saurolopus.* The presence of this structure in the embryo may answer a debate as the the function of the crestal structure.

Figure 3.1 First clutch of eggs from 2002

Ruler is 31.75 cm

Figure 3.2 Map of Montana and approximate location of egg finds

Figure 3.3 Clutch of two eggs from 2013

Ruler is 31.75 cm

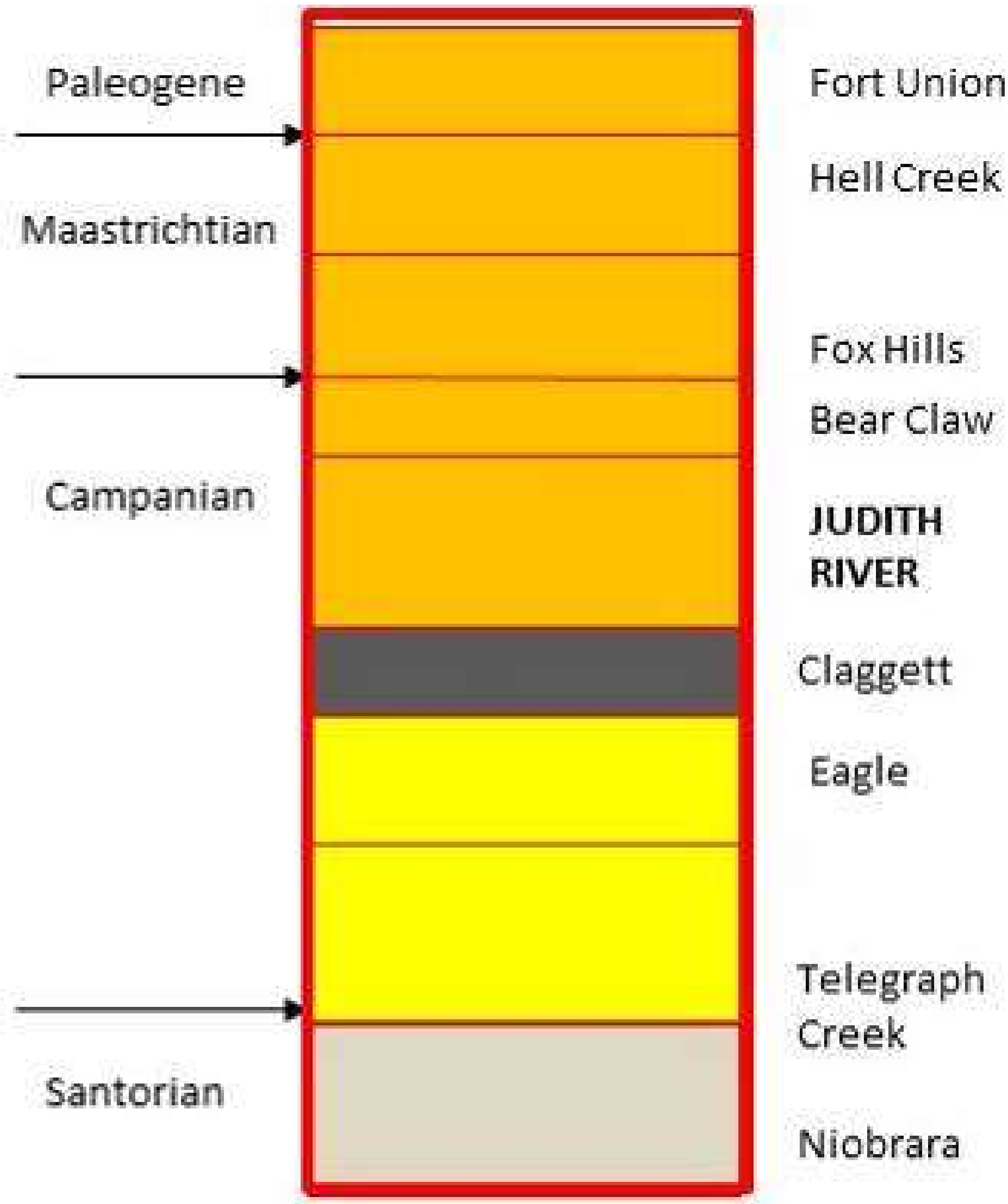

Figure 3.4 Stratigraphic column of South-Central Montana

Table 3.1 Variation in egg dimensions

	EGG 1	EGG 2	EGG 3	EGG 4	EGG 5	EGG 6
LENGTH IN CM	14.0	14.6	14.0	14.0	15.2	15.2
WIDTH IN CM	10.2	9.7	9.5	9.7	10.8	10.8

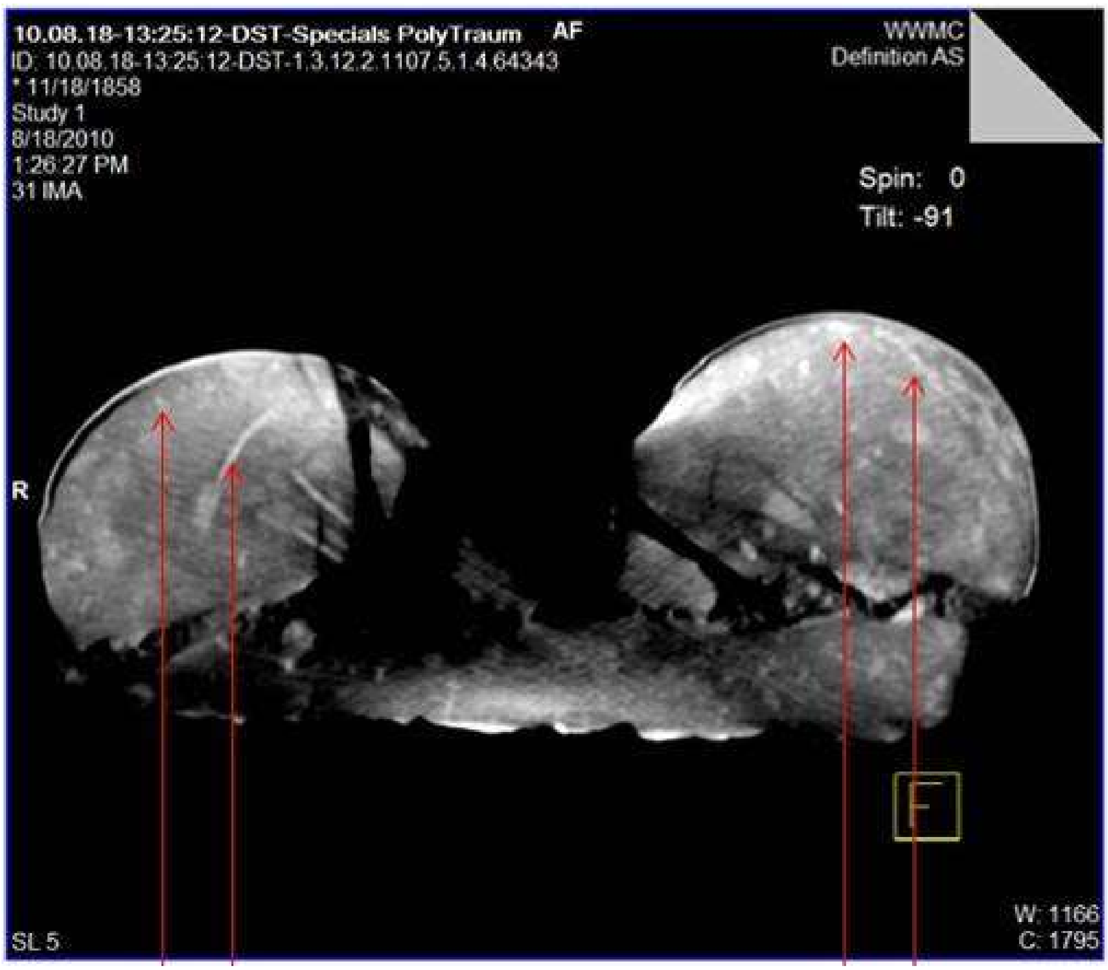

Figure 3.5 First CT scan performed at Wilson Clinic, Ft Walton Beach, FL.

Arrows indicate bones. The bones and shell are lighter in color due to their higher density. Bones indicated are probably vertebrata and long bones.

Figure 3.6 CT scan from Florida showing bones at the dorsal portion of eggs. Bones indicated are probably pelvis and ribs.

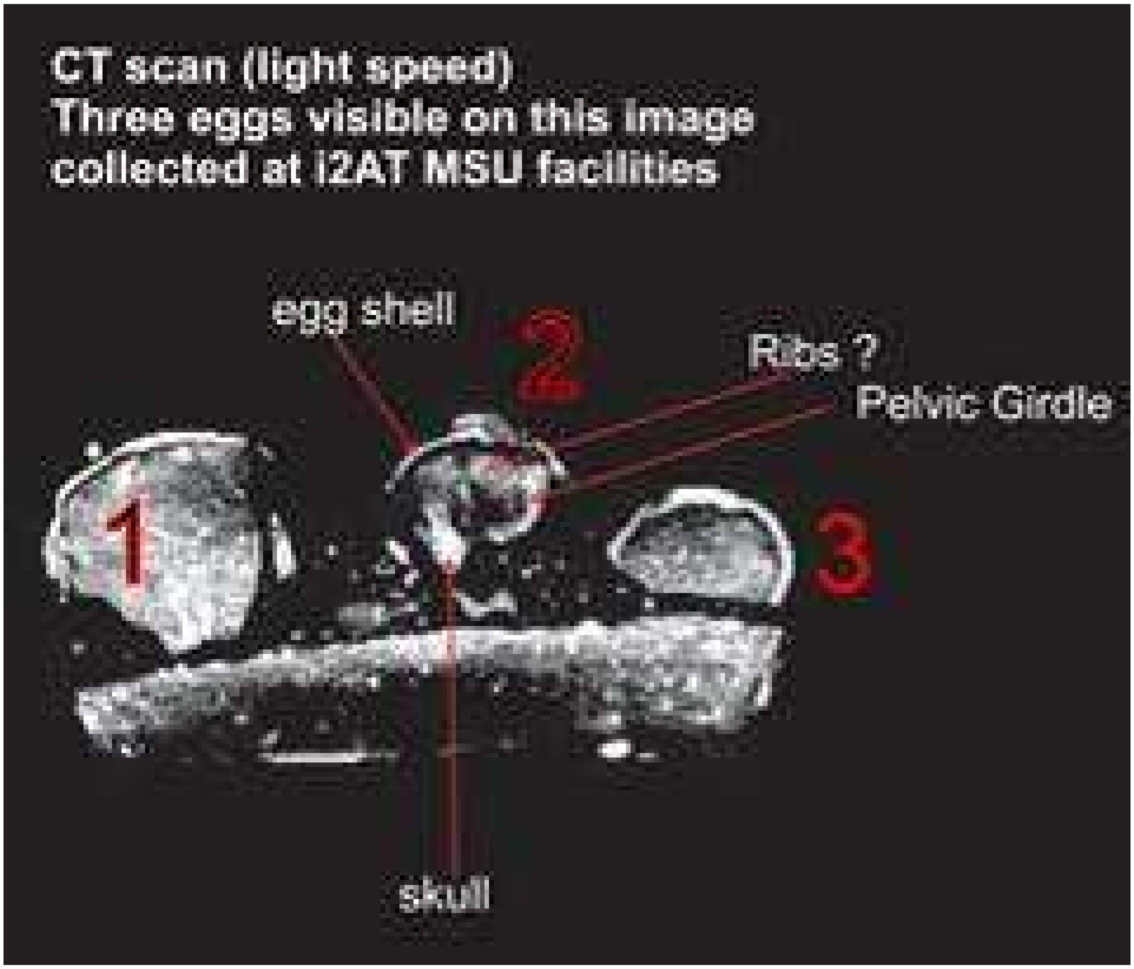

Figure 3.7 i2AT CT image of egg #2 showing embryo

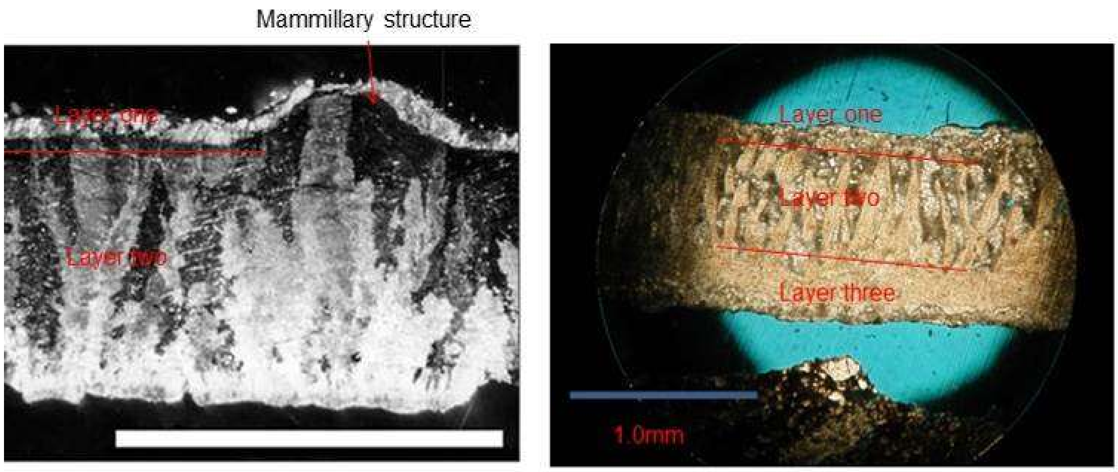

Figure 3.8 *Continoolithus canadadensis* (left) compared with egg shell from the study series (right)

Continoolithus canadadensis from Jackson & Varracchio, 2010

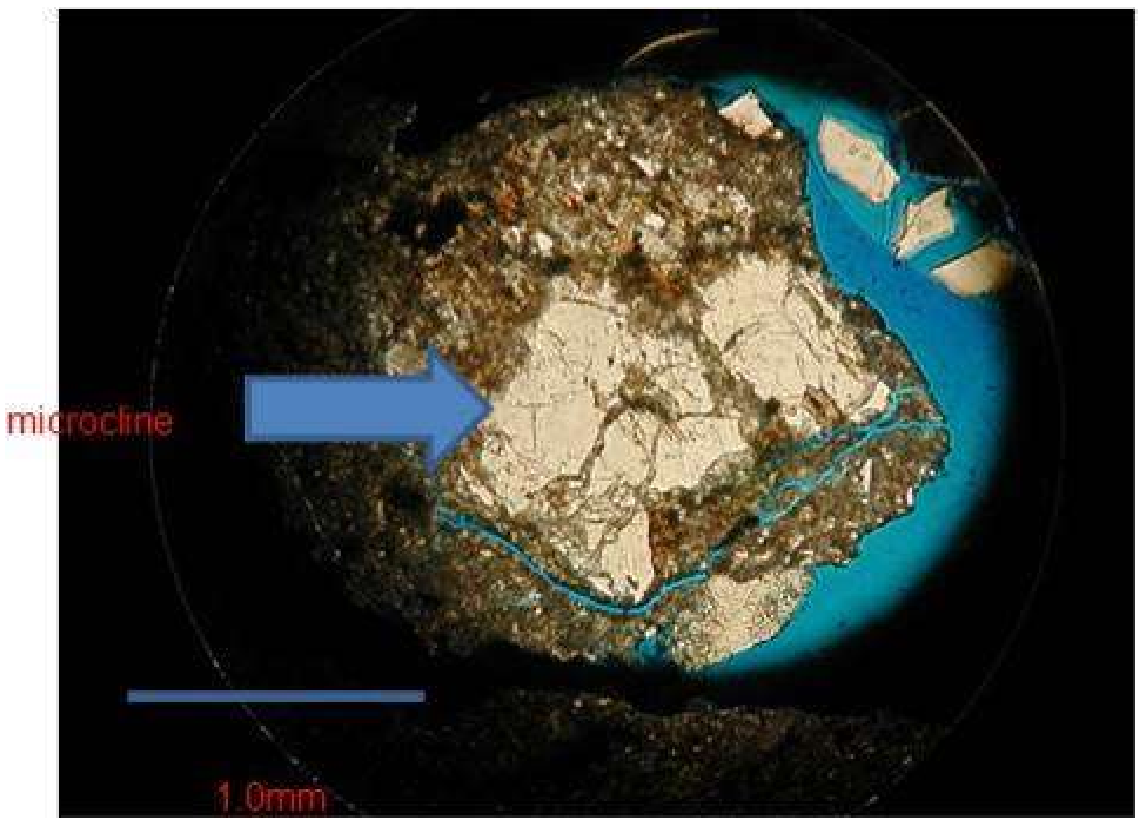

Figure 3.9 Thin section of ash, un-polarized light

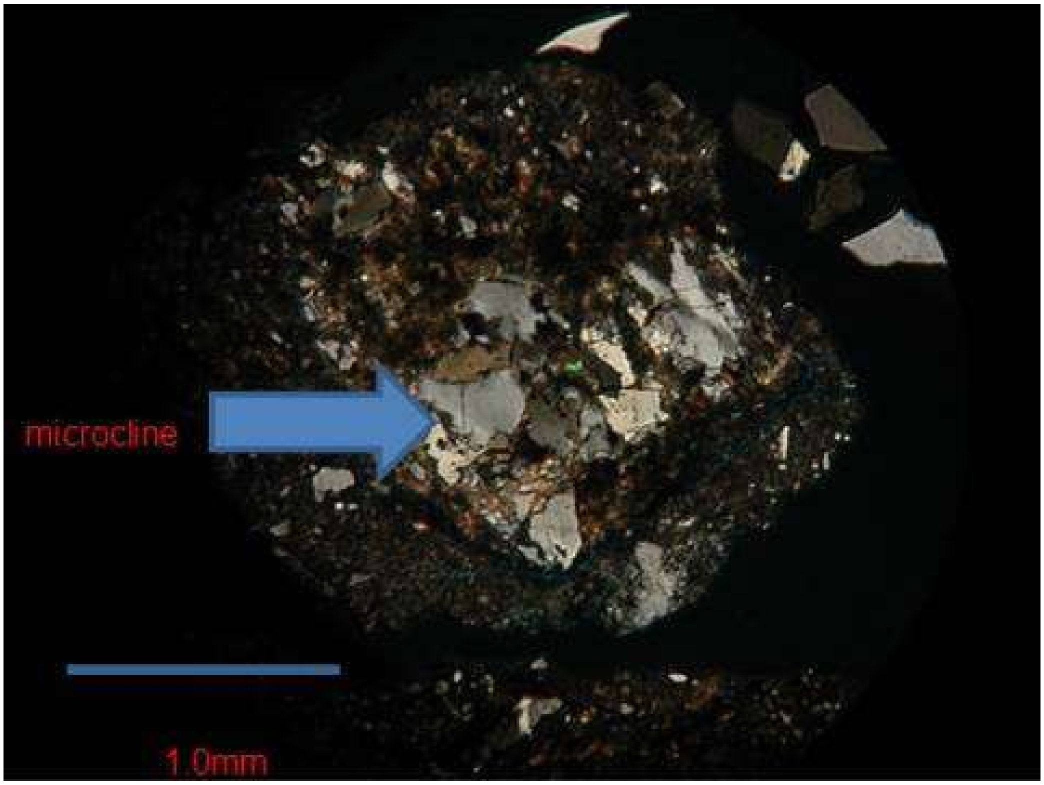

Figure 3.10 Thin section of ash in cross-polarized light

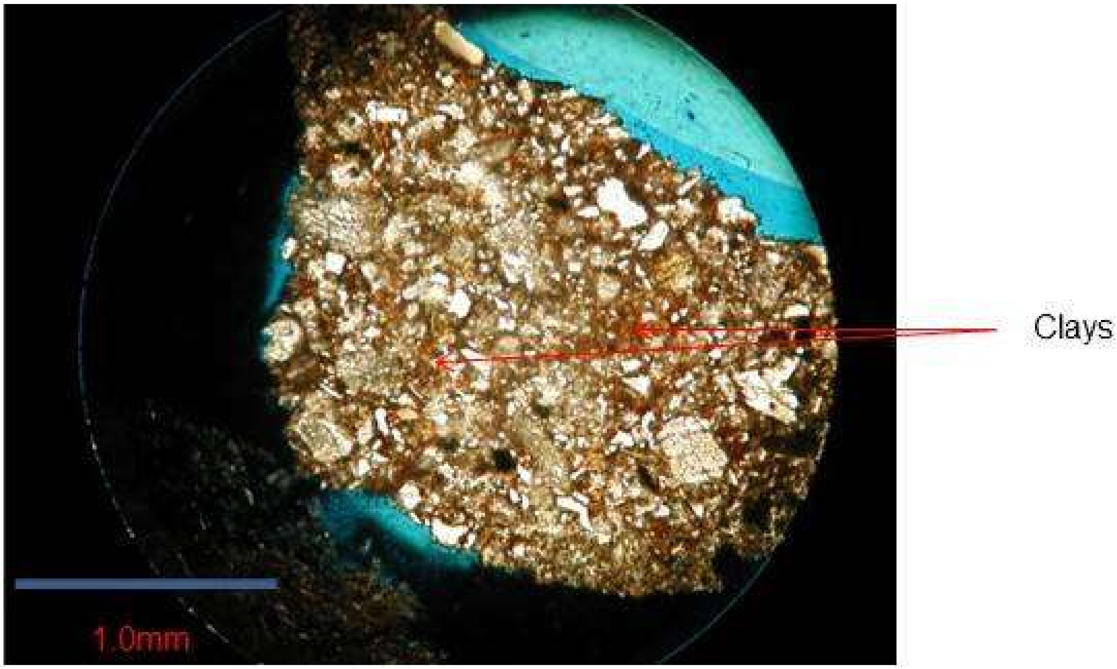

Figure 3.11 Sedimentary matrix in plane polarized light

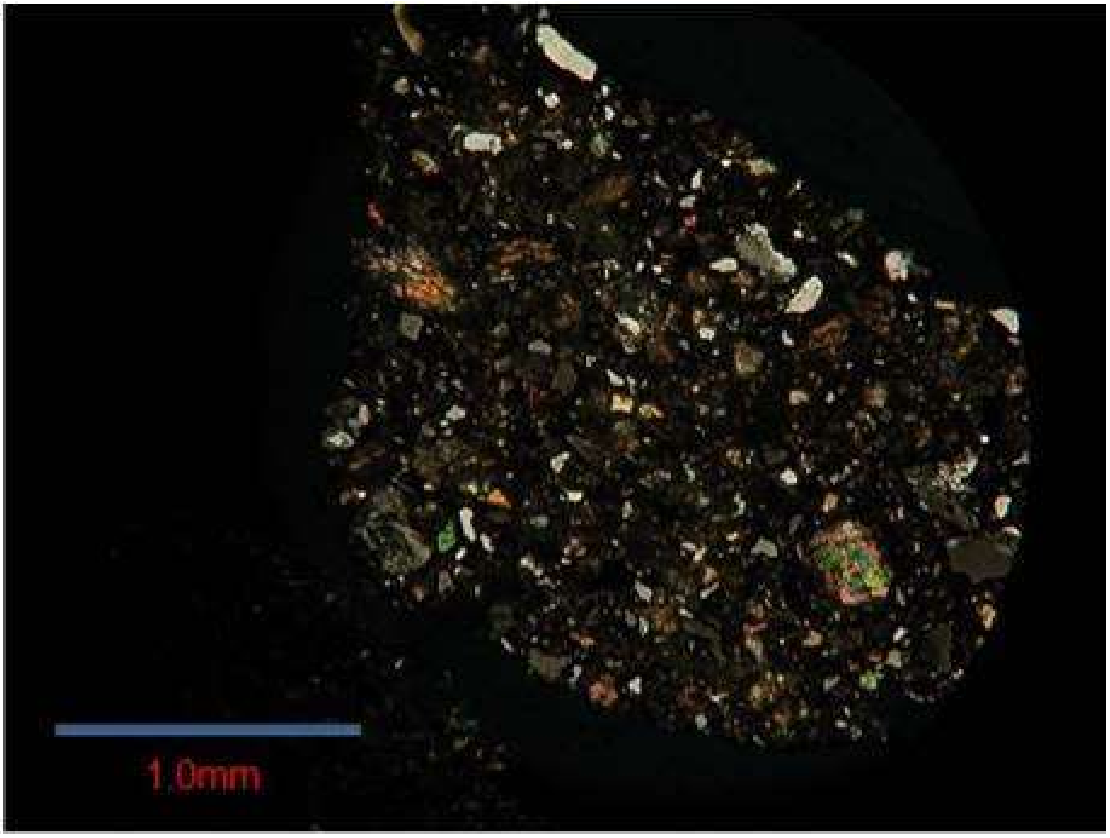

Figure 3.12 Sedimentary matrix under cross-polarized light

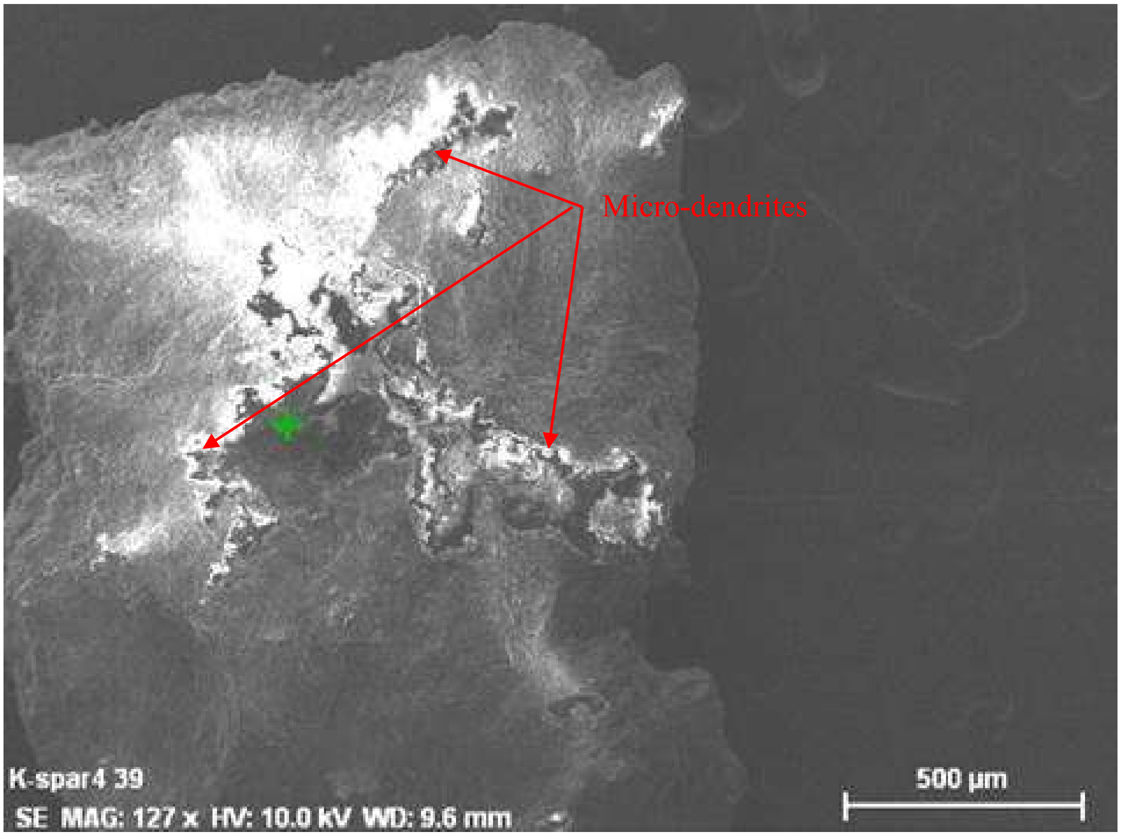

Figure 3.13 SEM showing Tungsten containing micro-dendrites

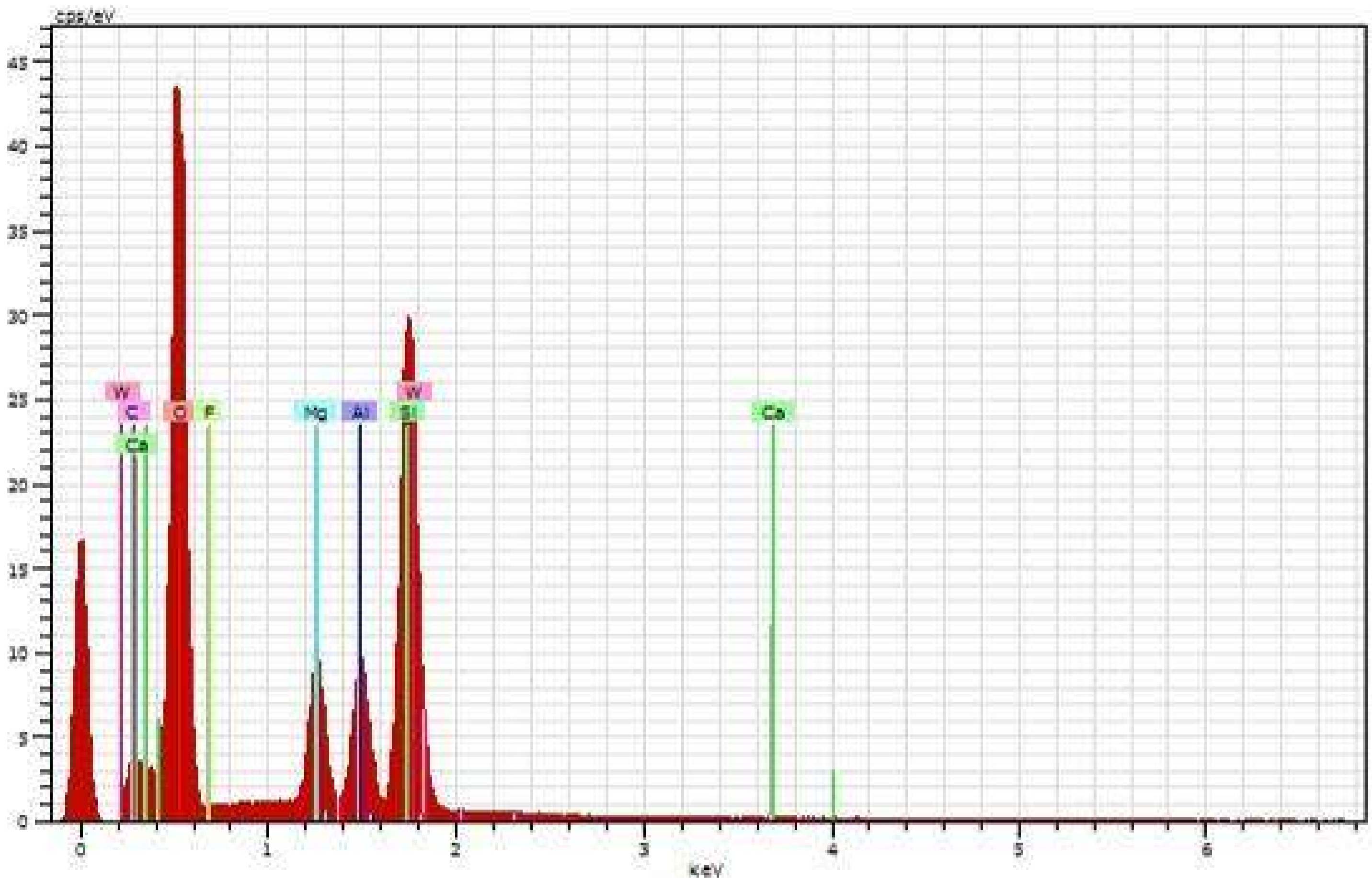

Figure 3.14 EDS of micro-dendrite

Table 3.2 Spectrum of micro-dendrites

ELEMENT	C. Norm (wt%)	C Atomic %	C. ERROR (1 SIGMA) (wt %)
Oxygen	51.38	65.81	7.91
Silicon	22.11	16.13	1.33
Aluminum	5.67	4.30	0.39
Magnesium	5.41	4.56	0.42
Carbon	3.93	6.71	0.78
Calcium	0.09	0.04	0.03
Tungstun	10.20	1.14	0.64
Fluorine	1.20	1.29	0.27

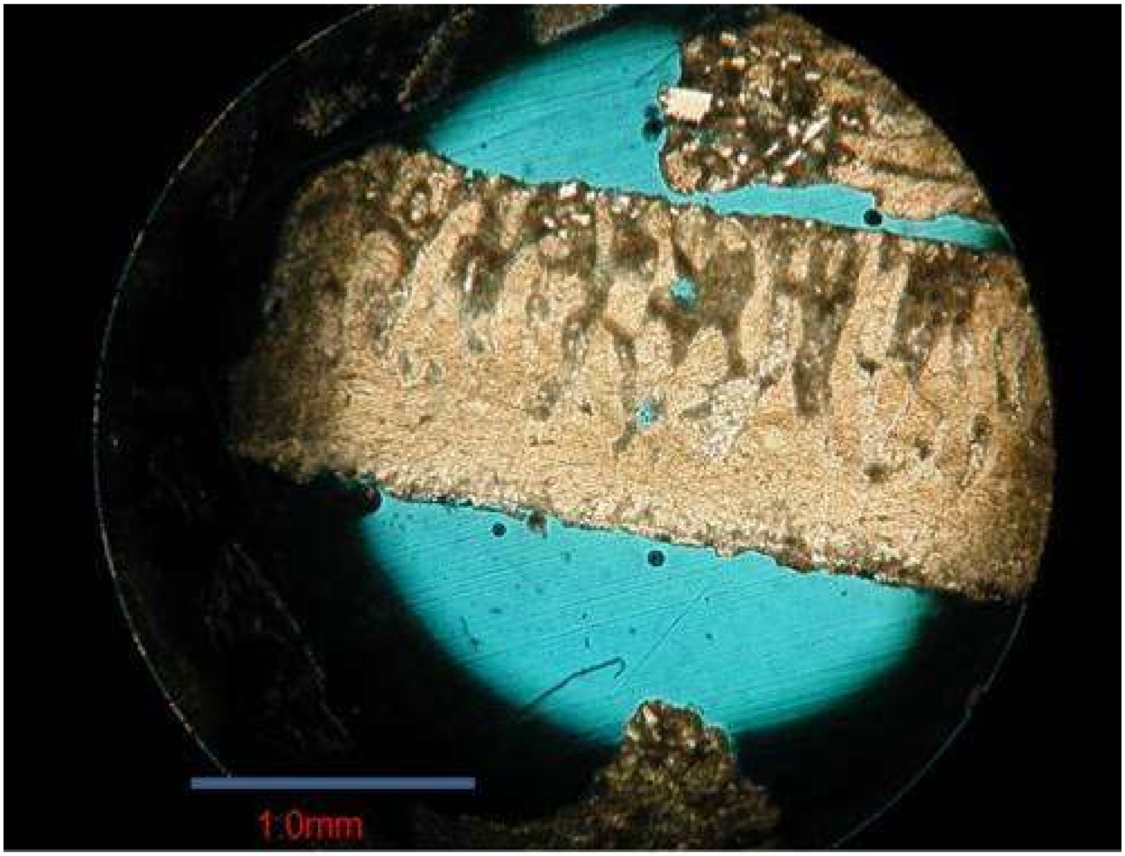

Figure 3.15 Thin section of egg-shell showing pore structure

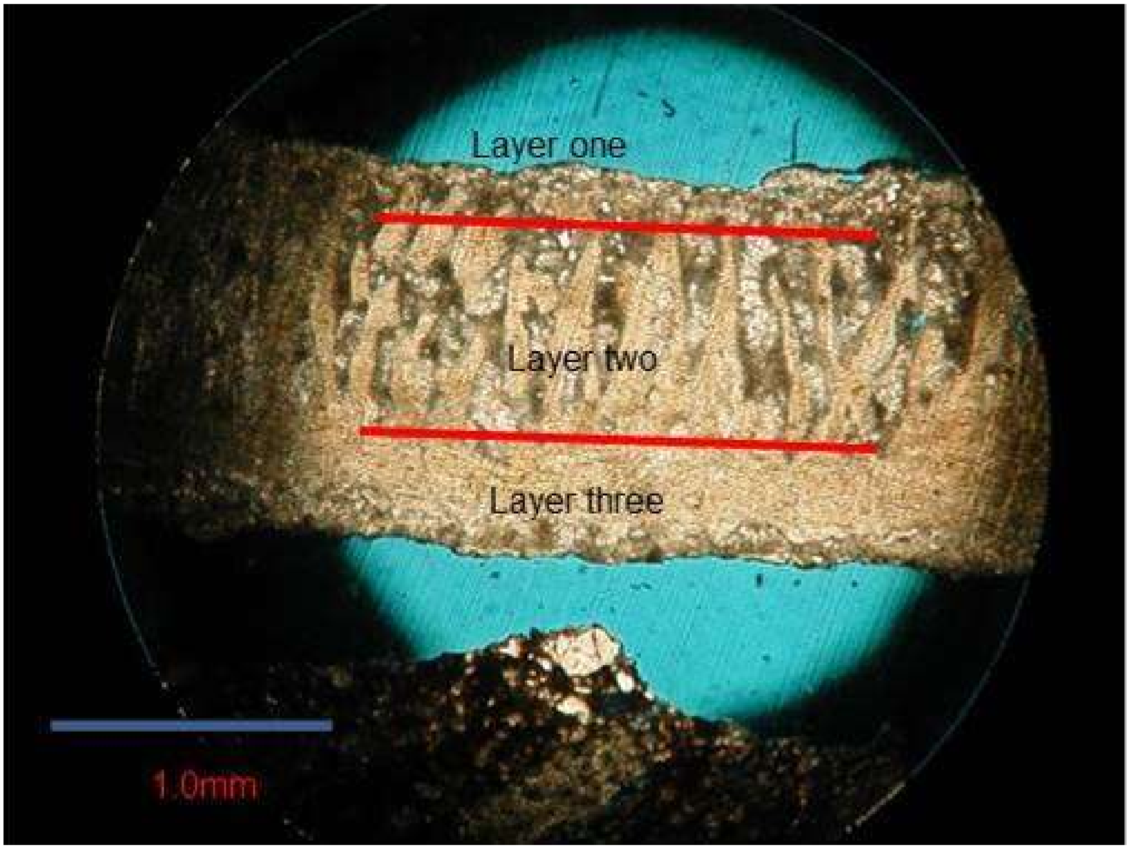

Figure 3.16 Thin section revealing three layers of egg-shell

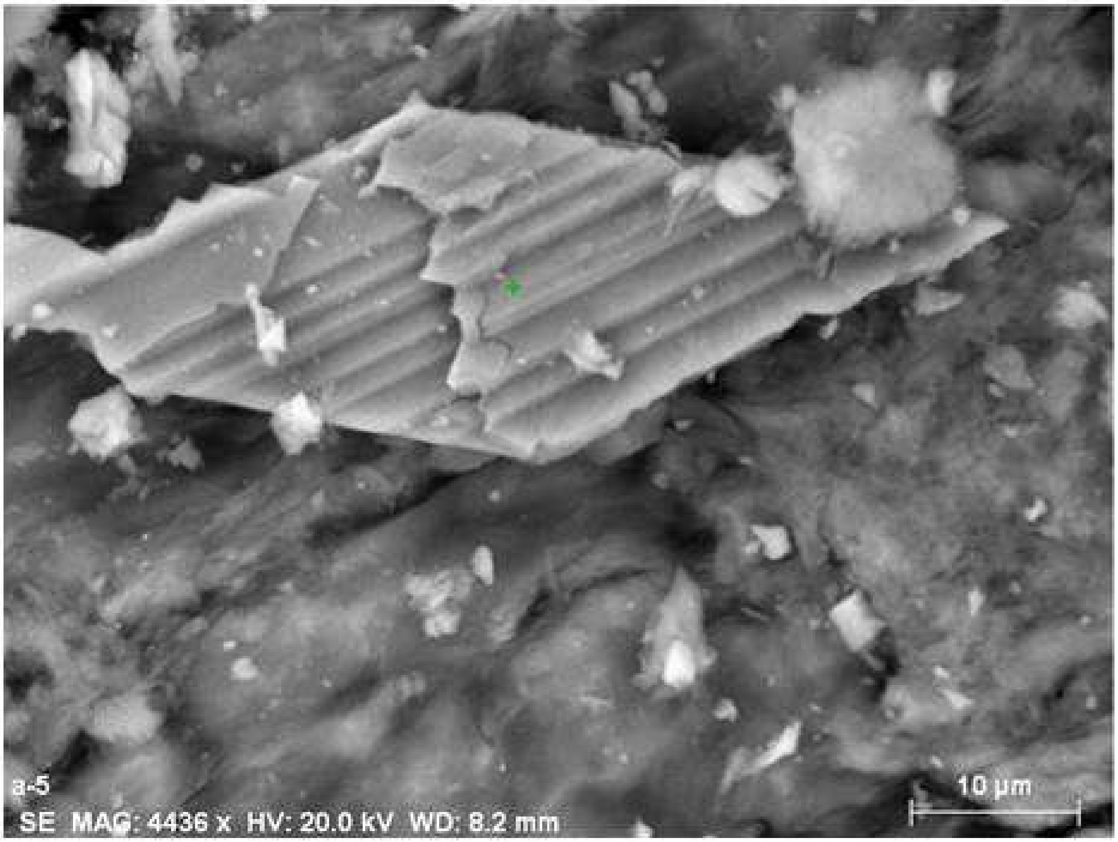

Figure 3.17 SEM of a potassium feldspar crystal in the ash

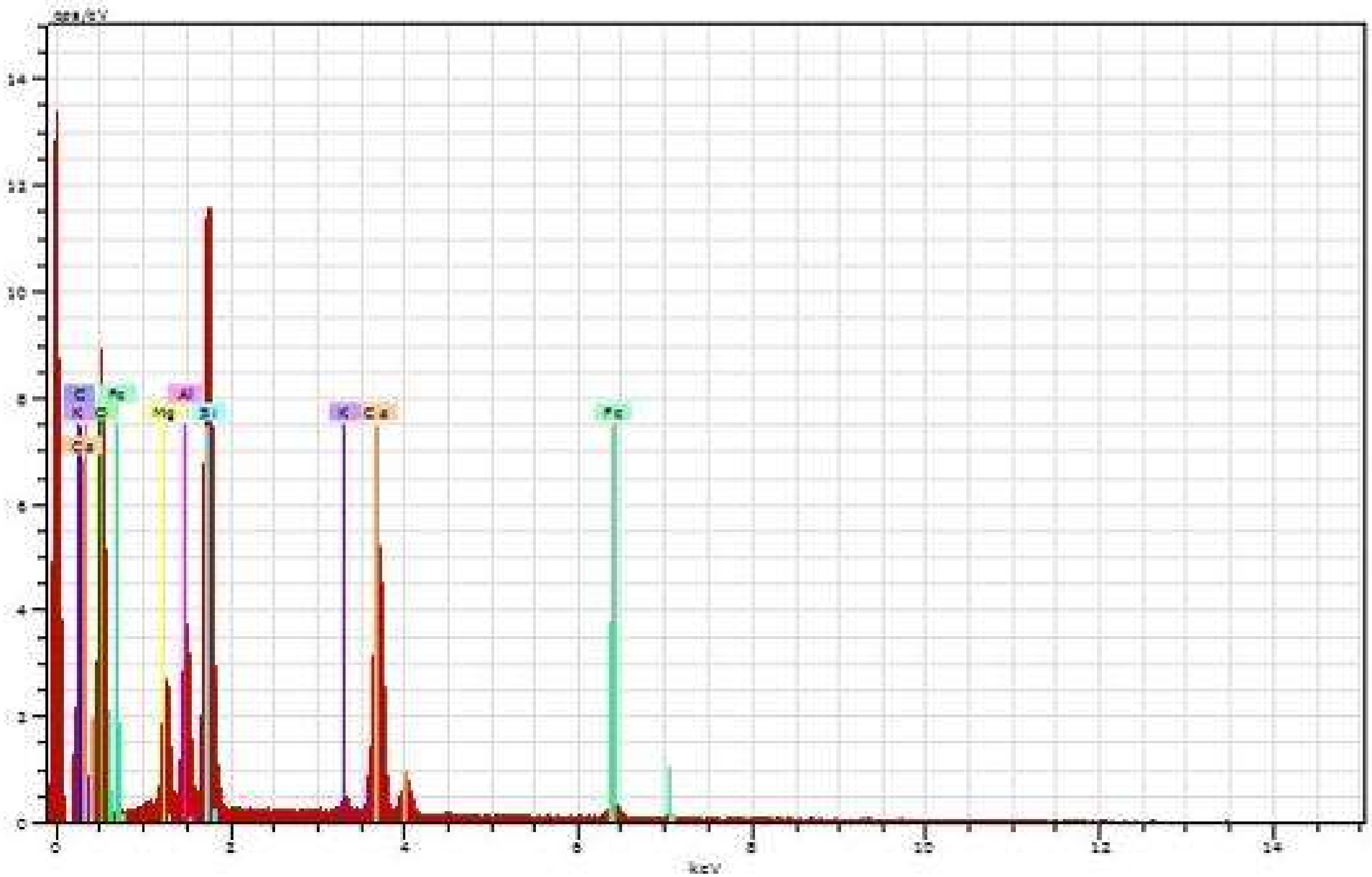

Figure 3.18 EDS analysis of feldspar crystal

Table 3.3 EDS spectral analysis of crystal

ELEMENT		WT %	Atomic %	Error Sigm
Oxygen		55.75	66.89	5.26
Carbon		6.27	10.02	0.86
Silicon		13.6	9.3	0.51
Aluminum		4.79	3.41	0.22
Magnesium		4.02	3.18	0.21
Calcium		13.38	6.41	0.35
Iron		1.9	0.65	0.07
Potassium		0.28	0.14	0.03
TOTAL		100	100	

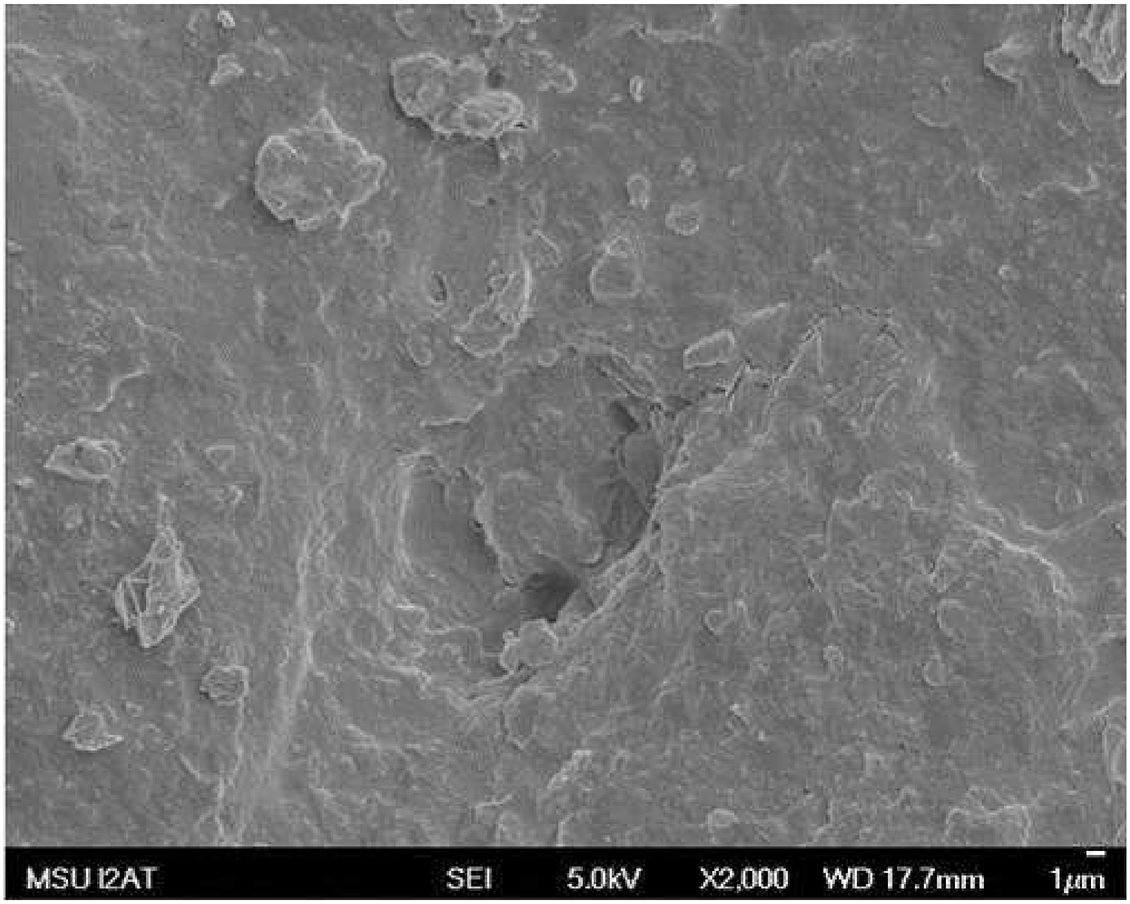

Figure 3.19 SEM showing pore shape and structure

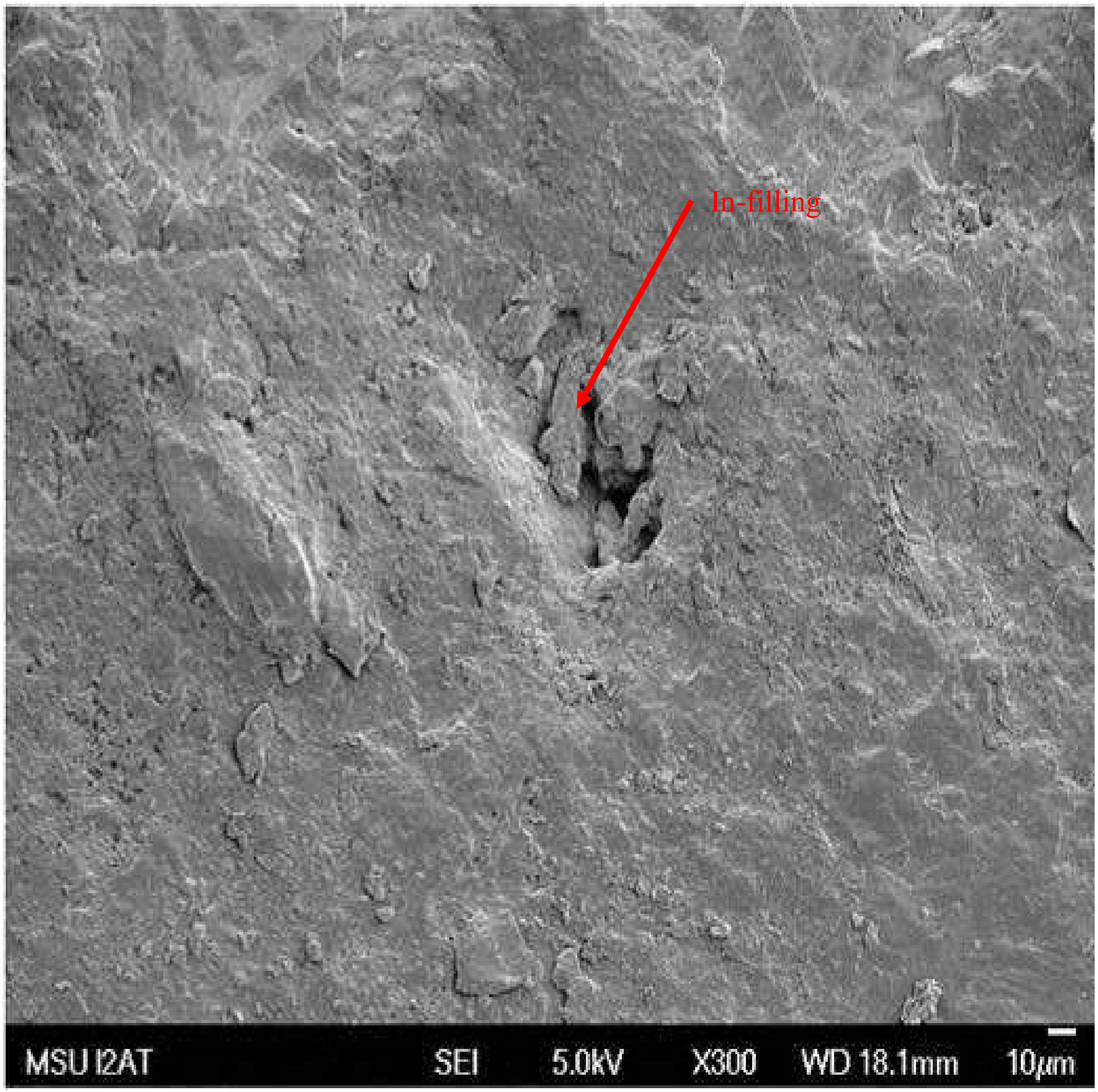

Figure 3.20 SEM of surface pores with in-filling

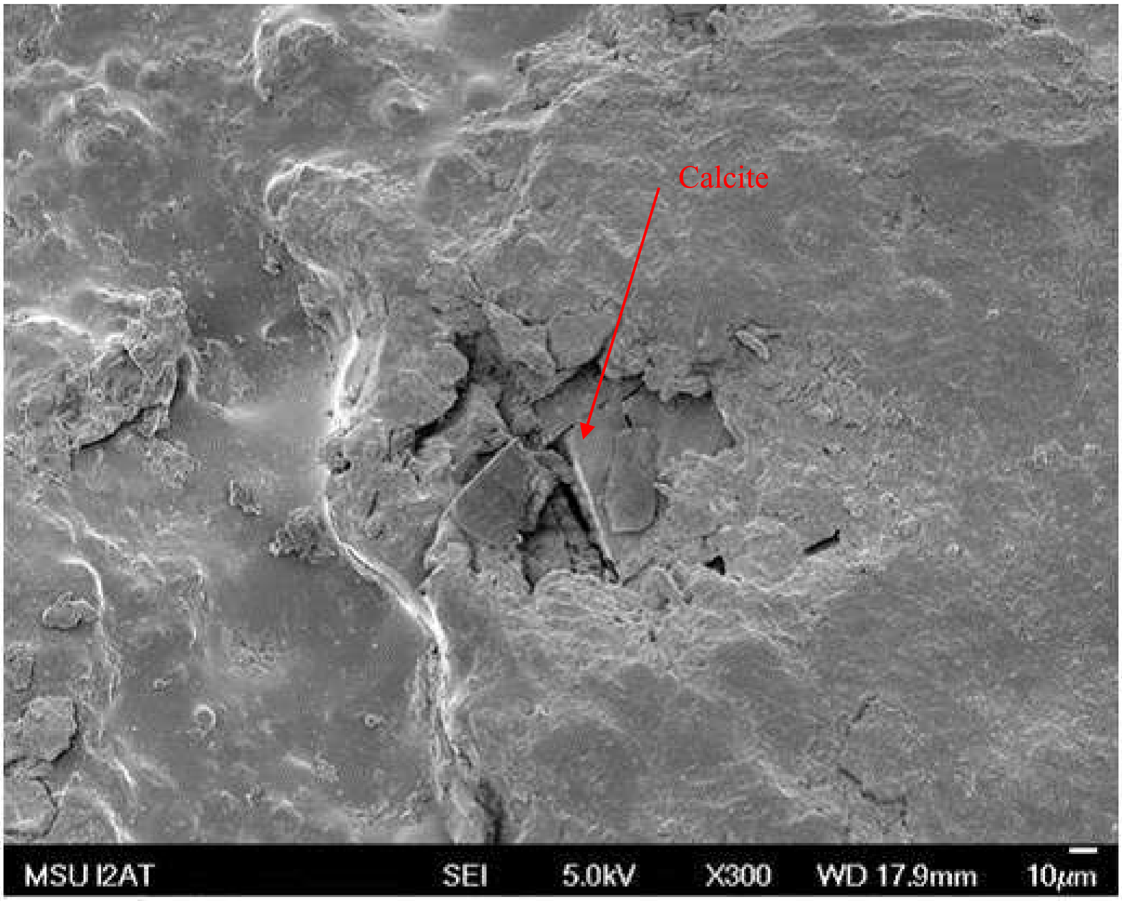

Figure 3.21 SEM of surface pore showing calcite crystals

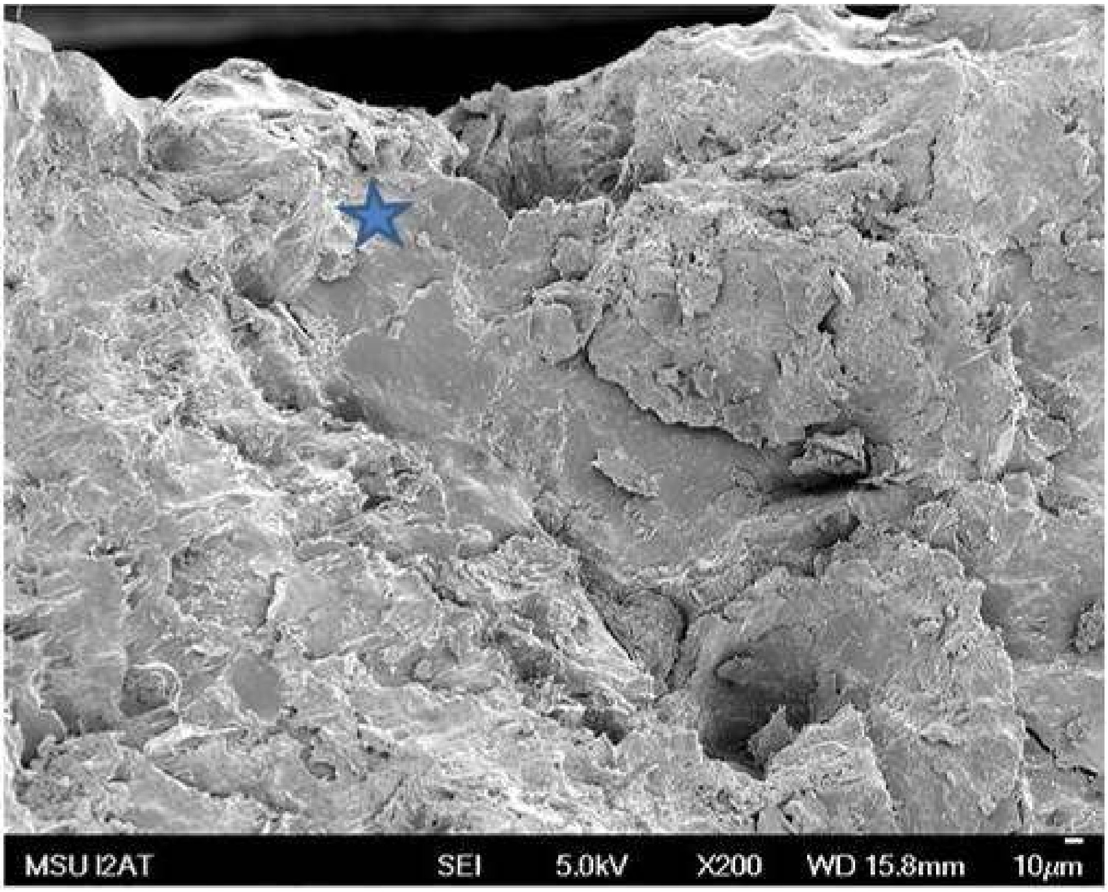

Figure 3.22 Side view of pore

EDS taken from star in upper section

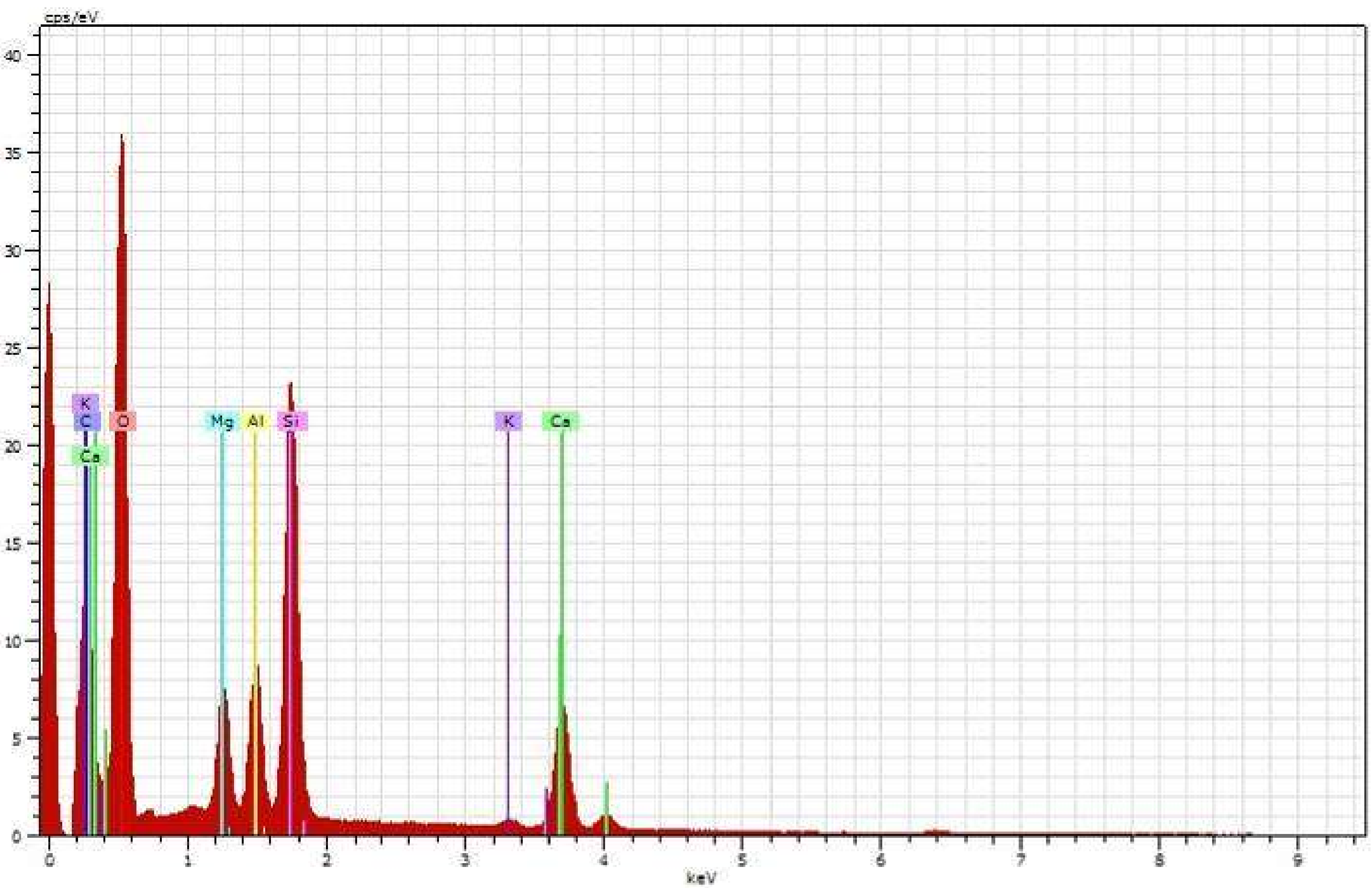

Figure 3.23 EDS spectra of upper pore structure, high magnesium.

Table 3.4 EDS Spectral Analyses of upper section of egg shell

ELEMENT	WT %	Atomic %	Error Sigm
Oxygen	52.33	66.09	5.14
Calcium	16.27	8.2	0.52
Carbon	2.78	4.67	0.37
Silicon	19.39	13.95	0.75
Magnesium	3.86	3.21	0.21
Aluminum	4.77	3.57	0.22
Potassium	0.61	0.32	0.05
Total	100	100	

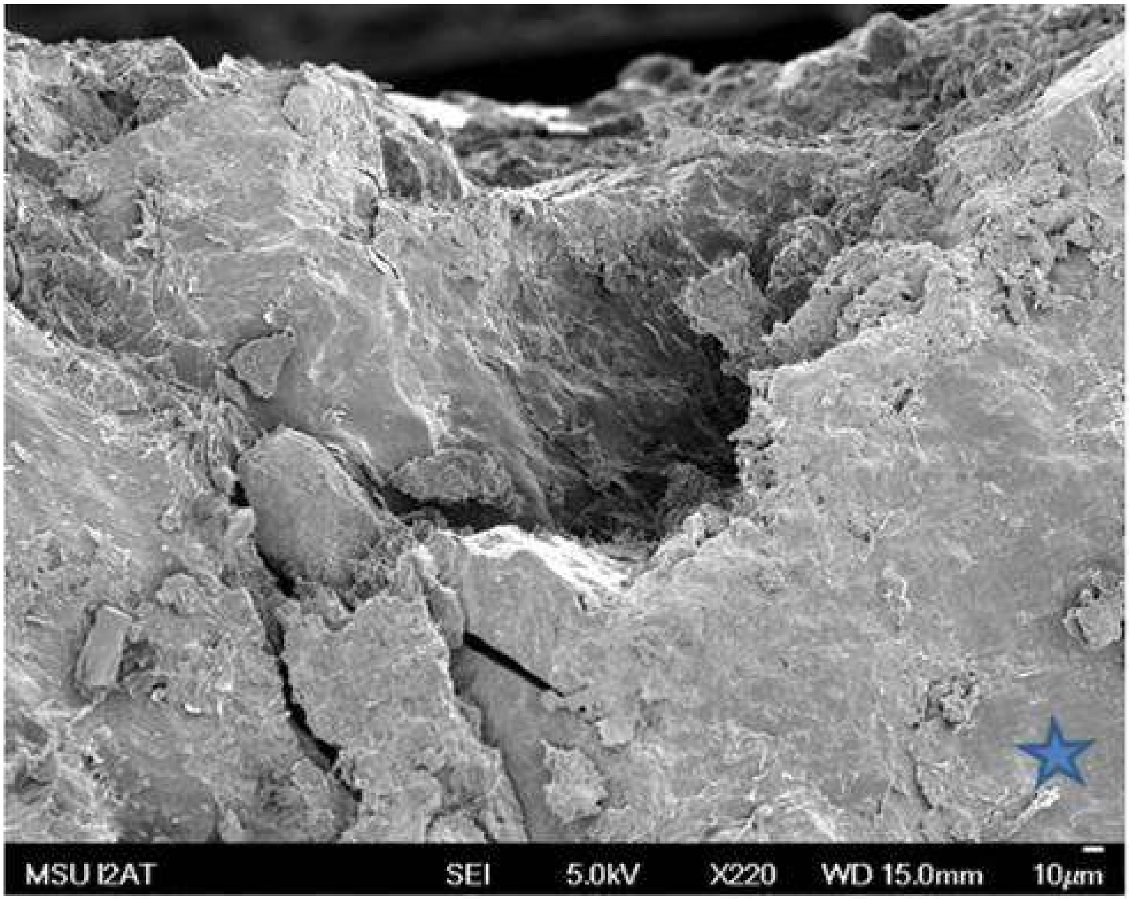

Figure 3.24 SEM of pore structure

EDS taken from star further down in shell

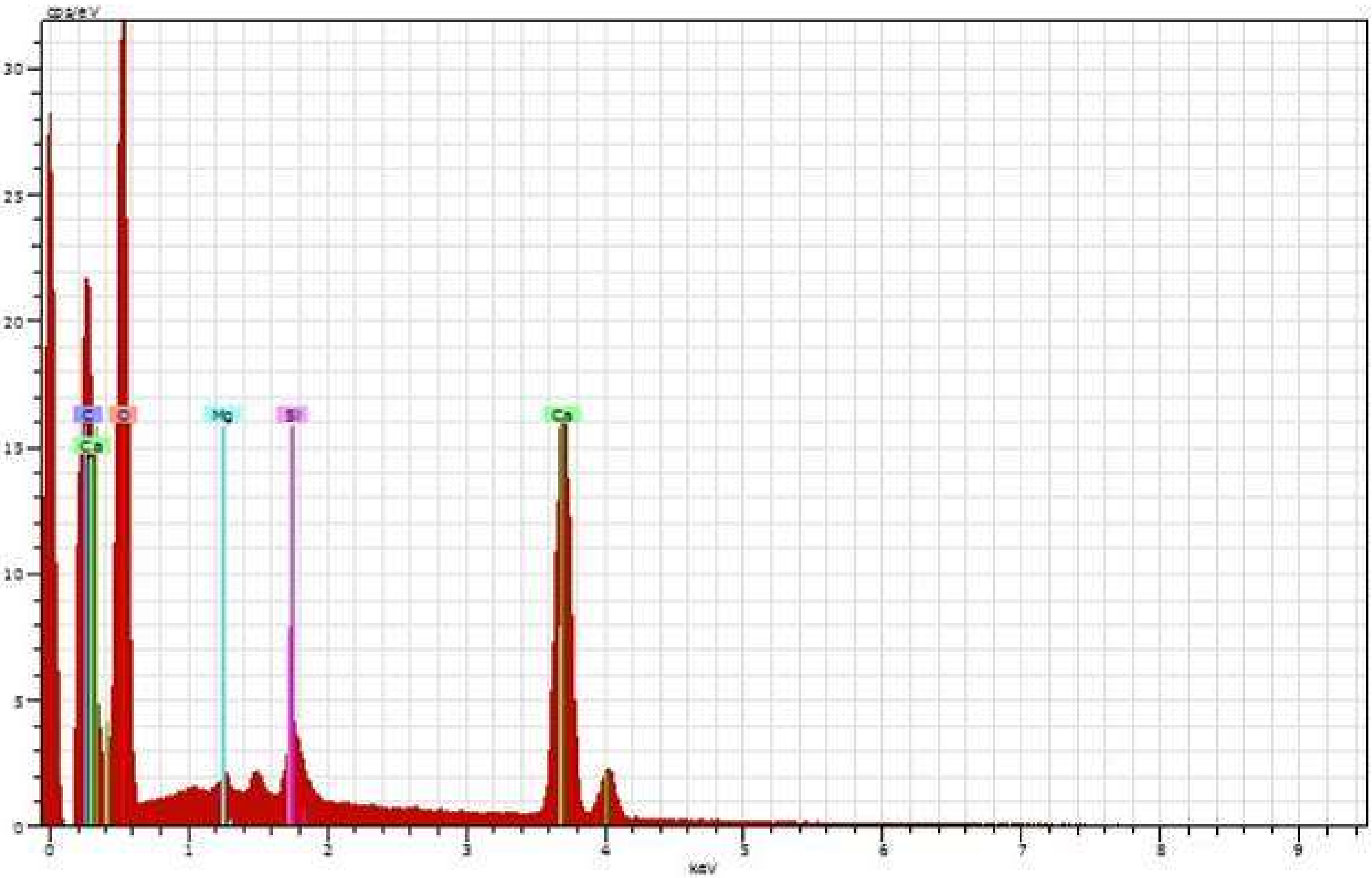

Figure 3.25 EDS spectra of egg shell further down in egg shell (blue star from figure 3.24), low magnesium.

Table 3.5 DS Spectral analyses of area lower down in pore

ELEMENT		WT %	Atomic %	Error Sigm
Oxygen		47.35	54.02	5.67
Calcium		30.18	13.75	1.14
Carbon		20.22	30.73	2.47
Silicon		1.91	1.24	0.11
Magnesium		0.34	0.26	0.05
Total		100	100	

References

Abel, R.L., Laurini, C.R., and Richter, M. (2012) A palaeobiologist's guide to 'virtual' micro-CT preparation. *Palaeontologia Electronica* Vol. 15, Issue 2, pp. 1-17.

Bennett, C., Williams, M., Leng, M., Siveter, D., Davies, S., Sloane, H., Wilkinson, I. (2011) Diagenesis of fossil ostracods: implications for stable isotope based environmental reconstruction. *Palaeogeography, Palaeoclimatology, Palaeoecology* Vol. 305 Issue 1-4, pp. 150-161.

Britt, B. & Naylor, B. (1994) An embryonic *Camarasaurus* (Dinosauria, Sauropoda) from the Morrison Formation (Dry Mesa Quarry, CO.). Dinosaur Eggs and Babies Cambridge University, Cambridge, MA. pp. 256-264.

Carpenter, K., Hirsch, K., Horner, J. (1994) Dinosaur Eggs and Babies Cambridge University Press, Cambridge, MA. pp.1-372.

Carpenter, K. (1999) Eggs, Nests, and Baby Dinosaurs Indiana University Press, Bloomington, Indiana. pp.1-337.

Deckker, P., Forester, R. (1988) The use of ostracods to reconstruct continental environmental records. Ostracoda in the Earth Sciences ed Deckker, P, Colin, J., Peypouquet, J. *Elsevier* pp. 175-199.

Deeming, D.C. (2005) Ultrastructural and functional morphology of eggshells supports the idea that dinosaur eggs were incubated buried in a substrate. *Palaeontology*, Vol. 49, part 1 pp.171-185.

Fastovsky, D., Weishampel, D., Watabe, M., Barsbold, R., Tsogtbaatar, K., Narmandakh, P. (2011) A nest of *Protoceratops andrewsi* (Dinosauria, Ornithischia). *Journal of Paleontology* Vol. 85, Issue 6 pp.1035-1041.

Garwood, R., Rahman, I.A., and Sutton, M.D. (2010) From Clergymen to computers—the advent of virtual palaeontology. *Geology Today*, Vol. 26, No. 3, May-June pp 96-100.

Golder, W. and Christian, A. (2002) Quantitative CT of Dinosaur Bones. *Journal of Computer Assisted Tomography* Vol 26 Issue 5 pp. 821-824.

Gould, G.C., Marcus, L.F., Gueziec, A.P., Daleo, G.F., and Reddy, D.P. (1996) Medical CT scan visualization and its applications for the study of fossils using Data Explorer and Interformat. *Journal of Vertebrate Paleontology*, Vol. 16 pp. 38A.

Grellet-Tinner, G., Chiappe, L., Norell, M., Bottjer, D. (2006) Dinosaur eggs and nesting behaviors: A paleobiological investigation. *Palaeogeography, Palaeoclimatology, Palaeoecology,* Vol. 232, pp. 294-321.

Grigorescu, D., Garcia, G., Csiki, Z., Codrea, V., Bojar, A.-V. (2010) Uppermost Cretaceous megaloothid eggs from the Hateg Basin, Romania, associated with hadrosaurs hatchlings: Search for explanation. *Palaeogeography, Palaeoclimatology, Palaeoecology* Vol. 293 pp.360-374.

Hirsch, K. (1994) Upper Jurassic eggshells from the Western Interior of North America. Dinosaur Eggs and Babies Cambridge Press pp.137-150.

Jackson, F., Horner, J., Varricchio, D. (2010) A study of a *Troodon* egg containing embryonic remains using epiflourescence microscopy and other techniques. *Cretaceous Research* Vol. 31, pp.255-262.

Jackson, F., Varricchio, D. (2010) Fossil Eggs and eggshells from the Lowermost Two Medicine Formation of Western Montana, Sevenmile Hill Locality. *Journal of Vertebrate Paleontology* Vol. 30, Issue 4, pp. 1142-1156.

Jensen, J. (1967) Dinosaur eggs from the Upper Cretaceous North Horn Formation of Central Utah. *Brigham Young University Research studies, Paleontology Series* Vol. 13, pp. 55-78.

Ketcham, R.A. and Carlson, W.D. (2001) Acquisition, optimization and interpretation of X-ray computed tomographic imagery: applications to the geosciences. *Computers and Geosciences*, Vol. 27, pp. 381-400.

Li, Y., Liu, Y., Chen, X., Zhao, G. (1996) Dinosaurian embryo; 2, young dinosaur bones in Ovaloolithus. *Journal of China University of Geosciences*, Vol. 21, Issue 6 pp. 608-610.

Liang, X., Wen, S., Yang, D., Zhou, S., Wu, S. (2009) Dinosaur eggs and dinosaur egg-bearing deposits (Upper Cretaceous) of Henan Province, China: Occurrences, palaeoenvironments, taphonomy, and preservation. *Progress Natural Science* Vol. 19, Issue 11, pp. 1587-1601.

Martins, R., Beckm ann, F., Castahinha, R., Mateus, O., Pranzas, P. (2010) Dinosaur and crocodile fossils from the Mesozoic of Portugal: Neutron tomography and synchrotron-radiation based micro-computed tomography. *Mater. Res. Soc. Symp.* Proc. 1319.

Mueller-Towe, I., Sander, P., Schuller, H., Theis, D. Hatching and infilling of dinosaur eggs as revealed by computed tomography. *Palaeontographica* Vol. 267, Part 1/6 pp. 119-168.

Norell, M., Clark, J., Demberelyin, D., Rhinchen, B., Chiappe, L., Davidson, A., McKenna, M., Altangeral, P., Novacek, M. (1994) A Theropod dinosaur Embryo and the Affinities of the Flaming Cliffs Dinosaur Eggs. *Science* Vol. 266, pp. 779-784.

Paul, G. (1994) Dinosaur reproduction in the fast lane: implications for size, success, and extinction. From: Dinosaur Eggs and Babies Cambridge University, Cambridge, MA.

Pfretzschner, H.-U., Tutken, T. (2011) Rolling bones-Taphonomy of Jurassic dinosaur bones inferred from diagenetic microcracks and mineral infillings. . *Palaeogeography, Palaeoclimatology, Palaeoecology* 310, pp. 117-123.

Scherzer, B. & Varricchio, D. (2010) Taphonomy of a juvenile Lambeosaurine bonebed from the Two Medicine Formation (Campanian) of Montana, United States. *PALAIOS* Vol. 25, pp.780-795.

Straight, W., Davis, G., Skinner, C., Haims, A., McClennan, B., Tanke, D. (2009) Bone lesions in Hadrosaurs: Computed tomography imaging as a guide for paleohistoric and stable-isotope analysis. *Journal of Vertebrate Paleontology* Vol. 29, Issue 3, pp.315-325.

Sutton, M. Garwood, R., Siveter, Da., Siveter, De. (2012) SPIERS and VAXML: A software toolkit for tomographic visualization and a format for virtual specimen interchange. . *Palaeontologia Electronica* Vol. 15, Issue 2, pp1-14.

Swapp, S. Scanning Electron Microscopy (SEM) *Geochemical Instrumentation and Analysis* pp. 1-6.

Varricchio, D., Jackson, F. (2004) A phylogenetic assessment of prismatic dinosaur eggs from the Cretaceous Two Medicine Formation of Montana. *Journal of Vertebrate Paleontology* Vol. 24, Issue 4, pp. 931-937.

Vila, B., Jackson, F., Galobart, A. (2010) First data on dinosaur eggs and clutches from Pinyes locality (Southern Pyrenees). *Ameghiniana* Vol. 47, Issue 1, pp. 79-87.

Wasser, G. (1988) A geological evaluation of the Judith River Formation (Belly River Formation) in the Pembina Region. *CSPG Special Publication Sequences, Stratigraphy, Sedimentary, Surface and Sub-surface-Memoir 15, pp.563*-569.

Weishampel, D., Norman, D., and Grigorescu, D. (1993) *Telatosaurus transsylvanicus* from the Late Cretaceous of Romania: The most basal hadrosaurid dinosaur. *Palaeontology,* Vol. 36 part 2, pp.361-386.

Zhao, Z., Mao, X., Chai, Z., Yang, G., Kong, P., Ebihara, M., Zhao, Z. (2002) A possible causal relationship between extinction of dinosaurs and K/T iridium enrichment in the Nanxiong Basin, South China: evidence from dinosaur eggshells. *Palaeogeography, Palaeoclimatology, Palaeoecology* Vol. 178 pp.1-17.

Zuo, Q., and Jing, W.-D. (1995) First report of studying dinosaur egg fossils with method of medical CT scanning. *Acta Palaeontologica Sinica*, Vol. 34 pp. 777-779.

CHAPTER IV

STUDY ON OXYGEN ISOTOPES AND ELEMENT:CALCIUM RATIOS IN REEF BUILDING CORALS

Abstract

Corals have long been used as proxies for the sea-water environment. However the existence of chemical and isotopic inconsistencies between different corals and within different architectural elements of the same corals grown simultaneously in the same environment suggests that factors besides ocean temperature and seawater composition affect isotopic and chemical records. Secondary Ion Mass Spectrometry (SIMS) analysis was conducted on the reef building coral (*Monastrae annularis*) from the Veracruz Reef in the Southern Gulf of Mexico in order to investigate the differences in stable oxygen isotope and elemental ratios between the different architectural elements of these corals. The microstructure of the coral reveals a few morphological different zones (architectural elements) such as the theca-wall (Th), septa (S), costae (C), exothecal and endothecal dissepiments (ExD) and (EnD). Theca, septa, costae, and ExD that grew at the same time are similar in $\delta^{18}O$ within one sigma error. However, $\delta^{18}O$ in EnD is isotopically heavier by 1‰ than those of simultaneously grown theca, septa, costae, and ExD. Indeed, the theca walls seem to provide the best correlation with temperature than any of the other elements. Variation with EnD was found, especially with regard to $\delta^{18}O$, but also with regard to Sr/Ca and U/Ca, and Ba/Ca. SIMS spot profiles in the coral growth direction

yielded weekly time resolution and demonstrate that factors other than temperature and seawater composition affect elemental and isotopic ratios in corallite aragonite. $\delta^{18}O$ positively correlates with Sr/Ca but is opposite to Mg/Ca. The $\delta^{18}O$-Sr/Ca relationship suggests that this is driven by temperature at least partially.

Introduction

Our understanding of climate change and oceanographic variability through time is largely derived from knowledge of oxygen isotopes ($\delta^{18}O$) (Land, et al., 1975; Stoll, et al., 2002; Suzuki, 2012; Giry, et al., 2013; Grottoli and Eakin, 2006; Hayashi, et al., 2012; Saenger, et al 2012; Storz, et al., 2013) and elemental ratios (X/Ca) signatures in coral reefs (Inoue, 2006: Dissard, et al., 2012; Gagnon, et al., 2007; Giry, et al., 2010; Hayashi, et al., 2012; Storz, D. et al., 2013), where X can be Mg, Sr, Ba, etc. Corals continue to provide valuable data as environmental proxies. $\delta^{18}O$ and strontium/calcium is especially valuable for temperature proxies. The use of corals as proxies has been complicated due to the many various architectural structures which make up most corals. Corals in this study were collected in the Verde Reef off of Veracruz, Mexico in the Bay of Campeche (Figure 4.1). Corals are composed of a theca in which the polyp resides, costa which form as bumps on top of the septa (as it grows upwards towards the surface and light), septa which divide the theca into various compartments. The theca is usually joined together by exothecal dissepiments and then endothecal dissepiments provide an upward growing base for the polyp within the theca (Figure 4.2). All of these structures grow at different rates and some have varying differences in their intake of elements and stable isotopes. The dissepiments for instance tend to grow at night (Watanabe, et al., 2002) as well as with-in a lunar cycle (Dávalos-Dehullu, et al., 2008).

This paper will seek to examine those differences, provide the best advice for researchers who seek to sample selective members of the skeleton which best represent the proxies desired and to answer if these differences are significant or not depending upon the mass percentage of the different architectural elements. In addition, a comparison of the volume of the architectural structures will be made to ascertain just how much of a difference sampling the whole bulk coral or select parts of the coral will make.

The complex microstructure of the coral reveals a few morphologically different zones (architectural elements). These are the Theca-wall (Th), Septa (S), Costae (C), Exothecal and Endothecal dissepiments (ExD) and (EnD) (Figure 4.1). The theca is the architectural element which the coral polyp lives in. It forms the wall and cup of the coral skeleton. Costae are the bumps at the surface surrounding the entrance to the theca and where the polyp extrudes. The ExD connect one thecal wall to another thecal wall of another coral polyp; the septa are those elements which divide the theca vertically. Finally the EnD are those structural elements which the polyp builds under its self as it grows the theca upward and outward. It also appears that the EnD grows the slowest and the last (since the other elements must be produced for the polyp to move up into). According to previous works dissepiments grow at night, while the other elements calcify during the day due to the photosynthetic effect (Watanabe, et al., 2002). Some architectural elements seem to reflect the temperature proxy more accurately than others (Leder, et al., 1996; Watanabe, et al., 2002; Cohen, et al., 2004) For example it was shown that $\delta^{18}O$ in theca (which is also the largest by mass) is the best representative for temperature records (Land, et al., 1975). Corals are being used as climate and seawater composition indicators through both the isotopic variations and X/Ca (e.g Land, et al., 1975; Stoll, et al., 2002; Giry, et al., 2010; Giry, et al., 2013; Goreau, 1977; Grottoli, & Eakin, 2006; Hemming, et al., 1998; Saenger, et al 2012; Storz, et al., 2013). Other factors also seem to influence the growth of coral, such as: reproductive cycles, sedimentation, fresh-water influence (from monsoons), nutrient availability (also related to run-off), wind-stress, storms, amount of sunlight and turbidity (Barnes and Lough, 1993). However, the differential incorporation of stable isotopes and X/Ca into EnD bring a source of error into these climate calculations previously not considered. It has also been found that $\delta^{18}O$ isotopes reflect not only annual temperature differences in some architectural elements (especially the theca, as already noted) (Land, et al., 1975), but even seasonal variation which helps prove its use as a proxy for Sea Surface Temperature (SST) (Cohen, et al., 2004; Watanabe, 2002; Guzman & Tudhope, 1998; Leder, et al., 1996). Therefore by thoroughly examining the $\delta^{18}O$, B/Ca, Mg/Ca, Ba/Ca, Sr/Ca, and U/Ca) in all the different architectural elements we can improve existing geochemical proxies. Another consideration is the fraction of architectural structures in the coral. The ratio of ExD mass to theca mass is 0.017:1 and the ratio of EnD mass to theca mass is 0.0070:1 (Dávalos-Dehullu, et al., 2008). The combined mass of the theca the costae and septa which are similar in thickness and which have similar $\delta^{18}O/\delta^{16}O$ ratios and similar calcium/elemental ratios, compared the amount of mass present in the dissepiments may mean that the difference the dissepiments influence proxy calculations may become trivial.

Coral sampling and analytical methods

Sample description and preparation

The coral species *Montastraea annularis* was collected at 10 m depth on the leeward slope of Isla Verde Reef, Veracruz Reef System, Southern Gulf of Mexico, in August 1991(Figure 4.1). Pieces 1 cm long were sliced from the most recent side of the coral (Figure 4.3a). Specimens were sliced in parallel and to the perpendicular directions of growth. Therefore, one of the sections exposed a time series of a continuously extended skeleton (Figure 4.3b); while another section represents simultaneously grown skeletal material (Figure 4.3c). Both sections were mounted in epoxy (EpoxiCure®, Buehler) and polished down to 1-µm size by diamond suspension. The parallel section consists of the last 7 mm of growth prior to coral collection and shows corallite aragonite crystallized under variable temperature due to seasonal change (Figure 4.3b). The perpendicular section exposed the 5 mm from the surface of the coral representing the corallite which precipitated simultaneously and therefore without temperature and compositional variability of seawater.

SIMS analysis

Oxygen isotopes

Analyses of the coral sections were conducted with CAMECA ims 1270 ion microprobe at the University of California Los Angeles (UCLA). The samples were analyzed while maintaining their structural integrity. This was done so that the different structural portions could be analyzed separately. Samples were examined with a 2-3 nA Cs^+ primary beam with a lateral dimension of 20-30 µm at the sample surface (see Gabitov et al. 2012 for details). Negative secondary ions ^{16}O and ^{18}O were simultaneously measured by Faraday Cups (FC) using multi-collection set-up for a mass resolving power (MRP) of ~2000, which was sufficient for resolving hydride interference with the ^{18}O peak (Fayek, et al., 2002). During two analytical sessions the raw intensity of ^{18}O varied from $6.7 \cdot 10^6$ to $7.1 \cdot 10^6$ counts per second (cps). The total sputtering time prior to acquisition was therefore 120 s, which was sufficient to reach a steady $^{18}O/^{16}O$ value over the 12 cycles of the analysis on a single spot. Ten spot analyses of calcium carbonate reference materials (calcites and aragonite) yielded standard deviation of 0.2-0.3‰. The standard was analyzed routinely after every 5-8 measurements of the aragonite sample. In order to quantify SIMS data, the sample raw $^{18}O/^{16}O$ ratios were normalized to those of the aragonite standard (which was located in the same mount), where $^{18}O/^{16}O$=0.002051. Natural clear-beige aragonite crystal (BB-Ar) from Belice, Bohemia and calcites (NBS-18, NBS-19, and MEX) were analyzed to determine SIMS instrumental mass fractionation [$IMF=10^3 \cdot \ln(^{18}O/^{16}O_{SIMS})/(^{18}O/^{16}O_{reference})$]. IMF values for calcite standards ($IMF_{calcite}$) were consistent to each other within analytical uncertainty, but lower than IMF of aragonite ($IMF_{BB\text{-}Ar}$), i.e. $IMF_{BB\text{-}Ar}$-$IMF_{calcite}$=0.8‰ in the analytical session 1 and 2 respectively. The reference isotopic ratios for NBS-18 ($\delta^{18}O_{PDB}$=-23‰) and NBS-19 ($\delta^{18}O_{PDB}$=-2.2‰) were obtained from Friedman et al. (1982). MEX $\delta^{18}O_{PDB}$=-10.39‰) and BB-Ar ($\delta^{18}O_{PDB}$=-7.79‰) were analyzed by gas source mass spectrometry at the University of Arizona. The oxygen isotope analyses were performed in two analytical sessions. After the first session the sample was ground down to 20-40 μm and additional $\delta^{18}O$ measurements were conducted followed by elemental ratios analyses on the same polished section.

Li/Ca, B/Ca, Mg/Ca, and Sr/Ca ratios

Samples were analyzed with a 1.8-7.7 nA $^{16}O^{-}$ primary beam at 20-30 μm lateral dimension of the sample surface. Positive secondary ions corresponding to mass/charge stations of 5.5 (background), ^{7}Li, ^{11}B, ^{24}Mg, ^{42}Ca, and ^{88}Sr were measured during three analytical sessions. Intensities were measured by peak switching with waiting times up to four seconds and counting times of 1, 10, 4, 2, 2, and 1 seconds for ^{6}Li, ^{7}Li, ^{24}Mg, ^{42}Ca, ^{88}Sr, and ^{138}Ba respectively. Each spot was pre-sputtered for 2 minutes. A mass resolving (MRP) of ~2900 achieved separation of molecular interferences such as $^{6}Li^{1}H$, $^{10}B^{1}H$, $^{23}Na^{1}H$, $^{26}Mg^{16}O$, $^{40}Ca^{1}H_2$ (Gabitov, et al. 2011). To reduce $^{44}Ca_2$ and $^{87}Sr^{1}H$ interferences, 88Sr was measured with the offset of -80V using the energy bandwidth of 50V (total voltage was 10 kV).

HUJ-AR is an aragonite reference material where Sr/Ca=8.21 mmol/mol (Gabitov et al. 2013). UCI-CC is a calcite reference material where Mg/Ca=3.45 mmol/mol. M-93 is a piece of *Porites* coral with B/Ca=0.364 mmol/mol. CAL-HTP is a synthesized calcite where Li/Ca=28.9 μmol/mol. NIST 610, 612 and 614 are glass wafers from the national Institute of Standards and Technology.

The technique used to measure elemental ratios of the corallite aragonite was Laser Ablation Inductive-Coupled Plasma Mass Spectrometry (LA-ICP-MS) and SIMS. This allowed for fine sampling of the different architectural elements and a high resolution for the different elemental isotopes. The LA-ICP-MS enabled measurements of the individual different architectural elements and did not require carbonate standards with a similar chemical composition, as SIMS does.

Calculation of Dissepiment ratios to theca

The thickness of the theca (costae and septa were very similar in thickness to the theca as well) was normalized to one with the thickness of each of the dissepiments to form a ratio thickness of septa/thickness of each dissepiment=1/X. Then the spacing of the dissepiments was accounted for by dividing the average dissepiment spacing into the thickness of the dissepiments. Finally since the EnD are roughly twice as numerous, the ratio number for EnD was multiplied by two.

Results and discussion

The existence of chemical and isotopic inconsistencies between different corals and within different architectural elements of the same corals grown simultaneously in the same environment suggests that factors besides ocean temperature and seawater composition affect isotopic and chemical records (Giry, et al., 2010). The microstructure of the coral reveals a few morphological different zones (architectural elements) such as the theca-wall (Th), septa (S), costae (C) exothecal and endothecal dissepiments (ExD) and (EnD). Th, S, and ExD (Figure 4.1) that grew at the same time are similar in $\delta^{18}O$ within one sigma error (Figure 4.4). However, $\delta^{18}O$ in EnD is isotopically heavier by 1‰ than those of simultaneously grown Th, S, C, and ExD. Indeed, the theca walls seem to provide the best correlation with temperature than any of the other elements (Giry, et al., 2010; Watanabe, et al., 2002). Others have found variation in $\delta^{18}O$ with-in EnD, being enriched with $\delta^{18}O$ notably Leder, et al in 1996, when working in Biscayne Bay. Leder and his team used micro-drill (micromils) to sample from the theca and the dissepiments. He found that a variation in growth rate, the slowest being 1.1 mm/yr and the fastest, being 8 mm/yr also corresponded to the different architectural elements. The dissepiments were the slowest growing and the theca the fastest. Isotopic ($\delta^{18}O$) variability corresponded as well as the theca was 0.1 to 2‰ more enriched in $\delta^{18}O$.

The ExD extension rates for our study were 0.913 mm/yr and for the EnD 0.72 mm/yr. This is close to Leder, and probably more accurate as with SIMS we were able to selectively sample just the dissepiments rather than getting part of the theca, as he admitted to with the more cumbersome drilling. Enrichment of $\delta^{18}O$ in slowly grown EnD is consistent with the $\delta^{18}O$ enrichment trend seen in inorganically precipitated aragonites (Gabitov, 2013). Theca however, does not fall into this trend.

It has already been mentioned that theca walls seem to provide the best correlation with SST than any other structures (Giry, et al., 2010; Watanabe, et al., 2002), however our SIMS $\delta^{18}O$ profiles with 2-23 day temporal resolution yielded scattered isotopic signals. This precludes accurate temperature evaluation from corallite $\delta^{18}O$. The actual SST increases from 23°C in February to a high of 29°C in August based on the direct measurements in the sample area during the year of 2001. This δ18O-T°C inconsistency demonstrates that factors other than temperature and sea-water composition affect elemental and isotopic ratios in corallite aragonite.

Sections parallel to the direction of growth are presented in Figure 4.8. SIMS spot profiles in the coral growth direction yielded weekly time resolution and demonstrate that factors other than temperature and seawater composition affect elemental and isotopic ratios in corallite aragonite. Sr/Ca and B/Ca were $\delta^{18}O$ positively correlated but was opposite to Mg/Ca (Figure 4.9 A, B, C). The $\delta^{18}O$-Sr/Ca relationship suggests that this is driven by temperature at least partially (Figure 4.9A). The Sr/Ca-

B/Ca relationship suggests a temperature effect on B/Ca because Sr/Ca was proven to preserve SST signals (Figure 4.9B).

It is shown that the fractionation differences in element/calcium ratios differ among the various architectural structures. For Sr/Ca, the EnD is lower but the ExD is higher than the Theca (Figure 4.12). Both the ExD and End are significantly lower than the Theca in Ba/Ca (Figure 4.13). The ratios are roughly the same in Mg/Ca (Figure 4.14) as they are for U/Ca (Figure 4.15).

It was reported that theca walls seem to provide the best correlation with temperature than any of the other structures (Giry, et al., 2010; Watanabe, et al., 2002;). Sea Surface Temperature varied from a low of 23°C (February) to a high of 29°C (August) based on direct measurement for the 1991 year. This $\delta^{18}O$-T°C inconsistency demonstrated that factors other than temperature and sea-water composition affect elemental and isotopic ratios in corallite aragonite. However our SIMS $\delta^{18}O$ profiles with 2-23 day temporal resolution (Figure 4.5) yielded a scattered isotopic signal precluding accurate temperature evaluation from corallite $\delta^{18}O$. In the sample area, the actual SST varies from 23 SIMS micro-analyses of the perpendicular section showed that $\delta^{18}O$ does not vary between three of the architectural elements; i.e. theca, septa, and ExD (Figure 4.6). Here the error is the standard deviation between multiple measurements. Sections parallel to the direction of the coral growth are presented on Figure 4.8. Theca, Septa, and ExD were analyzed at the similar distances from the surface of the coral (1860µm), and therefore, represented aragonite crystallized simultaneously (Figure 4.8). The exposed EnD are shown on Figure 4.8. These EnD are located within 4mm from theca, septa and ExD marked on figure 4.8, and therefore represent simultaneous growth

(Dávalos-Dehullu et al. 2008). The $\delta^{18}O$ of EnD is up to 1.5‰ higher than in the simultaneously grown Theca region. The results from session 2 also yielded $\delta^{18}O$ enrichment in EnD, but with a lower degree of 0.7‰.

The vertical section in parallel with the growth direction shows the last 7 mm of growth prior to coral collection (Figure 4.7). Here SIMS profiles through the time of coral growth could, and often do yield high resolution seasonal seawater temperature records. The spatial offset between EnD and the other architectural elements was estimated from its measured value of 4 mm (Devalos-Dehullu, et al., 2008) and the location of the latest EnD which appear on the sliced section, i.e. 5.1 mm (Figure 4.8). The averaged values of $\delta\ ^{18}O$ from Theca, Septa, and ExD grown between 4 and 5.1 mm are compared with simultaneously precipitated EnD (Figure 4.4, blue diamond areas). The data showed that average $\delta\ ^{18}O$ in Theca, Septa, and ExD are similar to each other to within 1 sigma error. However, the average $\delta\ ^{18}O_{\ EnD}$ is isotopically heavier by 1.5 ‰, i.e. $\delta^{18}O_{\ Th+S+ExD}$=-6.2 ‰ and $\delta\ ^{18}O_{EnD}$ =-4.7 ‰. This 1.5 ‰ difference corresponds to the large temperature offset of 6° C. All examined elements inside the blue boxes of Figure 4.4 were grown at the same time; therefore the $\delta\ ^{18}O$ difference was not caused by environmental growth differences such as seawater composition or temperature.

$\delta^{18}O$ positively correlates with Sr/Ca and B/Ca but is opposite to Mg/Ca (Figure 4.9A,B,C). The $\delta^{18}O$-Sr/Ca relationship suggests that this is driven at least partially by temperature (Figure 4.9A). The Sr/Ca-B/Ca relationship suggests a temperature effect on B/Ca because Sr/Ca has been shown to preserve SST signals (Figure 4.9B) (Cohen, et al., 2004).

LA-ICP-MS data showed that the fractionation differences in element/calcium ratios differ among the various architectural structures. The location of the laser burns were similar to SIMS data positions shown on Figure 4.10. Actual image is shown in Figure 4.11. Ratios of trace elements to calcium are shown in Table 4.1. The concentration ratio of Sr/Ca is higher in the EnD than in the theca, but lower in the ExD (Figure 4.11). The concentration of Ba/Ca ratio is higher in the EnD than the theca (Figure 4.12). In the Mg/Ca concentration the ratio is lower in the EnD (Figure 4.13). The U/Ca ratios showed inconclusive results (Figure 4.13). These variabilities are not fully consistent with the growth rat effect observed in inorganically precipitated aragonite in contrast to the oxygen isotope data ($\delta^{18}O$) in ExD and EnD (Gabitov, et al., 2008; Gabitov, 2013).

Conclusions

EnD are enriched in $\delta^{18}O$ by 1‰ compared to the other architectural structures (Theca, Septa, Costae and ExD) Trace element:Calcium ratios vary between architectural structures as well. Growth rate appears to be not the only factor controlling $\delta^{18}O$ and X/Ca distribution between architectural structures of *Montastrea annularis.* Despite EnD enrichment in $\delta^{18}O$, overall the isotopical input of EnD would be insignificant for bulk analyses in calculating proxies due to the over-all small percentage of EnD in the total mass of the coral skeleton.

In Ba/Ca ratios the EnD was found to be higher than the theca. In Mg/Ca the EnD was found to be lower and the Sr/Ca was lower in the ExD and higher in the EnD.

Better environmental proxies could be obtained by selectively sampling the theca, septa, and costae, however, the small amount of dissepimental mass would scarcely affect the out-come.

Figure 4.1 Location (red star) on coral collection in the Gulf of Mexico

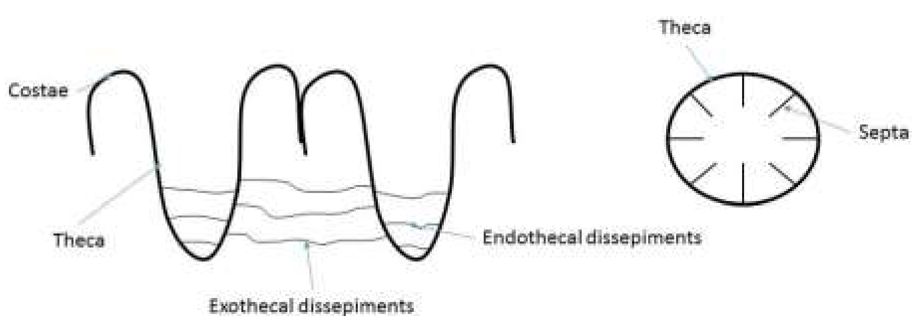

Figure 4.2 Coral skeleton showing Costae, Theca, Septa, Exothecal dissepiments and Endothecal dissepiments

Drawing by Jeremy Weremeichik and John Paul Jones

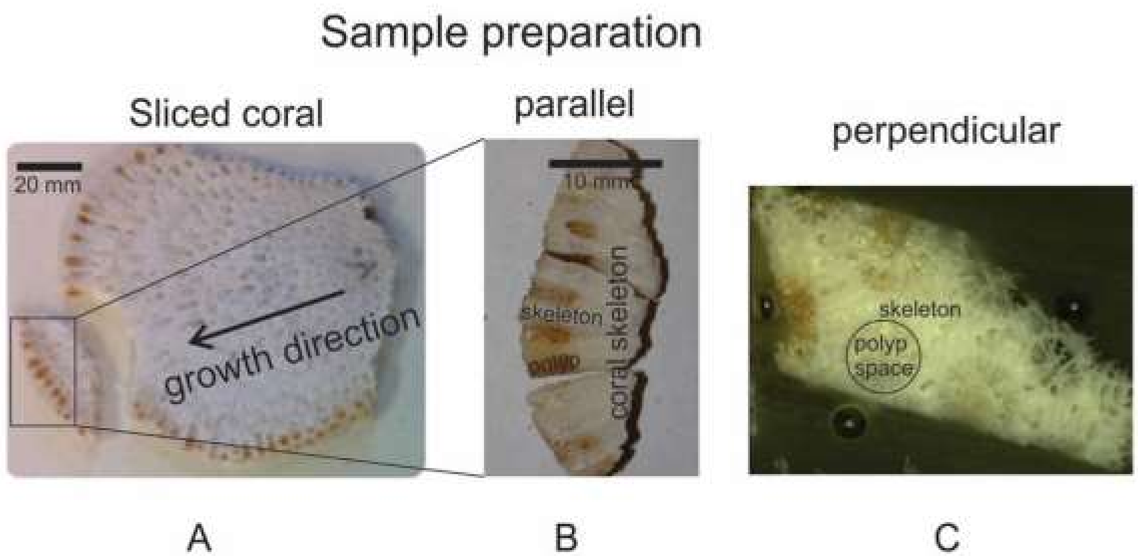

Figure 4.3 Three images showing orientation of coral preparation

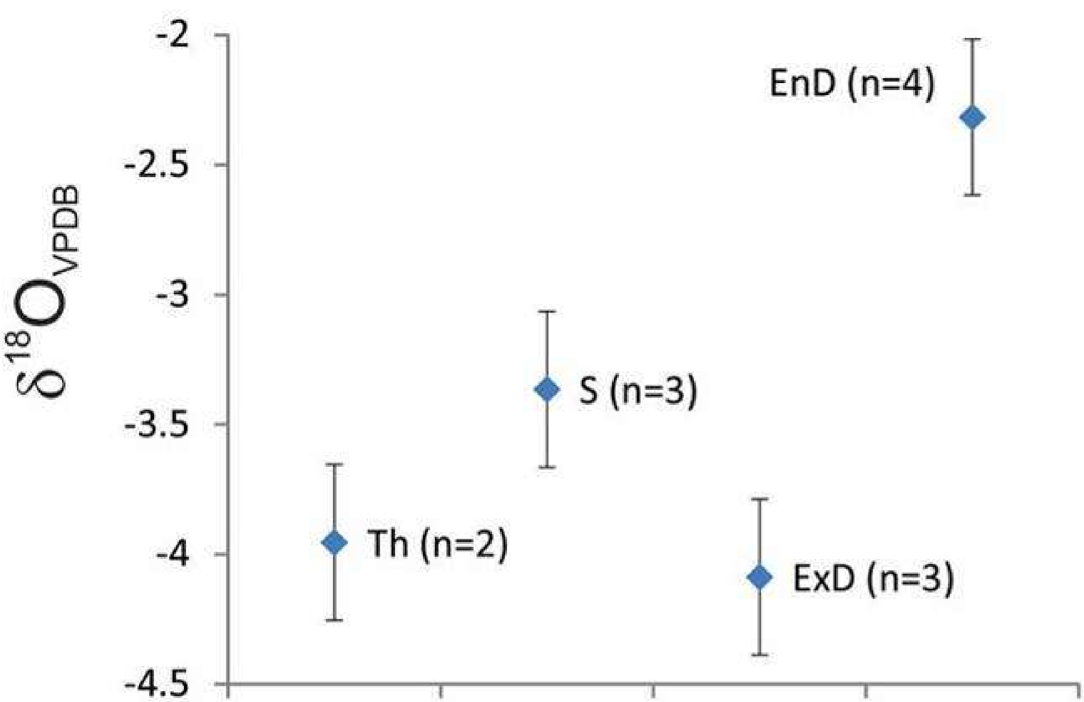

Figure 4.4 Oxygen isotope data of four different architectural structures grown simultaneously

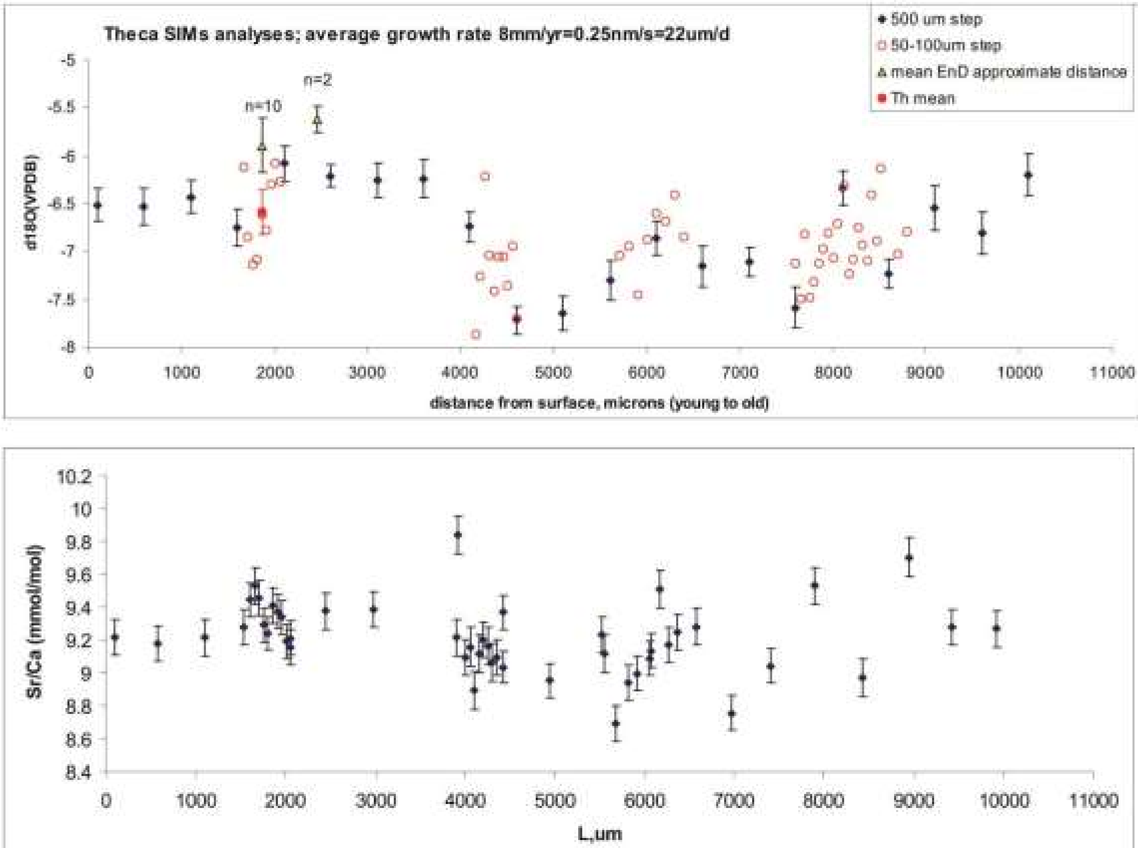

Figure 4.5 Temporal displacement of $\delta^{18}O$ and Sr/Ca ratios

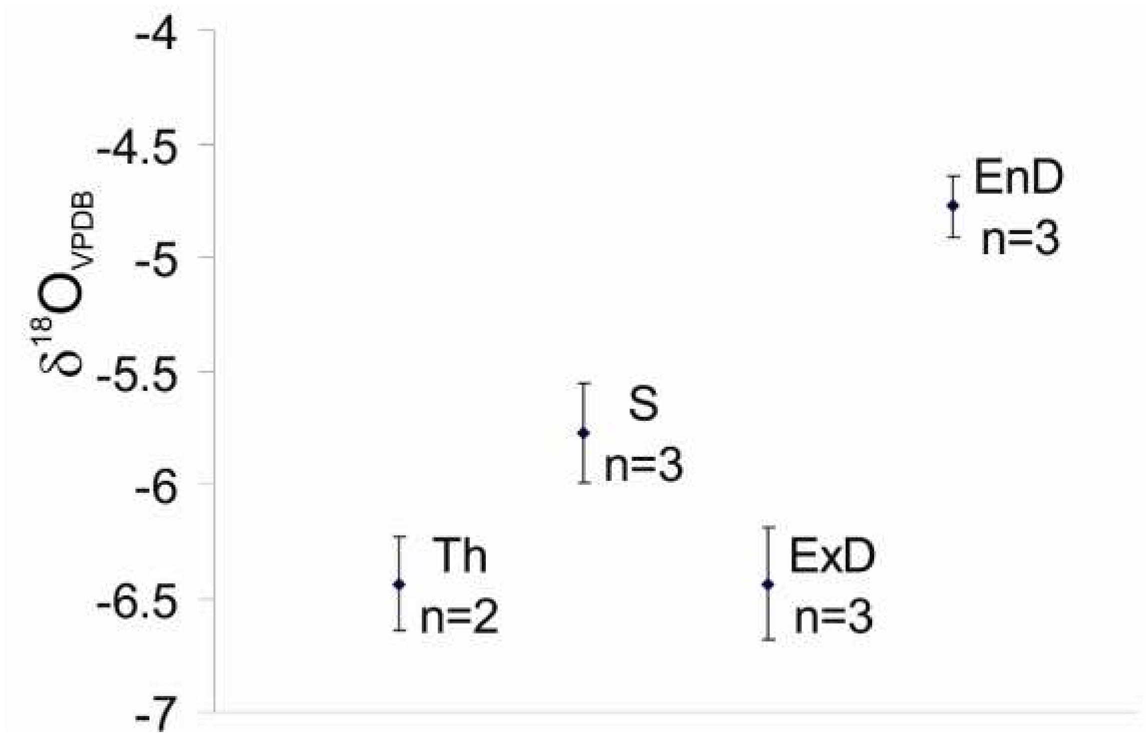

Figure 4.6 Parallel growth indicating equal theca, septa and ExD $\delta^{18}O$, enriched EnD.

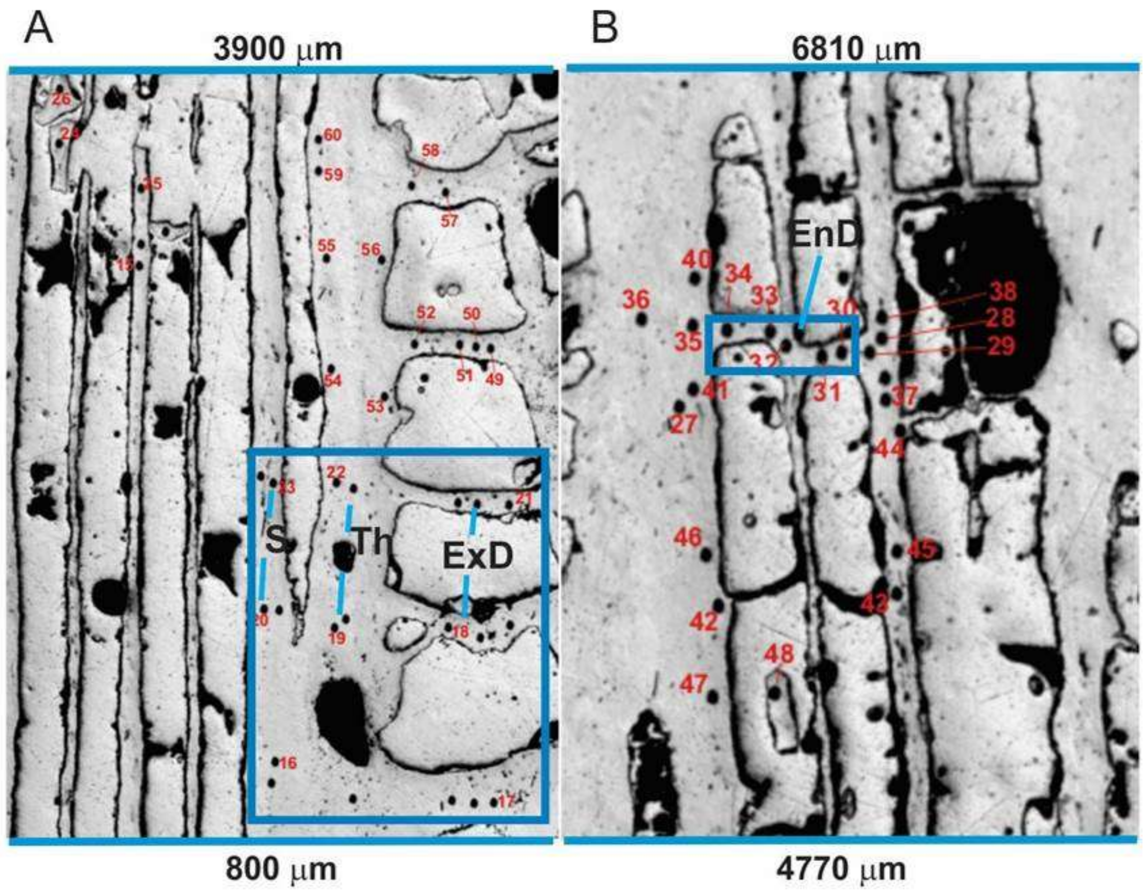

Figure 4.7 Image showing samples from various architectural structures

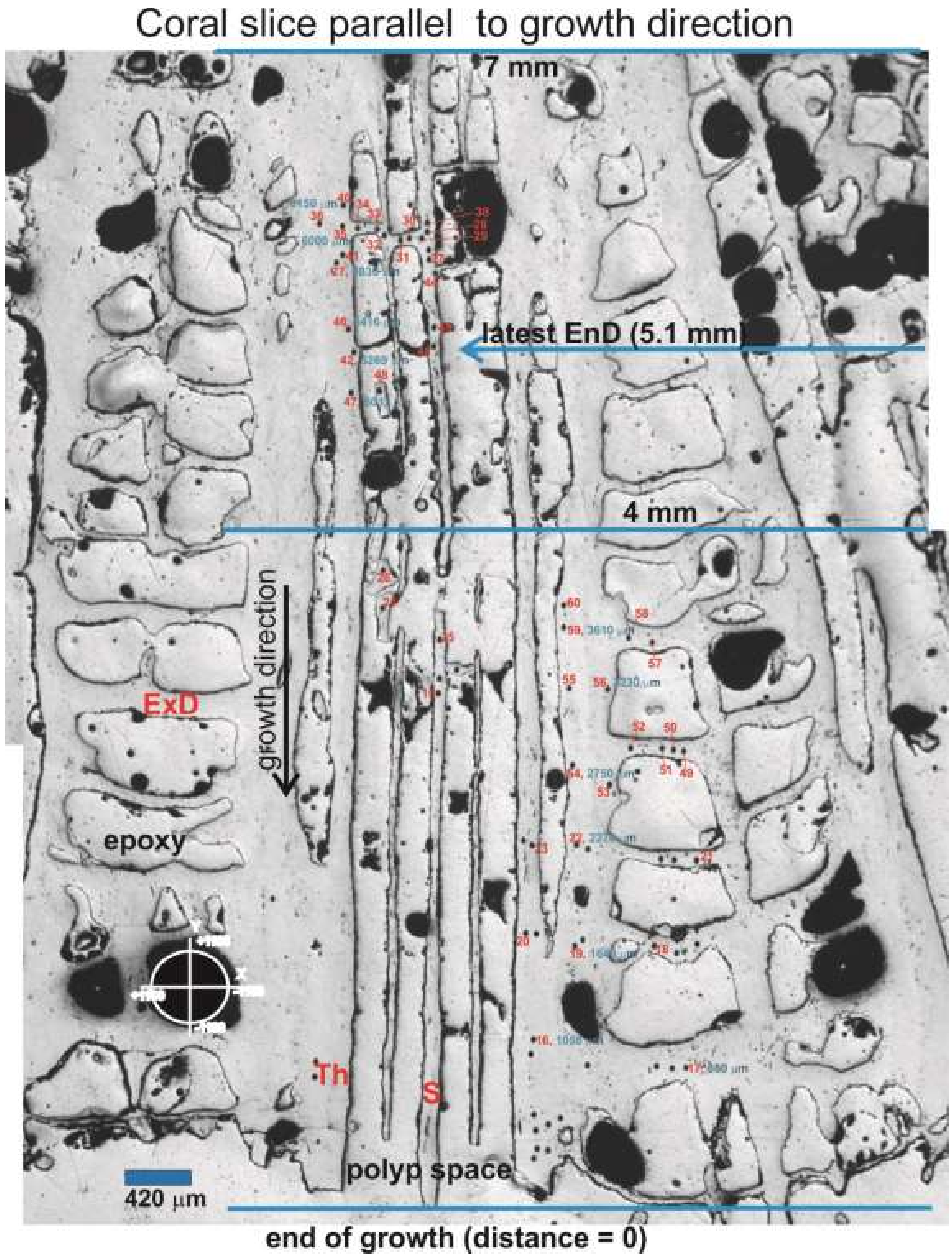

Figure 4.8 Sample parallel to growth

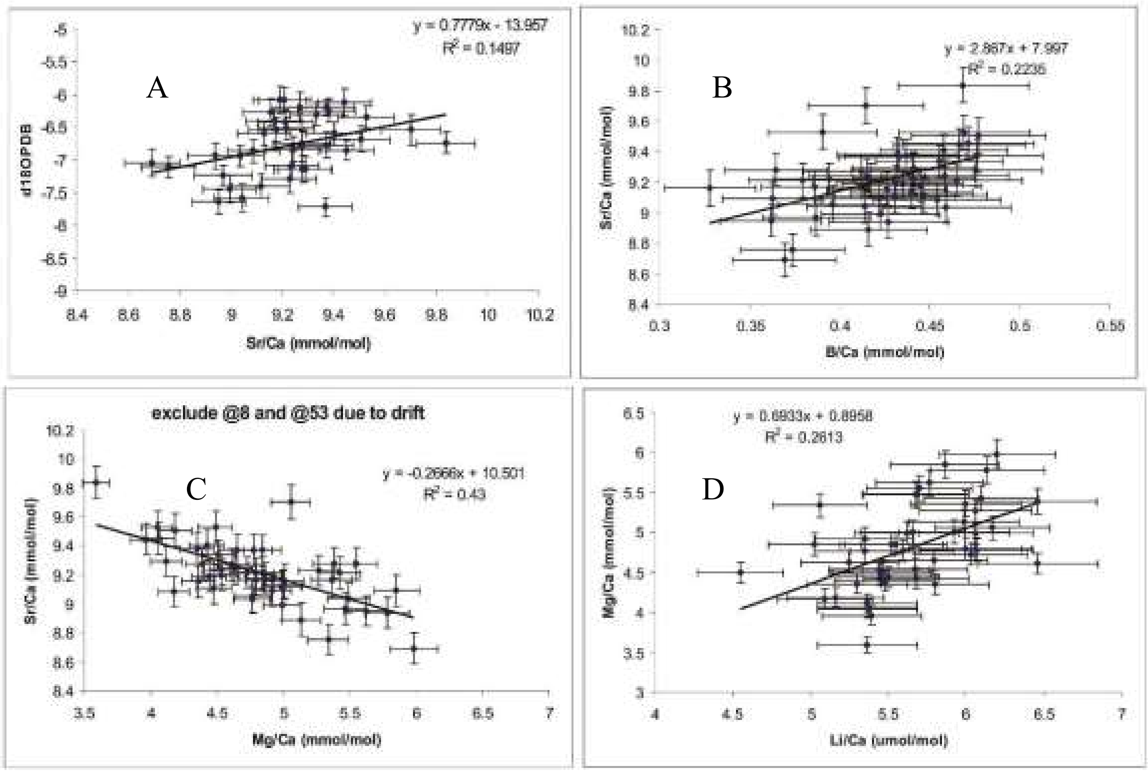

Figure 4.9 Elemental ratio and isotopic ratio comparisons

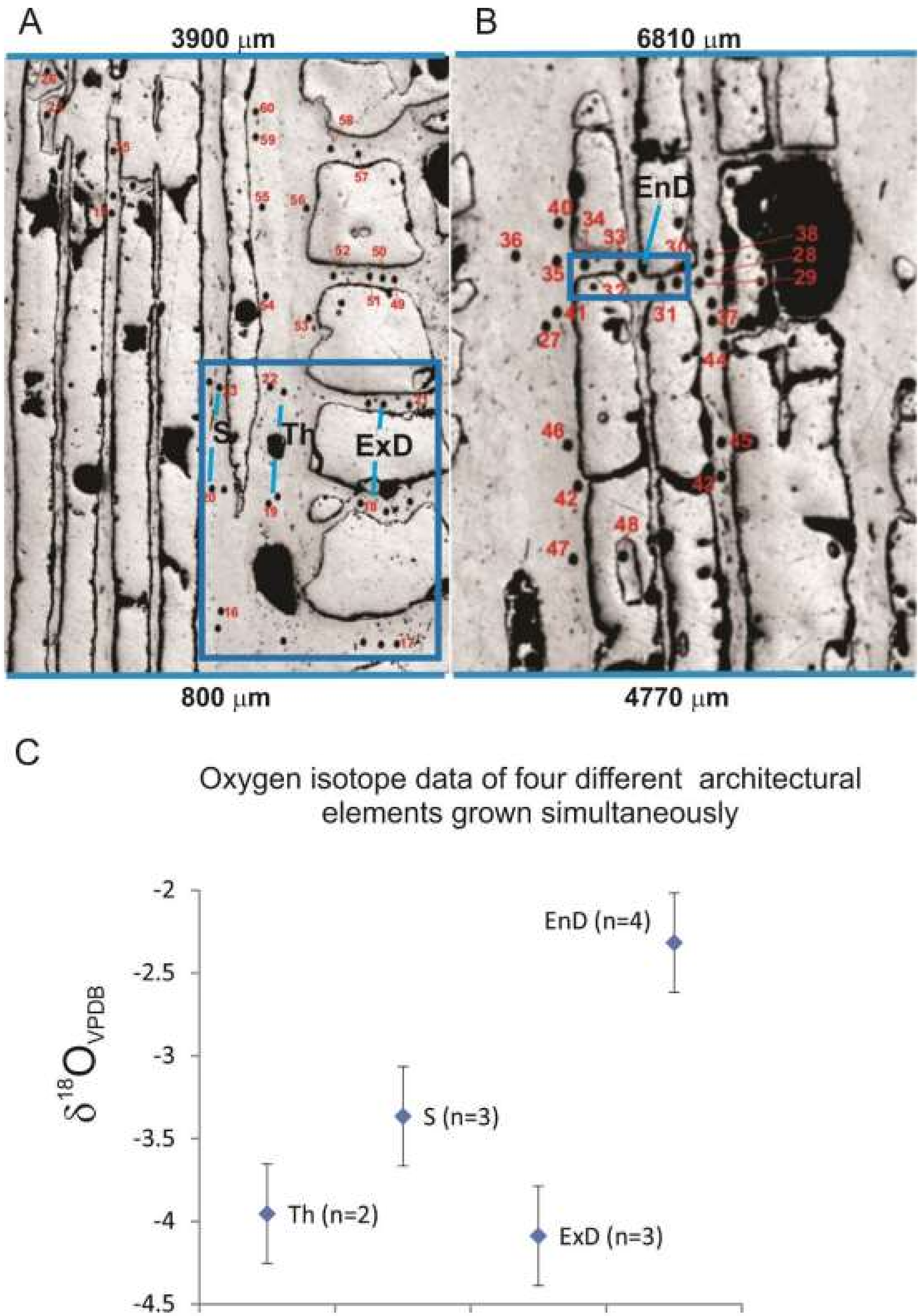

Figure 4.10 SIMS similar to laser burns

Figure 4.11 Image showing simultaneous growth and laser sampling of architectural structures

Table 4.1 Trace element to calcium ratios in various architectural structures

	Mmol/mol				
	Mg/Ca	Sr/Ca	Ba/Ca	U/Ca	B/Ca
ExD(1-2)	4.938114	8.522167	0.007849	0.000594	0.433022
Theca (1-4)	4.710074	8.844135	0.007885	0.00061	0.449925
EnD(1-6)	3.977032	9.062297	0.012749	0.000729	0.420399
s.d					
ExD(1-2)	0.196617	0.048755	0.000325	5.19E-05	0.003443
Theca (1-4)	0.041916	0.07225	0.000222	1E-05	0.0159
EnD (1-6)	0.454555	0.10043	0.002122	9.91E-05	0.032233

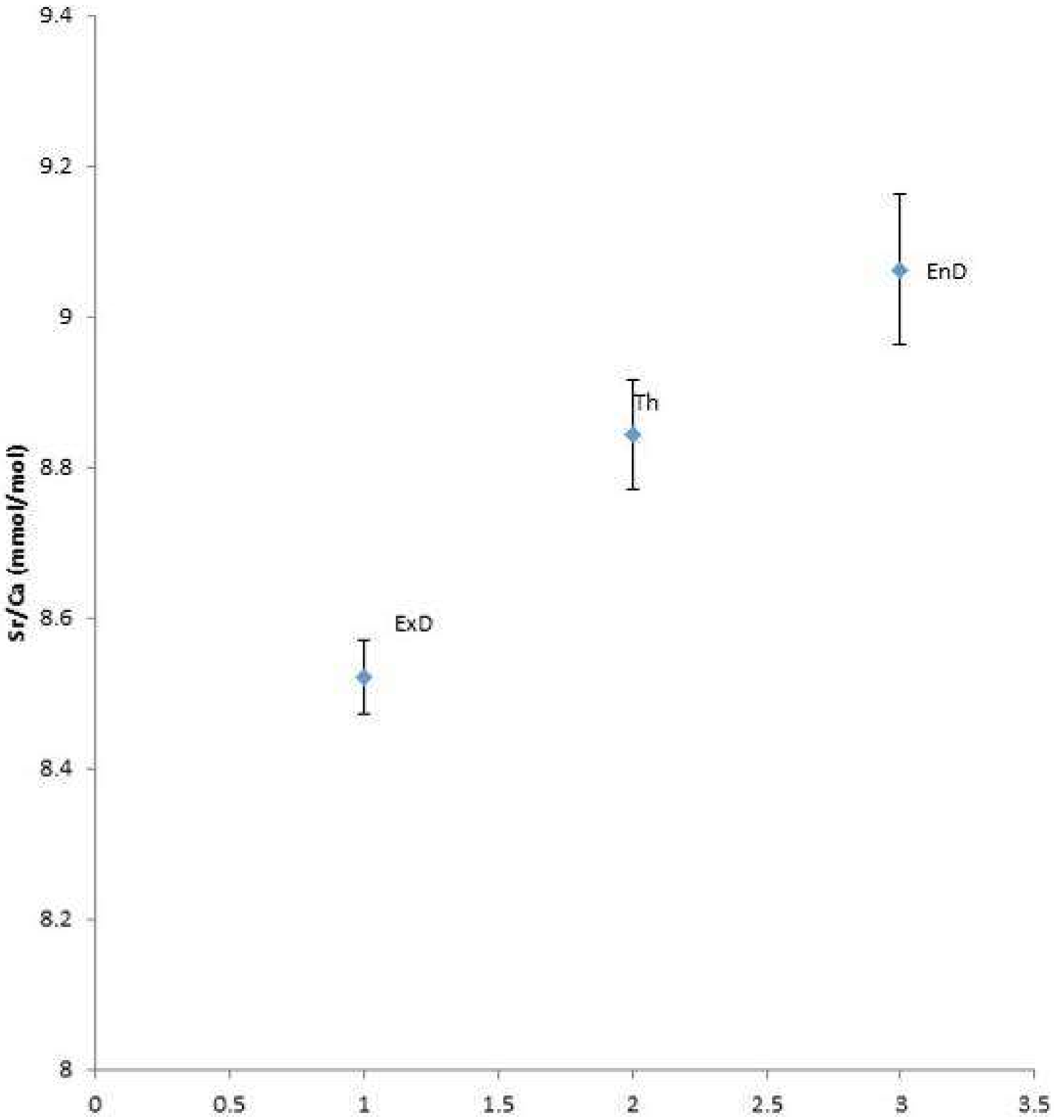

Figure 4.12 Strontium to calcium ratios in ExD, Theca, and EnD

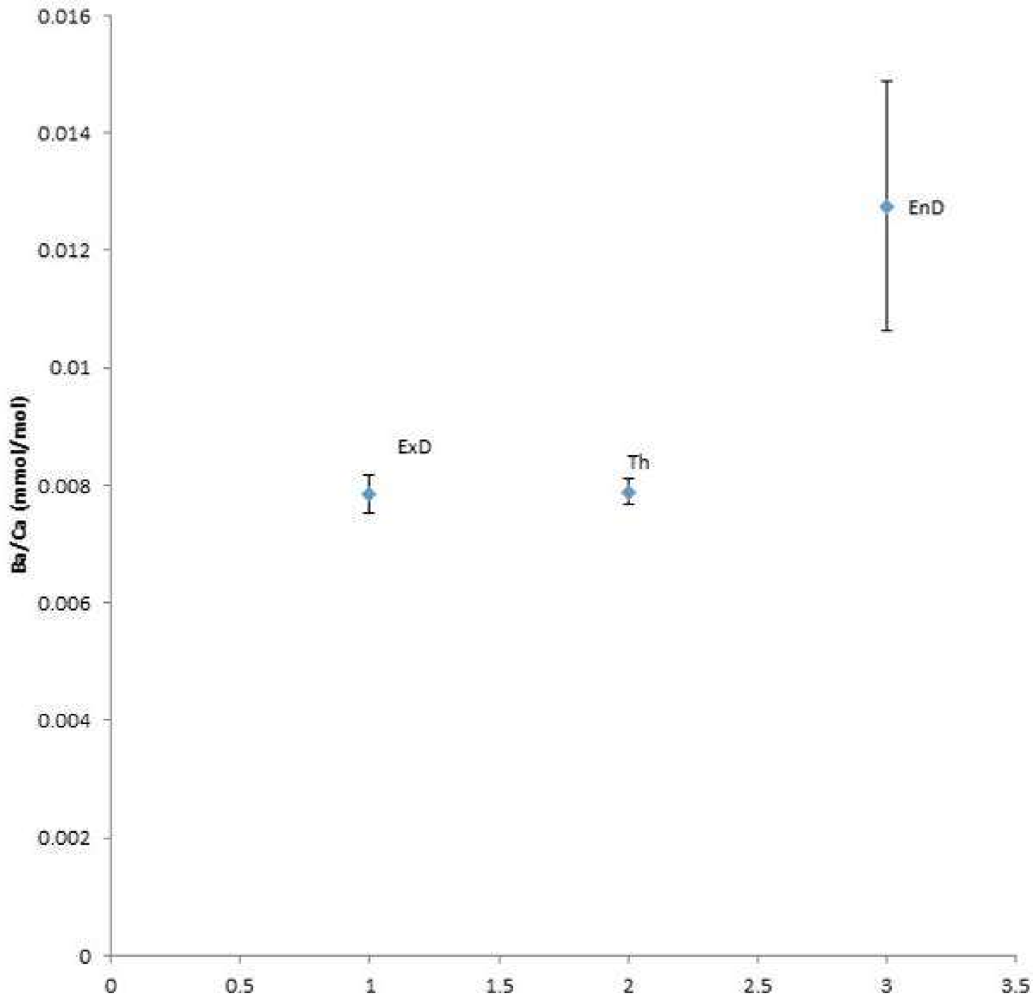

Figure 4.13 Barium to calcium ratios in ExD, Theca, and EnD

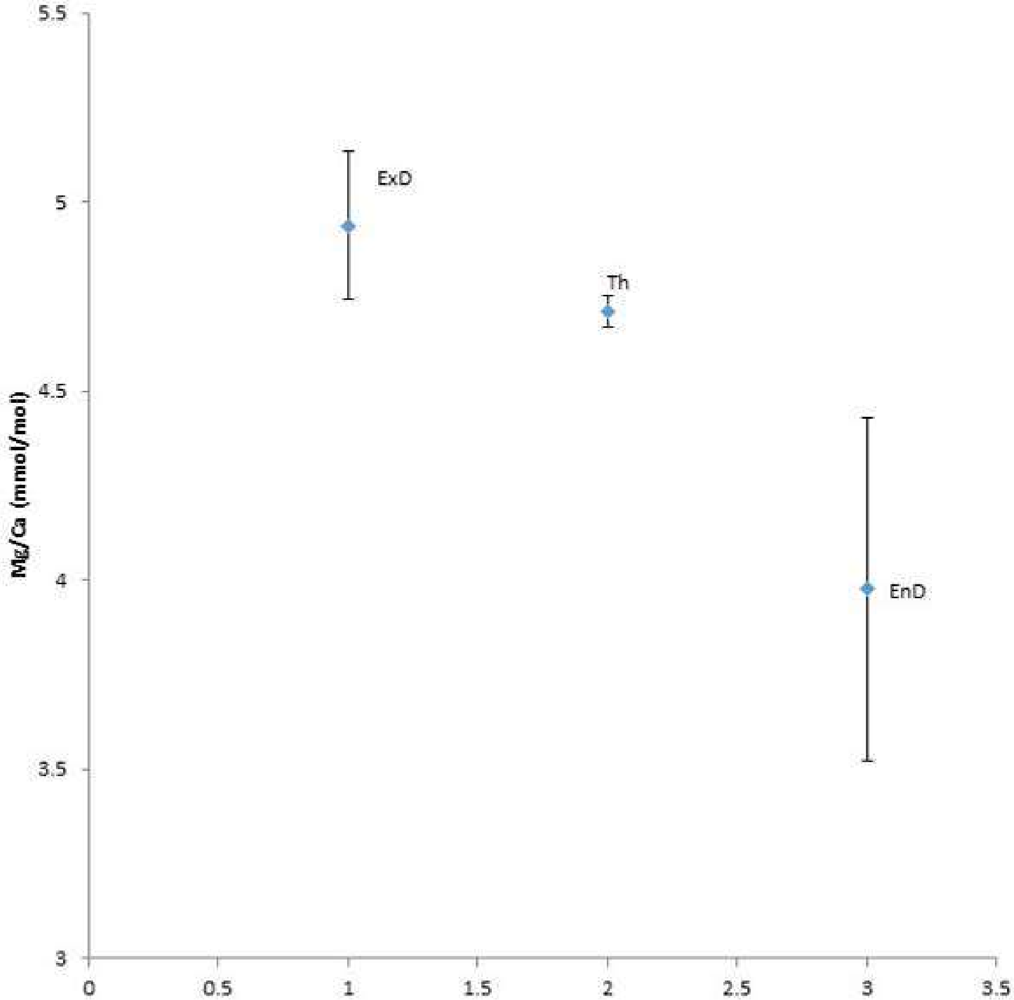

Figure 4.14 Magnesium to calcium ratios for ExD, Theca, and EnD

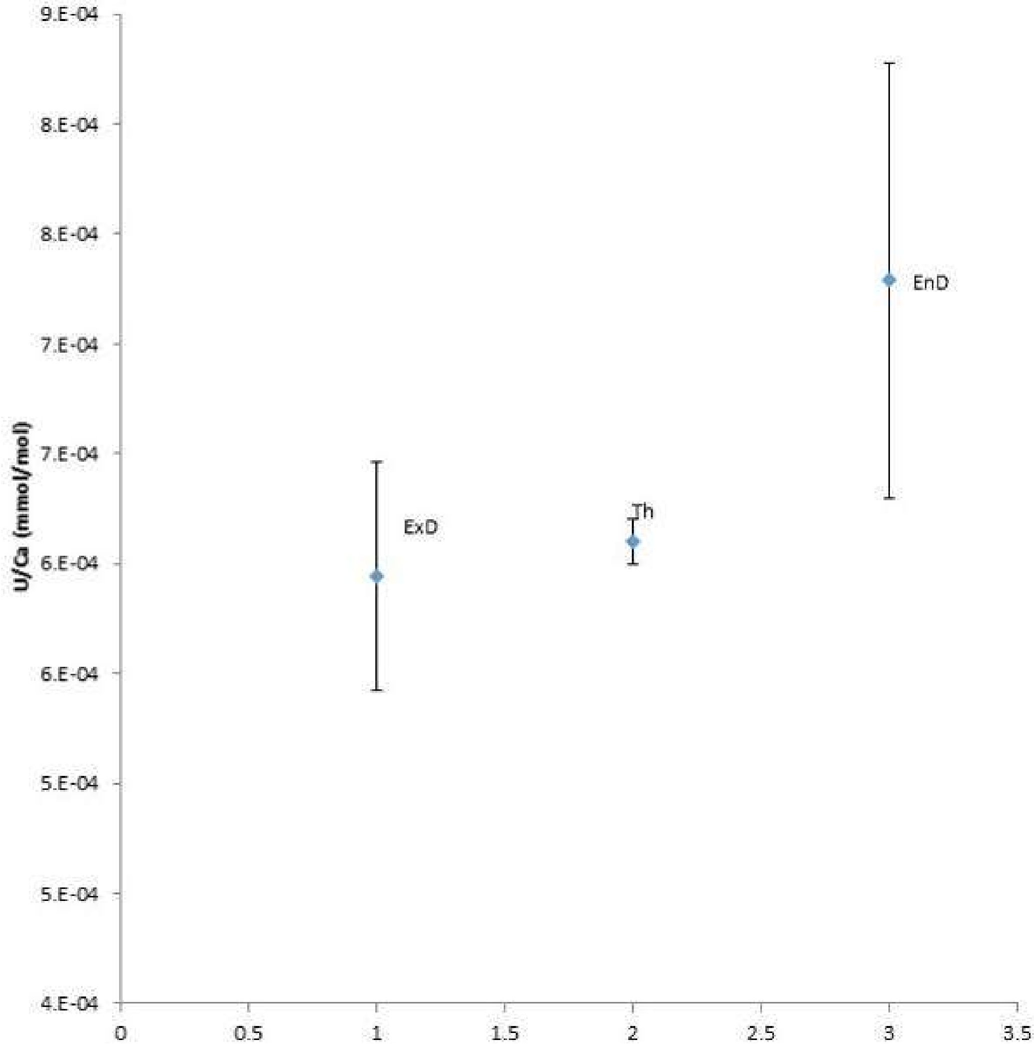

Figure 4.15 Uranium to calcium ratios in ExD, Theca, and EnD

References

Barnes, D., Lough, J. (1993) On the nature and causes of density banding in massive coral skeletons. *Journal of Experimental Biology and Ecology* Vol. 167, pp.91-108

Barnes, D., Taylor, R., Lough, J. (1995) On the inclusion of trace materials into massive coral skeletons Part II: distortion of skeletal records of annual climate cycles due to growth processes. *Journal of Experimental Biology and Ecology* Vol. 194, pp. 251-275

Carricart-Ganivet, J. (2011) Professional communication, September 2011.

Cohen, A., Smith, S., McCartney, M., van Etten, J. (2004) How brain corals record climate: An integration of skeletal structure, growth, and chemistry of *Diploria labyrinthiformis* from Bermuda. *Marine Ecology Progress Series,* Vol. 271, pp. 147-158

Dávalos-Dehullu, E., Hernández-Arana, H., Carricart-Ganivet, J. (2008) On the causes of density banding in skeletons of corals of the genus *Monastraea*. *Journal of Experimental Marine Biology and Ecology* 365 pp. 142-147

DeLong, K., Flannery, J., Maupin, C., Poore, R., Quinn, T. (2011) A coral Sr/Ca calibration and replication study of two massive corals from the Gulf of Mexico. *Palaeogeography, Palaeoclimatology, Palaeoecology* V. 307, pp 117-128

Dissard, D., Douville, E., Reynaud, S., Juillet-Leclerc, A., Montagna, P., Louvat, P., McCulloch, M (2012) Light and temperature effect on _11B and B/Ca ratios of the zooxanthellate coral *Acropora sp.*: results from culturing experiments. *Biogeosc. Discuss.,* 9 pp. 5969-6014

Fayek, M., Harrison, T., Ewing, R., Grove, M., Coath, C. (2002) O and Pb isotopic analyses of uranium minerals by ion microprobe and U-Pb ages from the Cigar Lake deposit. *Chemical Geology,* Vol. 185, pp. 205-225

Friedman, I., O'Neil, J., Cebula, G. (1982) Two new carbonate stable isotope standards. *Geostandards Newsletter,* Vol. 6 pp. 11-12

Gabitov, R. (2013) Growth-rate induced disequilibrium of oxygen isotopes in aragonite: An *in situ* study. *Chemical Geology* Vol. 351, pp. 268-275

Gabitov, R., Gaetani, G., Watson, E., Cohen, A., Ehrlich, H. (2008) Experimental determination of temperature and growth rate effects on U^{6+} and Mg^{2+} portioning between aragonite and fluid. *Geochim. Cosmochim. Acta,* 72, pp.4058-4068

Gabitov, R., Schmitt, A., Rosner, M., McKeegan, K., Gaetani, G., Cohen, A., Watson, E., Harrison, T. (2011) In situ d^7Li, Li/Ca, and Mg/Ca analyses of synthetic aragonites. *Geochem. Geophys. Geosvs.,* 12. 003001, doi:10.1029/2010GC003322.

Gabitov, R., Watson, E., Sadekov, A. (2012) Oxygen isotope fractionation between calcite and fluid as a function of growth *rate* and temperature: An in situ study. *Chem. Geol.,* 306-307 pp.92-102

Gaetani, G. and Cohen, A. (2006) Element portioning during precipitation of aragonite from seawater: A framework for understanding paleo-proxies. *Geochim. Cosmochim. Acta.,* 70 pp.4617-4634

Gagnon, A., Adkins, J., Fernandez, D., Robinson, L. (2007) Sr/Ca and Mg/Ca vital effects correlated with skeletal architecture in a scleractinian deep-sea coral and the role of Rayleigh fractionation. *Earth and Planet. Sci. Lett.,* 261, pp.280-295

Giry, C., Felis, T., Kölling, M., Scheffers, S. (2010) Geochemistry and skeletal structure of *Diplora strigosa,* implications for coral-based climate. *Palaeogeography, Palaeoclimatology, Palaeoecology 298,* pp.378-387

Giry, C., Felis, T., Kölling, M., Wei, W., Lohmann, G., Scheffers, S. (2013) Controls of Caribbean surface hydrology during the mid- to late Holocene: insights from monthly resolved coral records. *Climate of the Past* 9 pp.841-858

Goreau, T. (1977) Coral skeletal chemistry: Physiological and environmental regulation of stable isotopes and trace metals in *Montastrea annularis. Proceedings of the Royal Biological Sciences Society* 196, no. 1124 pp.291-315

Grottoli, A., and Eakin, C. (2006) A review of modern coral δ^{18}O and Δ^{14}C proxy records. *Earth Science Reviews* 81 pp. 67-91

Guzman, H. and Tudhope, A. (1998) Seasonal variation in skeletal extension rate and stable isotopic ($^{13}C/^{12}C$ and $^{18}O/^{16}O$) composition in response to several environmental variables in the Caribbean reef coral *Siderastrea siderea. Marine Ecology Progress Series,* Vol. 166, pp.109-118

Hayashi, E., Suzuki, A., Nakamura, T., Iwase, A., Ishimura, T., Iguchi, A., Sakai, K., Okai, T., Inoue, M., Araoka, D., Murayama, S., Kawahata, H. (2013) Growth-rate influences on coral climate proxies tested by a multiple colony culture experiment. *Earth and Planetary Science Letters* 362, pp. 198-206

Hemming, N., Reeder, R., Hart, S. (1998) Growth-step-selective incorporation of boron on the calcite surface. *Geochim., Cosmochim., Acta.,* 62, pp.2915-2922

Inoue, M. (2006) Re-evaluation of Sr/Ca ratio in coral skeletons as a proxy for temperature. *Geochemistry(Japan)* 40, pp. 209-219

Kita, N., Ushikubo, T., Fu, B., Valley, J. (2009) High precision SIMS oxygen isotope analysis and the effect of sample topography. *Chemi. Geol.*, 264, pp.43-57

Land, L., Lang, J., Barnes, D. (1975) Extension rate: A primary control on the isotopic composition of West Indian (Jamaican) Scleractinian reef coral skeletons. *Marine Biology* Vol. 33 pp. 221-233

Leder, J., Swart, P., Szmant, A., Dodge, R. (1996) The origins of variations in the isotopic record of scleractinian corals: I. Oxygen. *Geochimica et Cosmochimica,* Vol. 60., No. 15, pp. 2857-2870

Reed, W. (1992) Certificate of Analysis Standard Reference Materials 614, 615 trace elements in a glass matrix *National Institute of Standards and Technology (NIST)*

Saenger, C., Affek, H., Felis, T., Thiagarajan, N., Lough, J., Holcomb, M. (2012) Carbonate clumped isotope variability in shallow water corals: Temperature dependence and growth-related vital effects. *Geochim., Cosmochim. Acta,* 99, pp. 224-242

Stanley, G., Helmle, K. (2010) Middle Triassic coral growth bands and their implications for photosynthesis. *Palaios* Vol. 25, No. 12, pp.754-763

Stoll, H., Rosenthal, Y., Falkowski, P. (2002) Climate proxies from Sr/Ca of coccolith calcite: Calibrations from continuous culture of *Emiliania huxleyi. Geochim., Cosmochim., Acta* 66, pp. 927-936

Storz, D., Gischler, E., Fiebig, J., Eisenhauer, A., Garbe-Schönberg, D. (2013) Evaluation of oxygen isotopes and Sr/Ca ratios from a Maldivian scleractinian coral for reconstruction of climate variability in the Northwestern Indian Ocean. *Society for Sedimentary Geology* 28, pp. 42-55

Suzuki, A.(2012) Paleoclimate reconstruction and future forecast based on coral skeletal climatology. *Synthesiology* Vol. 5, No. 2, pp.80-88

Watanabe, T., Winter, A. Oba T., Anzai, R., Ishioroshi, H. (2002) Evaluation of the fidelity of isotope records as an environmental proxy in the coral *Montastraea. Coral Reefs* 21, pp.169-178